Imperial College London
Department of Physics

Quantum thermodynamics in the strong coupling regime

David Newman

Submitted in part fulfilment of the requirements for the degree of
Doctor of Philosophy in Physics of the University of London and
the Diploma of Imperial College, October 2018

Declaration

The work presented here is my own except for background material which is included so that this thesis may be self-contained. Any material which is not my own work is referenced appropriately.

Abstract

Quantum thermodynamics seeks to address the emergence of thermodynamic laws, which govern how energy is exchanged between physical systems, from a quantum mechanical description of light and matter. As such, the workhorse model for an underlying description of such energy exchange processes is the open quantum system: a quantum system which may interact with an external environment. Open quantum systems are well-understood in regimes where the interaction between the system and the environment is weak enough that perturbative methods may be employed to arrive at dynamical equations of motion for the evolution of the system. How to tackle the strong coupling regime is an open question and much research is still being devoted in this area. In this project we employ a technique developed for studying an open quantum system in regimes of strong reservoir coupling in problems in thermodynamics which have so far been restricted to the weak coupling regime. We spend some time developing our strong coupling framework and then use it to analyse a quantum heat engine to find that strong coupling leads to a particular set of operational costs which are not present in more well-understood weak coupling versions. We also identify effects purely quantum in nature, present in the engine cycle only at strong coupling, which lead to a degradation in the engine's performance. Finally we address the issue of quantum coherence more generally in archetypal open quantum system models beyond weak coupling, and identify a thermodynamic cost to its erasure.

Contents

List of Figures

Overview

Quantum thermodynamics is a term which encompasses recent efforts, both theoretical and experimental, directed towards reaching an understanding of how the laws of thermodynamics emerge from an underlying quantum theory of matter. Tremendous progress has been made in this field. However, this project stemmed from a desire to address an area which is conspicuous in its absence from the impressive results which have already been achieved to date in this topic.

Thermodynamics involves the study of energetic exchanges between physical systems as well as with their external environments. Classically, it is an emergent theory and the laws of thermodynamics are applicable in the limit of a large collection of individual microscopic systems, whose collective behaviour can be well described by classical laws of physics. Away from this limit, as the system size is reduced, naturally quantum physics is required to accurately describe the dynamics. In fact, this setting falls within the remit of a branch of quantum physics known as open quantum systems. This is a theory precisely designed to tackle the dynamics of quantum systems which interact with an environment.

In standard treatments of open quantum systems, one needs to make some approximations in order to work with equations of motion which are tractable. Except for a small number of exactly solvable models, computing the dynamics of a quantum system which interacts with an environment consisting of a large number of quantum particles is not possible analytically and difficult numerically without making some simplifying assumptions. These approximations typically restrict the treatment of the dynamics to a regime where the interaction between the system and the environment causes only a small perturbation on top of an otherwise interaction-free description.

When this toolbox from the theory of open quantum systems is employed in the study of quantum thermodynamics, one is therefore typically restricted to regimes where there is only weak system-environment coupling. In what follows, we shall be tackling circumstances which go beyond this restriction and discussing how the thermodynamics which emerge in this regime differ from those seen so far in weak coupling scenarios. In chapter 1, we will review the mathematical toolbox one requires to treat open quantum systems. We will clarify the approximations we have just alluded to, which restrict standard treatments to the weak coupling regime. This

chapter contains only material which is well-known in the field of open quantum systems and we will point out where the interested reader may find further detailed discussions of this topic. In chapter 2 we will move into the strong-coupling regime and discuss a mathematical formalism developed as part of this project specifically to treat open quantum systems beyond the approximations which would otherwise restrict us to the dynamics and thermodynamics of weak system-environment interactions.

In chapters 3 and 4, we will apply this framework in the analysis of a quantum heat engine, first at infinite cycle times and then at finite times. Quantum heat engines have been studied at weak system-reservoir coupling, however, a general treatment beyond this regime is breaking new ground and, we would argue, more relevant for practical realisations of such devices. We will seek to understand what differences arise at strong reservoir coupling and address what can be done in cases where these differences lead to a degradation in the engine's performance. On a more fundamental level, we shall also learn that there are purely quantum effects present in a finite time quantum engine only at strong coupling which hamper its performance, namely quantum coherence develops in the working system as a result of quantum correlations with the heat reservoirs.

In chapter 5, we shall look at quantum coherence in open quantum system models more broadly. We will identify a thermodynamic cost to its erasure, in the same spirit as Landauer's erasure principle, which explains the thermodynamic cost of classical information erasure. More generally we shall look at information flow between a quantum system and an environment beyond the realm of weak coupling and understand what thermodynamic signatures arise as a signal of strong reservoir coupling.

Chapter 1

The dynamics of open quantum systems

Before embarking on our study of thermodynamics, we shall devote a little time to some basic mathematical techniques that are required for the treatment of the dynamics of an open quantum system. An open quantum system is one which interacts with some external environment, which typically we do not wish or are unable to treat explicitly. A closed quantum system's dynamics are governed by the Schrödinger equation and specifically a Hamiltonian operator for the energy of the system. We shall see that the dynamics of an open quantum system can be described by a different equation of motion called a master equation, the derivation of which typically involves making some simplifying approximations about the behaviour of the environment with which the system interacts. As we review the technique of deriving such a master equation, we will place special emphasis on any approximations made and discuss how these typically restrict us to a regime of weak system-environment interactions. Later, we will relax these approximations and derive an alternative treatment of the dynamics of open quantum systems, known as the Reaction Coordinate (RC) formalism, which will allow us to treat the case where the open quantum system interacts more strongly with the environment.

The techniques reviewed in this chapter are all commonly employed in the framework of open

quantum systems and here we generally follow derivations presented in references [1, 2, 3]. Before treating the dynamics of an open quantum system we first review some of the basic mathematical formalism required.

1.1 Mathematical preliminaries

1.1.1 The Liouville-von Neumann equation for the evolution of a density operator

We begin with a very brief recap of how to describe the dynamics of closed quantum systems. Consider a system in a pure quantum state described by the vector $|\psi(t)\rangle$, belonging to some Hilbert space $\mathcal{H}^{\mathcal{S}}$. The time evolution of this vector is given by the time-dependent Schrödinger equation

$$i\frac{d}{dt}|\psi(t)\rangle = H(t)|\psi(t)\rangle, \tag{1.1}$$

where $H(t)$ is the Hamiltonian for the system, which may carry some time dependence. To keep expressions unencumbered, we will assume Hamiltonians have units of frequency. This means that $H(t)$ should read as $\frac{H(t)}{\hbar}$, where $\hbar$ is the reduced Planck constant. This is typically what is meant by the turn of phrase "setting $\hbar = 1$". The solution to equation (1.1) may be written as

$$|\psi(t)\rangle = U(t, t_0)|\psi(t_0)\rangle, \tag{1.2}$$

where $U(t, t_0)$ is a unitary operator acting on $\mathcal{H}^{\mathcal{S}}$ which evolves the system state vector at some initial time t_0 to its state vector at a later time t. To reach an explicit form for the time evolution operator we substitute the right hand side of equation (1.2) for $|\psi(t)\rangle$ into equation (1.1) and, cancelling the time-independent initial state vectors from either side, we obtain

$$i\frac{d}{dt}U(t, t_0) = H(t)U(t, t_0). \tag{1.3}$$

We may integrate equation (1.3) to give the following expression for the evolution operator from time t_0 to time t

$$U(t,t_0) = T_{\leftarrow} \exp\left[-i\int_{t_0}^{t} ds H(s)\right], \tag{1.4}$$

where $T_{\leftarrow}$ indicates that we take the time-ordered exponential in the expression which follows it. In the special case where the Hamiltonian is independent of time, a straightforward integration of Eq. (1.3) gives

$$U(t,t_0) = \exp\left[-iH(t-t_0)\right]. \tag{1.5}$$

So far we have restricted ourselves to pure quantum systems described by the time-dependent vector $|\psi(t)\rangle$. More generally, we may describe the state of a quantum system at an initial time t_0 by a density operator

$$\rho(t_0) = \sum_{\alpha} p_\alpha |\psi_\alpha(t_0)\rangle\langle\psi_\alpha(t_0)|. \tag{1.6}$$

We interpret p_α as the classical probability of the system being in the pure state $|\psi_\alpha(t_0)\rangle$ at time t_0. There are α different possible initial pure states for the system and we require $\sum_\alpha p_\alpha = 1$. In the case where the initial quantum state is pure, the summation index α only runs over one value and the density operator reduces to $\rho(t_0) = |\psi_\alpha(t_0)\rangle\langle\psi_\alpha(t_0)|$. If α runs over more than one value then the state is known as a mixed state.

To obtain the density operator for the system at some later time t we conjugate $\rho(t_0)$ with the time-evolution operator $U(t,t_0)$ such that

$$\rho(t) = U(t,t_0)\rho(t_0)U^\dagger(t,t_0). \tag{1.7}$$

From this expression we can obtain an equation of motion governing the time evolution of the density operator which is analogous to the Schrödinger equation governing the evolution of pure quantum systems. We differentiate equation (1.7), and, using equation (1.1), arrive at the Liouville-von Neumann equation

$$\frac{d}{dt}\rho(t) = -i\left[H(t),\rho(t)\right] \equiv \mathcal{L}(t)\rho(t). \tag{1.8}$$

In equation (1.8) we have defined a time-dependent Liouvillian superoperator $\mathcal{L}$, which maps a valid density operator to another valid density operator. The formal solution to equation (1.8) is

$$\rho(t) = T_{\leftarrow} \exp\left[\int_{t_0}^{t} ds \mathcal{L}(s)\right] \rho(t_0). \tag{1.9}$$

In the case of a Hamiltonian (and hence Liouvillian) that is independent of time this reduces to

$$\rho(t) = \exp\left[\mathcal{L}(t - t_0)\right] \rho(t_0). \tag{1.10}$$

The Liouville-von Neumann equation (1.8) will be the starting point for our derivation of the master equation for an open quantum system. But before diving into that, we will briefly introduce, in the next section, the concept of the interaction picture description of operators and quantum states as this will aid in the sections to follow.

1.1.2 The Interaction picture

We shall now briefly review the process of transforming operators and quantum state vectors into the interaction picture. This process forms a crucial step in treatments of open quantum system dynamics, since we will wish to treat the interaction between the open system and the environment as a perturbation on the non-interacting parts of a total system and environment Hamiltonian.

We consider a Hamiltonian of the form

$$H(t) = H_0 + H_I(t). \tag{1.11}$$

Here we suppose that H_0 describes the bare energy of a system and its environment (another, or several other quantum systems), and would appear alone in a Schrödinger equation governing the free evolution of all systems were they not interacting with each other. $H_I(t)$ is the term describing the interaction between the systems and may, in general, carry some time dependence. In what follows, we restrict ourselves to situations where this term is independent of time. The

expectation value of a Schrödinger picture observable $A(t)$, at some time t, is obtained by following the Born rule of standard quantum theory to yield

$$\begin{aligned} \langle A(t) \rangle &= \mathrm{tr}\left[A(t)\rho(t)\right] \\ &= \mathrm{tr}\left[A(t)U(t,t_0)\rho(t_0)U^\dagger(t,t_0)\right]. \end{aligned} \tag{1.12}$$

We define a unitary operator which resembles a time evolution operator based on the interaction-free Hamiltonian

$$U_0(t,t_0) \equiv \exp\left[-iH_0(t-t_0)\right]. \tag{1.13}$$

Noting that $U_0^\dagger(t,t_0)U_0(t,t_0) = U_0(t,t_0)U_0^\dagger(t,t_0) = I$, equation (1.12) may then be written as

$$\begin{aligned} \langle A(t) \rangle &= \mathrm{tr}\left[A(t)U_0(t,t_0)U_0^\dagger(t,t_0)U(t,t_0)\rho(t_0)U^\dagger(t,t_0)U_0(t,t_0)U_0^\dagger(t,t_0)\right] \\ &= \mathrm{tr}\left[U_0^\dagger(t,t_0)A(t)U_0(t,t_0)U_I(t,t_0)\rho(t_0)U_I^\dagger(t,t_0)\right] \\ &\equiv \mathrm{tr}\left[\tilde{A}(t)\tilde{\rho}(t)\right], \end{aligned} \tag{1.14}$$

where, in the second line, we have used the cyclic properties of the trace and defined the time evolution operator in the interaction picture as $U_I(t,t_0) = U_0^\dagger(t,t_0)U(t,t_0)$. In the third line we define the interaction picture form of an operator, denoted by the tilde, as $\tilde{A}(t) \equiv U_0^\dagger(t,t_0)A(t)U_0(t,t_0)$. The interaction picture at time t is therefore defined by the unitary transformation $U_0(t,t_0)$.

We may now determine an evolution equation for the density operator in the interaction picture,

$\tilde{\rho}(t)$. Differentiating the expression for the interaction picture form of the density operator yields

$$\begin{aligned}\frac{d}{dt}\tilde{\rho}(t) &= i\left[H_0, \tilde{\rho}(t)\right] + U_0^\dagger(t,t_0)\left(\frac{d}{dt}\rho(t)\right)U_0(t,t_0) \\ &= i\left[H_0, \tilde{\rho}(t)\right] - iU_0^\dagger(t,t_0)\left[H(t), \rho(t)\right]U_0(t,t_0) \\ &= -i\left[\tilde{H}_I(t), \tilde{\rho}(t)\right], \end{aligned} \tag{1.15}$$

where in the second line we have made use of the Liouville-von Neumann equation for the evolution of $\rho(t)$ to substitute in for $\frac{d}{dt}\rho(t)$ and in the last line we have used $I = U_0^\dagger(t,t_0)U_0(t,t_0)$ to notice that conjugation of the commutator with $U_0^\dagger(t,t_0)$ amounts to transformation of $H_I(t)$ and $\rho(t)$ into the interaction picture. Equation (1.15) is, therefore, the equivalent form of the Liouville-von Neumann equation describing the evolution of the density operator in interaction picture form. Both equation (1.15) and the definition of an operator in the interaction picture will prove useful tools in deriving a Born-Markov master equation in what follows.

1.1.3 The reduced density operator

There is one final key ingredient which we review briefly here, before turning to the description of the dynamics of an open quantum system by means of a master equation. In the case of a system S interacting with an environment E, the master equation formalism involves keeping track of the evolution of the system of interest S rather than that the global state for S and E. Consider a Hamiltonian of the form

$$H = H_S + H_E + H_I, \tag{1.16}$$

where H_S is the Hamiltonian for the free evolution of S ignoring any interaction with E, H_E the Hamiltonian for the evolution of E without any interaction with S and H_I the term treating the interaction between S and E. Any observable on the system alone may be written in the

form $A = A_S \otimes I_E$. The expectation value of any such observable will be given by

$$\begin{aligned} \langle A(t) \rangle &= \mathrm{tr}_{S+E} \left[(A_S(t) \otimes I_E) \, \rho(t) \right] \\ &= \mathrm{tr}_S \left[A_S(t) \rho_S(t) \right], \end{aligned} \tag{1.17}$$

where we have introduced the reduced density operator for the system, obtained by taking the partial trace over the environment degrees of freedom of the density operator for the total state, $\rho_S(t) = \mathrm{tr}_E \left[\rho(t) \right]$.

The evolution of the reduced density operator $\rho_S(t)$ is therefore obtained from equation (1.8) by performing a partial trace over the environment to give

$$\frac{d}{dt} \rho_S(t) = -i \, \mathrm{tr}_E \left[H(t), \rho_S(t) \right]. \tag{1.18}$$

We shall make use of equation (1.18), transformed into the interaction picture, now that we turn to the derivation of the master equation for the evolution of an open quantum system.

1.2 The Born-Markov master equation

1.2.1 Simplifying the Liouville-von Neumann equation

With these mathematical formalities now firmly in place, and with our grasp of the dynamics of closed quantum systems refreshed, we now turn to a treatment of the dynamics of an open quantum system which will culminate in our writing down a Born-Markov master equation. Although restricted to regimes of weak coupling, it will still serve as a foundation for our treatment of the strong coupling regime, on which we shall focus later. The derivation will rely on making some simplifications about how the environment behaves during its interaction with our system of interest, under what are collectively termed the Born-Markov approximations. We will highlight these at the relevant points. We begin by considering a Hamiltonian of the form of equation (1.16). Let us define $H_0 \equiv H_S + H_E$ and employ this to transform H_I into the

interaction picture according to the rules given in section 1.1.2, yielding

$$\widetilde{H}_I(t) = e^{i(H_S+H_E)t} H_I e^{-i(H_S+H_E)t}, \tag{1.19}$$

where we have chosen the initial time to be $t_0 = 0$. In the interaction picture, the global density operator for the composite system-environment state will obey equation (1.15) as its equation of motion. Integrating with respect to time, we may write the formal solution as

$$\widetilde{\rho}(t) = \widetilde{\rho}(0) - i \int_0^t ds \left[\widetilde{H}_I(s), \widetilde{\rho}(s) \right]. \tag{1.20}$$

Substituting the expression for $\tilde{\rho}(t)$ in equation (1.20) back into the right hand side of equation (1.15) yields

$$\frac{d}{dt}\widetilde{\rho}(t) = -i \left[\widetilde{H}_I(t), \widetilde{\rho}(0) \right] - \int_0^t ds \left[\widetilde{H}_I(t), \left[\widetilde{H}_I(s), \widetilde{\rho}(s) \right] \right]. \tag{1.21}$$

Performing a partial trace over the degrees of freedom of the environment we turn this into an equation of motion for the reduced density operator of the system S:

$$\frac{d}{dt}\widetilde{\rho}_S(t) = -i \mathrm{tr}_E \left[\widetilde{H}_I(t), \widetilde{\rho}(0) \right] - \int_0^t ds \ \mathrm{tr}_E \left[\widetilde{H}_I(t), \left[\widetilde{H}_I(s), \widetilde{\rho}(s) \right] \right]. \tag{1.22}$$

Let us assume that the interaction is switched on at $t = 0$ and that no correlations exist between the system and environment at that point, meaning that we may write the composite density operator as a product state: $\rho(0) = \rho_S(0) \otimes \rho_E(0)$. Although this step is often skimmed over and does not fall within the collective understanding of what are meant by the Born-Markov approximations, we wish to highlight at this stage that this assumption is in fact non-trivial. Without it, our subsequent derivation of the master equation would break down, but perhaps more importantly for the purposes of our later treatment of thermodynamic cycles, it is an assumption that is often vital for the validity of thermodynamic treatments of open quantum systems. Without it, interesting violations of the laws of thermodynamics are possible and indeed generalisations to account for the scenario of initially correlated systems are explored in

Ref. [4] and references therein.

Note also that $\widetilde{\rho}(0) = \rho(0)$, so we may drop the tilde in the first term on the right hand side of (1.22). We may also assume that the first term on the right hand side evaluates to zero, $\mathrm{tr}_E\left[\widetilde{H}_I(t), \rho(0)\right] = 0$. This may done without loss of generality: This term contributes to the unitary part of the dynamics of the system state ρ_S and as such any non-zero value may always be subsumed into a redefinition of the interaction-free terms in the Hamiltonian (H_0). Equation (1.22) now reduces to

$$\frac{d}{dt}\widetilde{\rho}_S(t) = -\int_0^t ds\ \mathrm{tr}_E\left[\widetilde{H}_I(t), \left[\widetilde{H}_I(s), \widetilde{\rho}(s)\right]\right]. \tag{1.23}$$

So far we have manipulated Eq. (1.15) for the global state into Eq. (1.23) for the reduced state of the system. But this latter equation is no simpler to solve: it is still an integro-differential equation where the state of the system at any given time t is conditional on the states at all previous times as far back as time $t_0 = 0$. We would like to have a time local equation in which $\frac{d}{dt}\rho_S(t)$ depends only on $\rho_s(t)$ at one particular time t: an ordinary differential equation which is more tractable. To make progress, we will make some simplifications known collectively as the Born-Markov approximations. Under the Born approximation we assume that the global state of system and environment remains separable at all times:

$$\rho(t) \approx \rho_S(t) \otimes \rho_E(t) \quad \forall t. \tag{1.24}$$

This assumption will be valid under the condition that the interaction term H_I is sufficiently small in magnitude compared with H_S, i.e. we are restricted to the regime of weak coupling. Furthermore we will make the assumption that the environment is static and remains in its initial state $\rho_E(0)$. If ρ_E is much larger in dimensionality than ρ_S then any changes to ρ_E due to the interaction with the system are small and safely negligible on the scale of changes to ρ_S. We also make the assumption that we may safely neglect any possible correlations between the system and the environment, meaning that we write the global state of environment and system

as separable at all times. Of course, in reality we are aware that correlations will develop as a result of a non-zero interaction term. However, we expect these correlations to be of the order of the interaction term, which we already assume to be but a small perturbation. Neglecting correlations therefore is reflective of our weak coupling assumption. The same assumptions carry through to the interaction picture, since H_0 does not contain any coupling terms. No correlations between the system and environment can be established, therefore, through the operation $e^{iH_0t}\rho(t)e^{-iH_0t}$.

Equation (1.23) now simplifies somewhat to

$$\frac{d}{dt}\widetilde{\rho}_S(t) = -\int_0^t ds\ \mathrm{tr}_E\left[\widetilde{H}_I(t), \left[\widetilde{H}_I(s), \widetilde{\rho}_S(s)\otimes\rho_E\right]\right]. \tag{1.25}$$

We have approximated away any time dependence for the environment state on the right hand side as well as explicitly imposed a separability restriction. One might, already at this stage, be uncomfortable about the approximations we have made and what restrictions they imply for the validity of any dynamics computed once we tackle solving this equation. We are restricted to regimes where the coupling is negligibly weak and we shall have to make do with our inability, because of the separability restriction, to track any system-environmental correlations. Later, when we discuss our approach to tackling the strong coupling regime in section 2, we shall overcome some of these restrictions and have the ability to track system-environmental correlations.

However, for the time being, restricted as we already are, we are still facing in equ. 1.25 an integro-differential equation which is not local in time. The evolution of $\widetilde{\rho}_S(t)$ depends on its past history through the integration of $\widetilde{\rho}_S(s)$ over the time variable s between $s = 0$ and $s = t$. This is still hard to solve and therefore the next step is to make the Markov approximation with the goal of localising Eq. (1.25) in time. This constitutes in replacing $\widetilde{\rho}_S(s)$ with $\widetilde{\rho}_S(t)$ in the integrand, removing the reference to a particular time $t = 0$ by shifting $s \to t - \tau$ and taking

the integral to infinity, to give a Born-Markov master equation:

$$\frac{d}{dt}\widetilde{\rho}_S(t) = -\int_0^\infty d\tau \ \mathrm{tr}_E \left[\widetilde{H}_I(t), \left[\widetilde{H}_I(t-\tau), \widetilde{\rho}_S(t)\otimes\rho_E\right]\right]. \tag{1.26}$$

Equation (1.26) is now a Markovian ordinary differential equation because only the state ρ_S at time t appears on the right hand side and is not part of the integration over the variable τ. The shifting of the integral back to infinity (there is a swap in the limits because of the minus sign in $s = t - \tau$) removes any dependence on a particular starting time. We will now spend a little time discussing the circumstances in which such simplifications are justified. In order to do so we shall define environment self-correlation functions.

1.2.2 Environment self-correlation functions

In an exact treatment of the open system, we can imagine that the system state would be influenced by its historical states because, at earlier times, these will have imprinted themselves on the environment through the interaction term H_I. In other words, the interaction term allows a system state to alter the initial state of the environment. Then at some later time, this changed environment will produce some back action, via H_I again, on the system.

If the environment is large compared with the system size and relaxes to an equilibrium state rapidly compared with any dynamics of the system, then even if an earlier system state has left its mark on the environment, this will quickly get washed away as the environment returns to equilibrium before there is any chance of some back action on the system. In the case of treating thermodynamics from the perspective of open quantum systems theory, it is very often assumed that the environment is initially in a thermal equilibrium state with respect to H_E at time $t = 0$, $\rho_E(0) = \frac{\exp[-\beta H_E]}{\mathrm{tr}_E[\exp[-\beta H_E]]}$, where the inverse temperature is given by $\beta \equiv \frac{1}{k_B T}$. We imagine, if the environment is taken to be a heat reservoir, that it rapidly rethermalises to this same equilibrium state whenever it is forced out of equilibrium through interactions with the system.

Markovian behaviour is therefore justified from this physical argument. To quantify this a little more precisely we employ the self-correlation time of the environment τ_{corr} as a measure of how quickly it relaxes to equilibrium. Then in the case where $\tau_{corr} \ll \tau_S$, the time scale for system dynamics, the simplifications in the previous section are justifiable.

Let us write a general form of H_I in terms of operators acting on the system Hilbert space and operators acting on the environment Hilbert space as follows

$$H_I = \sum_\alpha A_\alpha \otimes B_\alpha. \tag{1.27}$$

In the interaction picture this becomes

$$\begin{aligned} \widetilde{H}_I(t) &= \sum_\alpha \exp\left[iH_S t\right] A_\alpha \exp\left[-iH_S t\right] \otimes \exp\left[iH_E t\right] B_\alpha \exp\left[-iH_E t\right] && (1.28) \\ &= \sum_\alpha \widetilde{A}_\alpha(t) \otimes \widetilde{B}_\alpha(t). && (1.29) \end{aligned}$$

The environment self-correlation functions over two times t and s are defined as

$$C_{\alpha\beta}(t,s) \equiv \langle \widetilde{B}_\alpha(t)\widetilde{B}_\beta(s)\rangle_E = \mathrm{tr}_E\left[\widetilde{B}_\alpha(t)\widetilde{B}_\beta(s)\rho_E\right]. \tag{1.30}$$

Now, as discussed above, ρ_E is a stationary state and therefore commutes with H_E. So when substituting in for $\tilde{B}_{\alpha/\beta}(t)$ from (1.28) we can use the cyclic properties of the trace to show that

$$C_{\alpha\beta}(t,s) = \mathrm{tr}_E\left[\widetilde{B}_\alpha(t-s)B_\beta\rho_E\right] = C_{\alpha\beta}(t-s). \tag{1.31}$$

The self-correlation functions depend only on the time difference $t-s$. τ_{corr} is then the timescale over which these functions decay to zero and if they do so much more quickly than the timescale over which the system evolves, then the Markovian approximation is justified.

1.2.3 General form of the Born-Markov master equation

We now rewrite equation (1.26) in terms of the correlation functions $C_{\alpha\beta}(t-s)$ to explicitly show how environmental timescales enter the dynamics of an open quantum system. Expanding the commutators in equation (1.26) and substituting in from equations (1.31) and (1.28) we obtain

$$\frac{d}{dt}\widetilde{\rho}_S(t) = -\sum_{\alpha\beta}\int_0^\infty d\tau \left\{ \left[\widetilde{A}_\alpha(t), \widetilde{A}_\beta(t-\tau)\widetilde{\rho}_S(t)\right] C_{\alpha\beta}(\tau) + \left[\widetilde{\rho}_S(t)\widetilde{A}_\beta(t-\tau), \widetilde{A}_\alpha(t)\right] C_{\beta\alpha}(-\tau)\right\}. \tag{1.32}$$

The properties of the environment enter through the self-correlation functions in the terms on the right hand side of (1.32). The Markov approximation is justified when these decay rapidly to zero on the timescale over which $\widetilde{\rho}_S(t)$ varies, τ_S. In the interaction picture, we have transformed away any rapid evolution of the system due to its self-Hamiltonian and we are left with what we assume to be slow evolution governed by a very small interaction term. The Markov approximation therefore is based on the assumption that this slow evolution is in stark contrast to the rapid dynamics of a very large reservoir reflected in self-correlation functions which decay rapidly to zero compared with the timescale over which any significant changes are observed in the system.

We may now transform back to the Schrödinger picture to give

$$\begin{aligned}\frac{d}{dt}\rho_S(t) &= -i\left[H_S, \rho_S(t)\right] + \exp\left[-iH_S t\right]\left(\frac{d}{dt}\tilde{\rho}_S(t)\right)\exp\left[iH_S t\right] \\ &= -i\left[H_S, \rho_S(t)\right] \\ &\quad -\sum_{\alpha\beta}\int_0^\infty d\tau \left\{ \left[A_\alpha, \widetilde{A}_\beta(-\tau)\rho_S(t)\right] C_{\alpha\beta}(\tau) + \left[\rho_S(t)\widetilde{A}_\beta(-\tau), A_\alpha\right] C_{\beta\alpha}(-\tau)\right\}.\end{aligned} \tag{1.33}$$

Equation (1.33) gives a general form for the Born-Markov master equation, the equation of motion for an open quantum system in the limit of weak system-environment coupling. We will now discuss some examples of specific microscopic models and derive the Born-Markov equations which apply in each case.

1.3 The damped harmonic oscillator

We will consider, in this section, the case of a harmonic oscillator as the open quantum system of interest. We begin with this example because a damped harmonic oscillator is a ubiquitous model in studies of decoherence and dissipation in open quantum systems [1, 2, 3, 5]. It forms the basis for the quantum version of Brownian motion studied through the seminal Caldeira-Leggett model [6], a semi-empirical model of a Brownian system moving in a harmonic potential while coupled to a bosonic environment.

For our purposes we will consider a system moving in one spatial dimension, confined in a harmonic potential, linearly coupled to an environment which consists of a very large number of non-interacting harmonic oscillators maintained in thermal equilibrium at a particular temperature.

We will proceed now by deriving a master equation which relies on Born-Markov approximations and is therefore subject to weak coupling restrictions as discussed in section 1.2. Ultimately we will extend our treatment beyond weak coupling in sections to follow, employing the present treatment as a benchmark to ensure that our strong coupling treatment is also capable of reproducing well-established weak coupling results.

1.3.1 Born-Markov master equation for a quantum harmonic oscillator

A derivation of the Born-Markov master equation for a damped harmonic oscillator can be found in most good open quantum systems textbooks. Our derivation leans most heavily on that presented in Ref. [3] where the model is studied in the context of the decoherence of open quantum systems. Once again we begin with a global Hamiltonian of the form of equation (1.16), partitioned into a term describing the self-energy of the system S, a term for the self-energy of the environment E and an interaction term which couples the system with the environment. The environment self-energy is given by the sum of the self-energies of k harmonic oscillators

which do not interact with each other

$$H_E \equiv \sum_k \frac{1}{2}\left(P_k^2 + \omega_k^2 Q_k^2\right), \tag{1.34}$$

where P_k and Q_k are momentum and position operators, respectively, for the k^{th} environment oscillator. These obey canonical position-momentum commutation relations. The self-energy of the system oscillator of interest, written in terms of position x and momentum p, is given by

$$H_S = \frac{1}{2}\left(p^2 + \omega_0^2 x^2\right), \tag{1.35}$$

where ω_0 is the natural frequency of our system S.

We model the interaction between the system and the environment oscillators as linear in both the system position coordinate x and the coordinates Q_k, commonly referred to as bilinear coupling,

$$H_I = x \sum_k g_k Q_k, \tag{1.36}$$

where the g_k represent coupling constants for each interacting environmental oscillator.

We may write equation (1.36) in the form of equation (1.27) by making the definitions

$$A \equiv x \tag{1.37}$$

$$B \equiv \sum_k g_k Q_k. \tag{1.38}$$

The environment self-correlation function is then given by

$$C(\tau) = \mathrm{tr}_E\left[\tilde{B}(\tau) B \rho_E\right] = \sum_{kl} g_k g_l \ \mathrm{tr}_E\left[\tilde{Q}_k(\tau) Q_l \rho_E\right] = \sum_k g_k^2 \ \mathrm{tr}_E\left[\tilde{Q}_k(\tau) Q_k \rho_E\right], \tag{1.39}$$

We can simplify these expressions by rewriting the position operators for the environment in second quantised form

$$Q_k = \sqrt{\frac{1}{2\omega_k}}\left(a_k + a_k^\dagger\right), \tag{1.40}$$

where a_k and $a_k^\dagger$ are ladder operators for the k^{th} environment oscillator, satisfying the usual bosonic commutation relations. In the interaction picture this becomes

$$\tilde{Q}_k(\tau) = e^{iH_E\tau}Q_k e^{-iH_E\tau} = \sqrt{\frac{1}{2\omega_k}}\left(a_k e^{-i\omega_k\tau} + a_k^\dagger e^{i\omega_k\tau}\right). \tag{1.41}$$

We now substitute in for Q_k and evaluate the trace in equation (1.39) as follows

$$\begin{aligned}
\mathrm{tr}_E\left[\tilde{Q}_k(\tau)Q_k\rho_E\right] &= \frac{1}{2\omega_k}\left[\mathrm{tr}_E\left(a_k a_k^\dagger\rho_E\right)e^{-i\omega_k\tau} + \mathrm{tr}_E\left(a_k^\dagger a_k\rho_E\right)e^{i\omega_k\tau}\right] \\
&= \frac{1}{2\omega_k}\left\{\left[1+\mathrm{tr}_E\left(a_k^\dagger a_k\rho_E\right)\right]e^{-i\omega_k\tau} + \mathrm{tr}_E\left(a_k^\dagger a_k\rho_E\right)e^{i\omega_k\tau}\right\} \\
&= \frac{1}{2\omega_k}\left\{\left[1+N\left(\omega_k,T\right)\right]e^{-i\omega_k\tau} + N\left(\omega_k,T\right)e^{i\omega_k\tau}\right\} \\
&= \frac{1}{2\omega_k}\left\{\left[1+2N\left(\omega_k,T\right)\right]\cos\left(\omega_k\tau\right) - i\sin\left(\omega_k\tau\right)\right\} \\
&= \frac{1}{2\omega_k}\left\{\coth\left(\frac{\beta\omega_k}{2}\right)\cos\left(\omega_k\tau\right) - i\sin\left(\omega_k\tau\right)\right\}.
\end{aligned} \tag{1.42}$$

In the second line we have made use of the bosonic commutation relation $\left[a_k, a_k^\dagger\right] = 1$. In the third line we use the fact that the environment is in a thermal Gibbs state at temperature T, $\rho_E = \frac{1}{Z}e^{-\beta\omega_k a_k^\dagger a_k}$ with $Z \equiv \mathrm{tr}_E\left[\exp\left[-\beta\omega_k a_k^\dagger a_k\right]\right]$, giving $\mathrm{tr}_E\left(a_k^\dagger a_k\rho_E\right) = \left(e^{\beta\omega_k}-1\right)^{-1} \equiv N(\omega_k,T)$, with $\beta = \frac{1}{k_B T}$. The environment self-correlation function, in equation (1.39) is therefore given by

$$C\left(\tau\right) = \sum_k \frac{g_k^2}{2\omega_k}\left\{\coth\left(\frac{\beta\omega_k}{2}\right)\cos\left(\omega_k\tau\right) - i\sin\left(\omega_k\tau\right)\right\}. \tag{1.43}$$

It is common to define the noise kernel and dissipation kernel, $\nu\left(\tau\right)$ and $\eta\left(\tau\right)$ respectively, as follows

$$\nu\left(\tau\right) \equiv \sum_k \frac{g_k^2}{2\omega_k}\coth\left(\frac{\beta\omega_k}{2}\right)\cos\left(\omega_k\tau\right) = \int_0^\infty d\omega\frac{J\left(\omega\right)}{2\omega}\coth\left(\frac{\beta\omega}{2}\right)\cos\left(\omega\tau\right), \tag{1.44}$$

$$\eta\left(\tau\right) \equiv \sum_k \frac{g_k^2}{2\omega_k}\sin\left(\omega_k\tau\right) = \int_0^\infty d\omega\frac{J\left(\omega\right)}{2\omega}\sin\left(\omega_k\tau\right). \tag{1.45}$$

In equations (1.44) and (1.45), we have introduced the spectral density of the environment

$$J(\omega) \equiv \sum_k g_k^2 \delta(\omega - \omega_k), \tag{1.46}$$

characterising the environment density of states weighted by the strength of the system-environment coupling at each environment oscillator frequency. We also take the continuum limit for the environment replacing the sum over individual discrete oscillator frequencies ω_k by an integral over a continuous spectrum ω. The environment self-correlation function may then be written more concisely as

$$C(\tau) = \nu(\tau) - i\eta(\tau). \tag{1.47}$$

We may now substitute $C(\tau)$ from equation (1.47) and the system operator A from equation (1.37) into equation (1.33) and write down the following general expression for the master equation for a damped harmonic oscillator

$$\frac{d}{dt}\rho_S(t) = -i[H_S, \rho_S(t)] - \int_0^\infty d\tau \{\nu(\tau)[x, [\tilde{x}(-\tau)\rho_S(t)]] - i\eta(\tau)[x, \{\tilde{x}(-\tau), \rho_S(t)\}]\}. \tag{1.48}$$

The first term on the right hand side of equation (1.48) represents the unitary (dissipation-less) part of the evolution of the system oscillator. Environment induced decoherence and dissipation are described by the integrals over the noise and dissipation kernels in the second and third terms.

Using equation (1.35), we can evaluate the specific form of the interaction picture position operator appearing in equation (1.48) as

$$\tilde{x}(\tau) = e^{iH_S\tau} x e^{-iH_S\tau} = x\cos(\omega_0\tau) + \frac{1}{\omega_0} p\sin(\omega_0\tau), \tag{1.49}$$

where in the last step we have solved the Heisenberg equations of motion with respect to $H_0 = H_S + H_E$ for the system position and momentum operators. Substituting for $\tilde{x}(\tau)$ from equation (1.49) into equation (1.48), and after some algebraic manipulations, we obtain the

most common form of the Born-Markov master equation for a damped harmonic oscillator:

$$\frac{d}{dt}\rho_S(t) = -i\left[H_S + \frac{1}{2}\tilde{\omega}_0 x^2, \rho_S(t)\right] - i\gamma\left[x, \{p, \rho_S(t)\}\right] - D\left[x, [x, \rho_S(t)]\right] - f\left[x, [p, \rho_S(t)]\right]. \quad (1.50)$$

In equation (1.50) we have made the following definitions:

$$\tilde{\omega}_0^2 \equiv -2\int_0^\infty d\tau \eta(\tau, T)\cos(\omega_0\tau), \quad (1.51)$$

$$\gamma \equiv \frac{1}{\omega_0}\int_0^\infty d\tau \eta(\tau, T)\sin(\omega_0\tau), \quad (1.52)$$

$$D \equiv \int_0^\infty d\tau \nu(\tau, T)\cos(\omega_0\tau), \quad (1.53)$$

$$f \equiv -\frac{1}{\omega_0}\int_0^\infty d\tau \nu(\tau, T)\sin(\omega_0\tau). \quad (1.54)$$

The first term in equation (1.50) represents the unitary dynamics of a harmonic oscillator with natural frequency $\left(\omega_0^2 + \tilde{\omega}_0^2\right)^{\frac{1}{2}}$. This, then, is the first consequence of note of the interaction with the environment: it introduces a shift to the natural frequency of the oscillator of interest, commonly known as the Lamb Shift. The second term is responsible for momentum damping (dissipation) with rate proportional to γ. The remaining terms cause decoherence in the position basis at rates proportional to normal and anomalous diffusion coefficients D and f.

1.4 The spin-boson model

In section 1.3 we derived the weak coupling Born-Markov master equation for a damped harmonic oscillator as this quantum system is ubiquitous in generic models of open quantum systems. Another common starting point for modelling the dynamics of open quantum systems is to consider a quantum system restricted to two energy levels, interacting with a bath of bosonic modes. This model is known as the spin-boson model and is, in its own right, a paradigmatic model in the study of dissipation in open quantum systems [7, 8]. We will derive the weak

coupling master equation describing the dynamics of the spin of interest forthwith.

1.4.1 Born-Markov master equation for a two-level system

We begin by writing down the Hamiltonian for the spin-boson model:

$$H = \frac{\epsilon}{2}\sigma_z + \frac{\Delta}{2}\sigma_x + \sigma_z \sum_k g_k \left(b_k^\dagger + b_k\right) + \sum_k \omega_k b_k^\dagger b_k, \tag{1.55}$$

where σ_x and σ_z are the usual Pauli spin operators and $b_k^\dagger$ (b_k) are creation (annihilation) operators for each independent environment oscillator, satisfying bosonic commutation relations. We make the identification $H_S \equiv \frac{\epsilon}{2}\sigma_z + \frac{\Delta}{2}\sigma_x$ and $H_E \equiv \sum_k \omega_k b_k^\dagger b_k$, representing the self-energy of the spin and the bosonic environment respectively. ϵ is referred to as the bias and Δ the tunnelling. This terminology stems from this model being used to represent a double well potential truncated to lowest quantum state in each well. The bias is the energy splitting between each single quantum level contained in each potential well and the tunnelling mediates intrinsic (non-environmentally induced) transitions between these two levels. ω_k represents the natural frequency of each k environment oscillator. The remaining term is the interaction H_I with the coupling parameters given by g_k. We now proceed with the derivation of a weak coupling master equation for the dynamics of the spin, valid to second order in these coupling parameters. The steps are in line with those taken above for the damped oscillator so we will proceed more briskly.

The first step is to find the interaction picture version of the interaction term in equation (1.55), which yields (dropping the tildes and indicating the interaction picture by time dependence on operators)

$$\begin{aligned} H_I(t) &= e^{iH_S t}\sigma_z e^{-iH_S t} e^{iH_E t} \sum_k g_k \left(b_k^\dagger + b_k\right) e^{-iH_E t} \\ &= \sigma_z(t) \sum_k g_k \left(b_k^\dagger e^{i\omega_k t} + b_k e^{-i\omega_k t}\right), \end{aligned} \tag{1.56}$$

where

$$\sigma_z(t) = \frac{1}{\mu^2}\left[\left(\epsilon^2 + \Delta^2\cos(\mu t)\right)\sigma_z + \Delta\epsilon\left(1-\cos(\mu t)\right)\sigma_x + \Delta\mu\sin(\mu t)\sigma_y\right], \tag{1.57}$$

and

$$\mu = \sqrt{\epsilon^2+\Delta^2}. \tag{1.58}$$

We now substitute for H_I from equation (1.56) into equation (1.25) to yield

$$\begin{aligned}\frac{d}{dt}\widetilde{\rho}_S(t) = &- \sum_{k,k'}\int_0^t ds\left(\sigma_z(t)\sigma_z(s)\widetilde{\rho}_S(t) - \sigma_z(s)\widetilde{\rho}_S(t)\sigma_z(t)\right)\mathrm{tr}_E B_1\rho_E \\ &- \sum_{k,k'}\int_0^t ds\left(\widetilde{\rho}_S(t)\sigma_z(s)\sigma_z(t) - \sigma_z(t)\widetilde{\rho}_S(t)\sigma_z(s)\right)\mathrm{tr}_E B_2\rho_E. \end{aligned}\tag{1.59}$$

Here we have replaced $s \to t$ in $\widetilde{\rho}_S(s)$ in line with the Markov approximation. B_1 and B_2 are given by

$$B_1 = g_k\left(b_k^\dagger e^{i\omega_k t} + b_k e^{-i\omega_k t}\right)g_{k'}\left(b_{k'}^\dagger e^{i\omega_{k'} s} + b_{k'}e^{-i\omega_{k'}s}\right). \tag{1.60}$$

$$B_2 = g_{k'}\left(b_{k'}^\dagger e^{i\omega_{k'} s} + b_{k'}e^{-i\omega_{k'}s}\right)g_k\left(b_k^\dagger e^{i\omega_k t} + b_k e^{-i\omega_k t}\right). \tag{1.61}$$

Let us assume the environment is a thermal equilibrium state $\rho_E = \sum_k \frac{e^{-\beta H_E}}{(1-e^{-\beta\omega_k})^{-1}}$. Performing the trace over the environmental degrees of freedom, taking the continuum limit for the k environment oscillators, and a little algebraic manipulation yields the environment self-correlation function:

$$C_1(t-s) = \mathrm{Tr}_E[B_1\rho_E] = \int_0^\infty d\omega J(\omega)\cos\omega(t-s)\coth\frac{\beta\omega}{2}, \tag{1.62}$$

$$C_2(t-s) = \mathrm{Tr}_E[B_2\rho_E] = \int_0^\infty d\omega J(\omega) i\sin\omega(t-s), \tag{1.63}$$

where $J(\omega)$ is the spectral density and the inverse temperature is $\beta = \frac{1}{k_B T}$. Substituting back into equation (1.59) we can write down the interaction picture master equation

$$\frac{d}{dt}\widetilde{\rho}_S(t) = -\int_0^t ds\left(\nu(t-s)\left[\sigma_z(t),\left[\sigma_z(s),\widetilde{\rho}_S(t)\right]\right] - i\eta(t-s)\left[\sigma_z(t),\left\{\sigma_z(s),\widetilde{\rho}_S(t)\right\}\right]\right), \tag{1.64}$$

where curly brackets $\{,\}$ denote the anti-commutator and

$$\nu(t-s) = \int_0^\infty d\omega J(\omega)\cos\omega(t-s)\coth\frac{\beta\omega}{2}, \tag{1.65}$$

$$\eta(t-s) = \int_0^\infty d\omega J(\omega)\sin\omega(t-s). \tag{1.66}$$

We may now transform equation (1.59) back into the Schrödinger picture. To do this, we make use of the definition of the interaction picture density operator, rearrange and then differentiate with respect to time to give

$$\begin{aligned}\rho_S(t) &= e^{-i(H_S+H_E)t}\widetilde{\rho}_S(t)e^{i(H_S+H_E)t},\\ \frac{d}{dt}\rho_S(t) &= -i[H_S,\rho_S(t)] + e^{-i(H_S+H_E)t}\frac{d}{dt}\widetilde{\rho}_S(t)e^{i(H_S+H_E)t}.\end{aligned} \tag{1.67}$$

Noting that

$$e^{-iH_St}\frac{d}{dt}\sigma_z(t)e^{iH_St} = \sigma_z, \tag{1.68}$$

and

$$e^{-i(H_S+H_E)t}\sigma(s)e^{i(H_S+H_E)t} = \sigma(t-s), \tag{1.69}$$

we can substitute $\frac{d}{dt}\widetilde{\rho}_S(t)$ from equation (1.64) into equation (1.67) to yield

$$\frac{d}{dt}\rho_S(t) = -i[H_S,\rho_S(t)] - \int_0^t d\tau\left(\nu(\tau)\left[\sigma_z,[\sigma_z(-\tau),\widetilde{\rho}_S(t)]\right] - i\eta(\tau)\left[\sigma_z,\{\sigma_z(-\tau),\widetilde{\rho}_S(t)\}\right]\right). \tag{1.70}$$

Here, we have changed the integration variable $t-s\rightarrow\tau$. Omitting much unenlightening algebraic manipulation, substituting in for H_S and $\sigma_z(t)$ yields the following full version of the Schrödinger picture master equation for the spin-boson model

$$\begin{aligned}\frac{d}{dt}\rho_S(t) = &- i\left[\frac{\epsilon}{2}\sigma_z + \left(\frac{\Delta}{2}+\Gamma_2(t)\right)\sigma_x + \Gamma_1(t)\sigma_y,\rho_s(t)\right] - D(t)\left[\sigma_z,[\sigma_z,\rho_S(t)]\right]\\ &+ \left(\Gamma_1(t)-i\kappa_1(t)\right)\sigma_x\rho_S(t)\sigma_z + \left(\Gamma_1(t)+i\kappa_1(t)\right)\sigma_z\rho_S(t)\sigma_x\\ &- \left(\Gamma_2(t)-i\kappa_2(t)\right)\sigma_y\rho_S(t)\sigma_z - \left(\Gamma_2(t)+i\kappa_2(t)\right)\sigma_z\rho_S(t)\sigma_y\\ &- \kappa_1(t)\{\sigma_y,\rho_S(t)\} - \kappa_2(t)\{\sigma_x,\rho_S(t)\},\end{aligned} \tag{1.71}$$

where we have made the following definitions

$$D(t) = \frac{1}{\mu^2}\int_0^t d\tau\nu(\tau)\left(\epsilon^2+\Delta^2\cos(\mu\tau)\right), \tag{1.72}$$

$$\Gamma_1(t) = \frac{\Delta\epsilon}{\mu^2}\int_0^t d\tau\nu(\tau)\left(1-\cos(\mu\tau)\right), \tag{1.73}$$

$$\Gamma_2(t) = \frac{\Delta}{\mu}\int_0^t d\tau\nu(\tau)\sin(\mu\tau), \tag{1.74}$$

$$\kappa_1(t) = \frac{\Delta\epsilon}{\mu^2}\int_0^t d\tau\eta(\tau)\left(1-\cos(\mu\tau)\right), \tag{1.75}$$

$$\kappa_2(t) = \frac{\Delta}{\mu}\int_0^t d\tau\eta(\tau)\sin(\mu\tau). \tag{1.76}$$

Solving equation (1.71) and evaluating the integrals in equations (1.72 - 1.76) often requires resorting to numerical techniques, although in certain circumstances analytical solutions are obtainable. One such situation is when the bias is set to zero, $\epsilon \to 0$. This situation is often treated in good open quantum systems textbooks, for example in Ref. [3]. We will focus, in the next section, on another simplified version of the model which is analytically solvable, because we shall later draw on this as a benchmark against which to compare the reaction coordinate technique for strongly coupled open quantum systems.

1.4.2 An exactly solvable model: the independent boson model

We consider, in this section, a simplified version of the spin-boson model with Hamiltonian differing from that of equation (1.55) only in the absence of a tunnelling term. Setting $\Delta \to 0$ allows for an exact analytic solution for the reduced dynamics of the spin.

Let us begin by defining the unitary operator $V_P \equiv e^S$, where $S \equiv \sigma_z \sum_k \frac{g_k}{\omega_k}\left(b_k^\dagger - b_k\right)$. We note that, with $|\psi\rangle_P = V_P|\psi\rangle$ and $H_P = V_P H V_P^\dagger$, the Schrodinger equation in this new frame is written as one expects:

$$i\partial_t|\psi\rangle_P = H_P|\psi\rangle_P. \tag{1.77}$$

The formal solution to equation (1.77) is

$$|\psi(t)\rangle_P = U_P(t)|\psi(0)\rangle_P, \tag{1.78}$$

where the time-evolution operator is given by

$$U_P(t) = e^{-iH_P t}. \tag{1.79}$$

The astute reader may recognise the operator V_P as one which shifts the position of each oscillator in the environment. The presence of the spin space σ_z operator in the exponent ensures this shift is spin state-dependent: for the spin in the excited state, the shift is positive, and for the ground state it is negative. This collective excitation of the lattice, in microscopic models employed in branches of solid state physics, is called a polaron. Hence our usage of the subscript label P. We will refer to the frame defined by the transformation V_P as the polaron frame.

It is a straightforward task, making use of the Hadamard Lemma, to evaluate H_P and $U_P(t)$ in the polaron frame, yielding

$$H_P = \frac{\epsilon}{2}\sigma_z + \sum_k \omega_k b_k^\dagger b_k - \sum_k \frac{g_k^2}{\omega_k}, \tag{1.80}$$

$$U_P(t) = e^{-i\frac{\epsilon}{2}\sigma_z t} e^{-i\sum_k \omega_k b_k^\dagger b_k t} e^{i\sum_k \frac{g_k^2}{\omega_k} t}. \tag{1.81}$$

We notice that the polaron transformation reduces the interaction term in H_P to a scalar and that this is what enables us to write down an analytic solution to the Schrödinger equation in the polaron frame. Making the definitions

$$H_0 \equiv \frac{\epsilon}{2}\sigma_z + \sum_k \omega_k b_k^\dagger b_k, \tag{1.82}$$

$$H_1 \equiv \sigma_z \sum_k g_k \left(b_k^\dagger + b_k\right), \tag{1.83}$$

we move into the interaction picture with respect to H_0 and seek an expression for the time

evolution operator in the original frame:

$$\tilde{U}(t) \equiv e^{iH_0t}U(t) = e^{iH_0t}e^{-S}U_P(t)e^{S}. \tag{1.84}$$

Introducing the identity, $I = e^{-iH_0t}e^{iH_0t}$, this expression may be evaluated piecewise as follows:

$$\begin{aligned} e^{iH_0t}e^{-S}e^{-iH_0t} &= \exp\left[e^{iH_0t}\left[-\sigma_z\sum_k\frac{g_k}{\omega_k}\left(b_k^\dagger - b_k\right)\right]e^{-iH_0t}\right] \\ &= \exp\left[-\sigma_z\sum_k\frac{g_k}{\omega_k}e^{iH_0t}\left(b_k^\dagger - b_k\right)e^{-iH_0t}\right] \\ &= \exp\left[-\sigma_z\sum_k\frac{g_k}{\omega_k}\left(b_k^\dagger e^{i\omega_k t} - b_k e^{-i\omega_k t}\right)\right]. \end{aligned} \tag{1.85}$$

Noting that $e^{iH_0t}U_P(t) = e^{i\sum_k\frac{g_k^2}{\omega_k}t}$, we are left with

$$\tilde{U}(t) = e^{i\sum_k\frac{g_k^2}{\omega_k}t}\exp\left[-\sigma_z\sum_k\frac{g_k}{\omega_k}\left(b_k^\dagger e^{i\omega_k t} - b_k e^{-i\omega_k t}\right)\right]\exp\left[\sigma_z\sum_k\frac{g_k}{\omega_k}\left(b_k^\dagger - b_k\right)\right]. \tag{1.86}$$

Making use of the Baker-Campbell-Hausdorff formula to combine exponents and evaluating the relevant commutators yields

$$\tilde{U}(t) = e^{i\sum_k\frac{g_k^2}{\omega_k}t}e^{-i\sum_k\frac{g_k^2}{\omega_k^2}\sin(\omega_k t)}e^{\sigma_z\sum_k\frac{g_k}{\omega_k}\left(b_k^\dagger\left(1-e^{i\omega_k t}\right)-b_k\left(1-e^{-i\omega_k t}\right)\right)}, \tag{1.87}$$

which we may write more succinctly as

$$\tilde{U}(t) = e^{-i\phi(t)}e^{\sigma_z\sum_k\left[\alpha_k(t)b_k^\dagger-\alpha_k^*(t)b_k\right]}, \tag{1.88}$$

where $\phi(t) = \sum\frac{g_k^2}{\omega_k^2}\sin(\omega_k t)$ and $\alpha_k(t) = \frac{g_k}{\omega_k}\left(1-e^{i\omega_k t}\right)$. We shall drop the time arguments for

these functions in what follows to make expressions less cumbersome. Finally we note that,

$$\begin{aligned}\exp\left[\sigma_z\sum_k \alpha_k b_k^\dagger - \alpha_k^* b_k\right] &= I\cosh\left(\sum_k \alpha_k b_k^\dagger - \alpha_k^* b_k\right) + \sigma_z \sinh\left(\sum_k \alpha_k b_k^\dagger - \alpha_k^* b_k\right)\\ &= I\frac{1}{2}\left(\prod_k D(\alpha_k) + \prod_k D(-\alpha_k)\right) + \sigma_z\frac{1}{2}\left(\prod_k D(\alpha_k) - \prod_k D(-\alpha_k)\right)\\ &= |0\rangle\langle 0|\prod_k D(\alpha_k) + |1\rangle\langle 1|\prod_k D(-\alpha_k), \end{aligned} \tag{1.89}$$

where the displacement operator is given by $D(\alpha_k) \equiv \exp\left[\alpha_k b_k^\dagger - \alpha_k^* b_k\right]$. The interaction picture time-evolution operator is therefore given by

$$\tilde{U}(t) = e^{-i\phi}\left(|0\rangle\langle 0|\prod_k D\left(\alpha_k\right) + |1\rangle\langle 1|\prod_k D\left(-\alpha_k\right)\right). \tag{1.90}$$

Let us, as usual, consider an initial state of the form

$$\rho(0) = \rho_S(0)\otimes\rho_B, \tag{1.91}$$

with $\rho_B = \frac{e^{-\beta H_B}}{Z_B}$, a thermal state of the environment with respect to H_B for some given inverse temperature β, with $Z_B = \mathrm{tr}\left(e^{-\beta H_B}\right)$. The matrix elements of the reduced state on the spin, in the interaction picture, are given by

$$\tilde{\rho}_{ij}(t) = \langle i|\mathrm{Tr}_B\left[\tilde{U}\rho(0)\tilde{U}^\dagger\right]|j\rangle, \tag{1.92}$$

where $i, j = 0, 1$. As expected for an interaction term which is diagonal in the spin energy basis, the excited and ground state populations remain constant:

$$\begin{aligned}\tilde{\rho}_{00}(t) &= \langle 0|\mathrm{Tr}_B\left[\tilde{U}\rho(0)\tilde{U}^\dagger\right]|0\rangle\\ &= \langle 0|\rho_S(0)|0\rangle\mathrm{Tr}_B\left[\prod_k D\left(\alpha_k\right)\rho_B\prod_k D^\dagger\left(\alpha_k\right)\right]\\ &= \rho_{00}(0), \end{aligned} \tag{1.93}$$

and similarly,

$$\begin{aligned}\tilde{\rho}_{11}(t) &= \langle 1|\mathrm{Tr}_B\left[\tilde{U}\rho(0)\tilde{U}^\dagger\right]|1\rangle \\ &= \langle 1|\rho_S(0)|1\rangle \mathrm{Tr}_B\left[\prod_k D\left(-\alpha_k\right)\rho_B\prod_k D^\dagger\left(-\alpha_k\right)\right] \\ &= \rho_{11}(0). \end{aligned} \tag{1.94}$$

These equations make the spin state-dependent shift of the oscillator environment explicit. The coherences evolve according to

$$\begin{aligned}\tilde{\rho}_{01}(t) &= \rho_{01}(0)\mathrm{Tr}_B\left[\prod_k D\left(\alpha_k\right)\rho_B\prod_k D^\dagger\left(-\alpha_k\right)\right] \\ &= \rho_{01}(0)\mathrm{Tr}_B\left[\prod_k D\left(2\alpha_k\right)\rho_B\right]. \end{aligned} \tag{1.95}$$

This enables us to define a decoherence function $\Gamma(t)$ as

$$\tilde{\rho}_{01}(t) = \rho_{01}(0)e^{\Gamma(t)}, \tag{1.96}$$

where $\Gamma(t) = \ln \mathrm{Tr}_B\left[e^{\sum_k 2\alpha_k b_k^\dagger - 2\alpha_k^* b_k}\rho_B\right] = \sum_k \ln\left\langle e^{2\alpha_k b_k^\dagger - 2\alpha_k^* b_k}\right\rangle$, with the angular brackets denoting the expectation value with a thermal state of the environment with respect to H_B. Noticing that the expression inside angular brackets is the Wigner characteristic function for the bath mode k, and that it is a Gaussian function, we may write

$$\left\langle e^{2\alpha_k b_k^\dagger - 2\alpha_k^* b_k}\right\rangle = e^{-\frac{1}{2}|2\alpha_k|^2\left\langle\left\{b_k, b_k^\dagger\right\}\right\rangle}. \tag{1.97}$$

The expectation value of the anticommutator can readily be evaluated to $\coth\left(\frac{\omega_k}{2k_BT}\right)$ and the pre-factor to $-4\frac{|g_k|^2}{\omega_k^2}\left(1-\cos\omega_k t\right)$. The decoherence function may therefore finally be written in the form

$$\Gamma(t) = -\sum_k \frac{4|g_k|^2}{\omega_k^2}\coth\left(\frac{\omega_k}{2k_BT}\right)\left(1-\cos\omega_k t\right). \tag{1.98}$$

In terms of the spectral density $J(\omega)$ the decoherence function may be written as:

$$\Gamma(t) = -\int_0^\infty d\omega 4\frac{J(\omega)}{\omega^2}\coth\left(\frac{\omega}{2k_BT}\right)(1-\cos\omega t)\,. \tag{1.99}$$

We may now move back into the Schrödinger picture with the time evolution of the reduced state on the spin fully determined as

$$\begin{aligned}\rho_S(t) &= e^{-i\frac{\epsilon}{2}\sigma_z t}\tilde{\rho}_S(t)e^{i\frac{\epsilon}{2}\sigma_z t}\\ &= \begin{pmatrix} e^{-i\frac{\epsilon}{2}t} & 0\\ 0 & e^{i\frac{\epsilon}{2}t}\end{pmatrix}\begin{pmatrix}\rho_{00}(0) & \rho_{01}(0)e^{\Gamma(t)}\\ \rho_{10}(0)e^{\Gamma(t)} & \rho_{11}(0)\end{pmatrix}\begin{pmatrix} e^{i\frac{\epsilon}{2}t} & 0\\ 0 & e^{-i\frac{\epsilon}{2}t}\end{pmatrix}\\ &= \begin{pmatrix}\rho_{00}(0) & \rho_{01}(0)e^{\Gamma(t)}e^{-i\epsilon t}\\ \rho_{10}(0)e^{\Gamma(t)}e^{i\epsilon t} & \rho_{11}(0)\end{pmatrix}.\end{aligned} \tag{1.100}$$

Equation (1.100) gives us the exact time evolution of each element of the density operator for the TLS in the independent boson model.

We finish this section by noting that equation (1.100), obtained here from a manipulation of the Hamiltonian and via the Schödinger equation, is equivalent to setting $\Delta \to 0$ in the spin-boson master equation derived in the previous section, equ. (1.71), to obtain

$$\frac{d}{dt}\rho_S(t) = -i\left[\frac{\epsilon}{2}\sigma_z, \rho_s(t)\right] - D^{\Delta\to 0}(t)\left[\sigma_z,[\sigma_z,\rho_S(t)]\right]. \tag{1.101}$$

This form of the master equation, second order in coupling parameter $g(\omega)$, is exact in the environment oscillator continuum limit, therefore, in the case of zero tunnelling.

Chapter 2

The Reaction Coordinate formalism for strong system-reservoir coupling

With the exception of the exactly solvable model seen in section (1.4.2), we have, thus far, been dealing with the dynamics of open quantum systems under restrictions imposed by our inability to solve integro-differential equations of the form of equation (1.23). By imposing the simplifications collectively known as the Born-Markov approximations, we are restricted to situations where the open quantum system is only weakly coupled to its environment. Concretely, this means that the term responsible for the interaction in the global Hamiltonian is much smaller than the term representing the energy of the free open system of interest. This weak coupling theory can therefore only describe situations where the environment remains static, correlations between the system and environment never build up, and there is no feedback from the environment based on any changes the interaction with the system may have brought about. Circumstances where the environment is dragged out of equilibrium, where the system and environment become entangled and where excitations emitted into the environment may in turn act back on the system cannot be captured by weak coupling theory.

How to solve for the dynamics of open systems when these restrictions are relaxed is an active field of research. The polaron transformation, which we met in section (1.4.2) has been used

in conjunction with variational techniques to obtain the dynamics for open quantum systems at strong coupling, particularly in the context of quantum dots embedded within a phonon lattice [9]. Numerical techniques, such as the hierarchical equations of motion, can be used to evaluate the dynamics of the open system observables, given suitable computing power [10, 11]. But these fail to capture any environmental dynamics and cannot track system-environment correlations. Here we will focus on the reaction coordinate formalism, which also involves a unitary transformation of the global Hamiltonian and permits the study of open quantum systems beyond weak coupling approximations. Our primary motivation for focusing on this technique is its ability to retain some information about the environment and any correlations between it and the system. Later, we will put the technique to use in the field of quantum thermodynamics where system-environment correlations and non-equilibrium environmental dynamics is proving to be an active and exciting avenue of research. The formalism is reviewed in Ref. [12], has been discussed in the general context of open quantum systems in Refs. [13, 14] and applied to problems in thermodynamics in Refs [15, 16, 17]. We shall discuss the features of this formalism in this chapter and, in sections 2.1 and 2.2, we shall derive, in detail, master equations capable of treating the damped harmonic oscillator and spin-boson model at strong system-reservoir coupling. We shall see how these reaction coordinate master equations not only capture system dynamics accurately but also enable one to keep track of system-environment correlations.

The RC formalism is pictured conceptually in figure 2.1. The scenario depicted is that of a quantum system S which is coupled to an environment consisting of k independent harmonic oscillators. We shall focus on how the formalism functions for this type of bosonic environment. However, the formalism has also been applied to fermionic environments, details of which may be found in Refs. [12, 17]. This star shaped configuration of a quantum system linearly interacting with an environment of bosons is mapped to an enlarged system S' which interacts linearly with an altered environment of bosons E'. The enlarged system S' comprises the original quantum system Hamiltonian as well as a collective degree of freedom from the environment, the RC, and a coupling term between S and the RC. It is then only the RC which is coupled to the residual environment E'. The purpose of this transformation is to enable the use of the Born-Markov

master equation formalism to treat the enlarged system S' as the new open system of interest. In the original picture, the coupling is considered to be too strong to validate a Born-Markov approach, whereas, under the mapping, one incorporates the strong coupling within the enlarged system and leaves only weak coupling terms between the RC and the environment.

Denoting the original environment annihilation operators a_k, one can perform this mapping through a series of Bogoliubov transformations such that

$$a_k = u_{k1} b_1 + v_{k1} b_1^\dagger + \sum_{q>1} u_{kq} b_q + \sum_{q>1} v_{kq} b_q^\dagger. \tag{2.1}$$

The first two terms represent the RC mode and the remaining sums representing the mapped residual environment E'. In general, the preservation of bosonic commutation relations requires that the matrices U and V formed by the complex coefficients u_{kq} and v_{kq}, $U = (u_{kq})$ and $V = (v_{kq})$, must obey $UU^\dagger + VV^\dagger = \mathbf{0}$ and $UV^T + VU^T = \mathbf{0}$. Further conditions are then implied by our restriction for the type of interactions we wish to be present in the mapped picture.

We require that an original Hamiltonian of the form

$$H = H_S + A \sum_k (g_k a_k + g_k^* a_k^\dagger) + \sum_k \omega_k a_k^\dagger a_k, \tag{2.2}$$

where A is an operator acting on the Hilbert space of the system S, be transformed into a Hamiltonian of the form

$$H = H_S + \lambda A (b_1 + b_1^\dagger) + \Omega_1 b_1^\dagger b_1 + (b_1 + b_1^\dagger) \sum_{k>1} (f_k b_k + f_k^* b_k^\dagger) + \sum_k \Omega_k b_k^\dagger b_k. \tag{2.3}$$

In equation (2.3) the system self-Hamiltonian, H_S, is left unchanged. The second two terms represent the RC self-energy and its coupling with the system with everything else encompassed within the definition of the residual environment. This mapping can be achieved with the

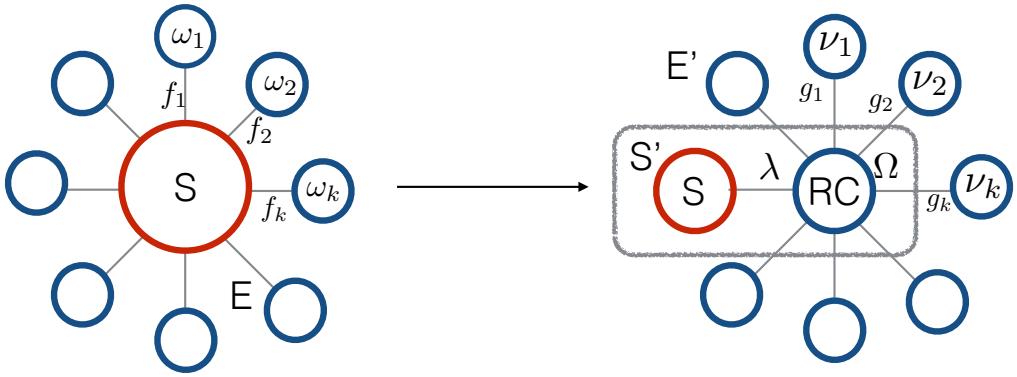

Figure 2.1: Schematic of the RC mapping. A model of a quantum system S interacting separately with k environment oscillators, each with natural frequency denoted by ω_k, with coupling parameters f_k. This model is transformed into the reaction coordinate (RC) picture. In the new picture, we incorporate a collective degree of freedom of the environment, the RC oscillator with natural frequency Ω, into the definition of an enlarged system S'. S' also includes the system-RC interaction, parametrised with coupling constant λ. The mapping results in a redefined environment E', which contains $k-1$ oscillators (although in practice the continuum limit is often applied and hence we retain the k label in the schematic). The environment oscillators' natural frequencies are shifted to ν_k, and these individually interact with the RC oscillator with coupling parameters g_k.

following Bogoliubov transformation

$$u_{kq} = \frac{1}{2}\left(\sqrt{\frac{\omega_k}{\Omega_q}} + \sqrt{\frac{\omega_q}{\omega_k}}\right)\Lambda_{kq}, \tag{2.4}$$

$$v_{kq} = \frac{1}{2}\left(\sqrt{\frac{\omega_k}{\Omega_q}} - \sqrt{\frac{\omega_q}{\omega_k}}\right)\Lambda_{kq}. \tag{2.5}$$

Here, the preservation of bosonic commutation relations imposes that the real-valued matrix (Λ_{kq}) obey $\sum_q \Lambda_{kq}\Lambda_{k'q} = \delta_{kk'}$. We obtain that $\Lambda_{k1} = \frac{g_k}{\lambda}\sqrt{\frac{\omega_k}{\Omega_1}}$ and from this can write down equations for the RC parameters in terms of the original frame spectral density $J(\omega) \equiv \sum_k |g_k^2|\delta(\omega - \omega_k)$:

$$\lambda^2 = \frac{1}{\Omega_1}\int_0^\infty \omega J(\omega) d\omega, \tag{2.6}$$

$$\Omega_1^2 = \frac{\int_0^\infty \omega^3 J(\omega) d\omega}{\int_0^\infty \omega J(\omega) d\omega}. \tag{2.7}$$

The spectral density defining the coupling to the residual reservoir may also be written down in terms of the original spectral density to complete the mapping. This is done by manipulating the equations of motion governed by the Hamiltonians in equations (2.2) and (2.3). We shall illustrate this with two example derivations, for the damped harmonic oscillator and the spin-boson model in the two sections which follow.

2.1 Reaction Coordinate Mapping for the Brownian oscillator Hamiltonian

In this section we will apply the RC mapping to the Hamiltonian for the damped harmonic oscillator which was studied under Born-Markov approximations in section 1.3. Our goal is to reach a Hamiltonian which will allow us to treat the strong coupling between the central system oscillator and the reaction coordinate exactly, therefore moving beyond the weak coupling regime, while the interaction to the residual environment may be treated under the Born-Markov approximations. We begin with the global Hamiltonian separated into system, environment and

interaction terms $H = H_S + H_I + H_E$, with (neglecting zero point energy terms)

$$H_S \equiv \omega_0 a^\dagger a, \tag{2.8}$$

$$H_E \equiv \sum_k \omega_k c_k^\dagger c_k, \tag{2.9}$$

$$H_I \equiv \sum_k g_k \left(a + a^\dagger\right)\left(c_k + c_k^\dagger\right). \tag{2.10}$$

Here, a is the annihilation operator for excitations in the oscillator of interest with natural frequency ω_0, and c_k are annihilation operators for the k environment oscillators with natural frequencies ω_k. We choose to work directly in second quantised form here, rather than with position and momentum operators, as we did in section 1.3. The interaction is parametrised by coupling constants g_k.

We wish to map to a Hamiltonian of the form

$$H' = H_{S'} + H_{E'} + H_C, \tag{2.11}$$

where

$$H_{S'} = \omega_0 a^\dagger a + \lambda\left(a^\dagger + a\right)\left(b^\dagger + b\right) + \Omega b^\dagger b, \tag{2.12}$$

$$H_{E'} = \left(b^\dagger + b\right)\sum_k f_k\left(r_k^\dagger + r_k\right) + \sum_k \omega_k r_k^\dagger r_k, \tag{2.13}$$

$$H_C = \left(b^\dagger + b\right)^2 \sum_k \frac{f_k^2}{\omega_k}. \tag{2.14}$$

For ease of notation we have labelled b as the annihilation operator for the RC and r_k as annihilation operators for the residual environment. Additionally we have required a counter term, H_C, which we shall discuss further below.

We proceed now as in Ref. [13]. We shall derive equations of motion for classical canonical coordinates from the Hamiltonians H and H'. It is also possible to proceed by deriving Heisenberg equations of motion and this is done explicitly in Ref. [12]. We re-express H and H' in terms of position and momentum coordinates for the system q, p_q, for the RC x, p_x, and for

the environment X_k and P_k. The Hamiltonian in the original frame becomes

$$H_q = \frac{p_q^2}{2} + \frac{1}{2}\omega_0^2 q^2 + q\sum_k \tilde{g}_k X_k + q^2 \sum_k \frac{\tilde{g}_k^2}{2\omega_k^2} + \frac{1}{2}\sum_k \left(P_k^2 + \omega_k^2 X_k^2\right), \tag{2.15}$$

where $\tilde{g}_k = \sqrt{4\omega_0\omega_k}$. We have introduced a counter term here, quadratic in the system position coordinate q. The motivation for this is discussed in Ref. [1] and Ref. [5]. It ensures the Hamiltonian remains always bounded from below, for any strength of interaction. One ought to write an interaction term based on a Hooke's law interaction between oscillators where the coupling involves the relative position of the coordinates of each oscillator, for example $H_{Hooke} = \frac{1}{2}\kappa(x_1 - x_2)^2$, where κ is some arbitrary spring constant. In writing interaction terms as we have been in Hamiltonians so far, we have been selecting out the term linear in each position coordinate (as is the convention in the literature), and neglected the terms involving position squared. If one begins with such an interaction Hamiltonian and includes the squared terms, the counter terms appear naturally.

We may use Hamilton's equations and equation (2.15) to write down the following equations of motion for the coordinates q for the system, and X_k for the environment oscillators:

$$\ddot{q}(t) = -\omega_0^2 q(t) - \sum_k \widetilde{g}_k X_k(t) - q(t)\sum_k \frac{\widetilde{g}_k^2}{\omega_k^2} \tag{2.16}$$

$$\ddot{X}_k(t) = -\widetilde{g}_k q(t) - \omega_k^2 X_k(t). \tag{2.17}$$

We make use of the Fourier transform $\widetilde{h}(z) = \int_{-\infty}^{\infty} h(t)e^{-izt}dt$ and inverse transform $h(t) = \frac{1}{2\pi}\int_{-\infty}^{\infty}\widetilde{h}(z)e^{izt}dz$ in order to eliminate the environment coordinates from the equation of motion for q as follows,

$$z^2\widetilde{q}\,(z) = \omega_0^2\tilde{q}(z) + \sum_k \widetilde{g}_k\widetilde{X}_k(z) + \tilde{q}(z)\sum_k \frac{\widetilde{g}_k^2}{\omega_k^2}, \tag{2.18}$$

$$z^2\tilde{X}_k(z) = \widetilde{g}_k\tilde{q}(z) + \omega_k^2\widetilde{X}_k(z). \tag{2.19}$$

Substituting into equation (2.18) for $\widetilde{X}_k(z)$ from equation (2.19) and rearranging gives

$$z^2\left(1-\frac{\omega_0^2}{z^2}+\sum_k \frac{\tilde{g_k}^2}{\omega_k^2\left(\omega_k^2-z^2\right)}\right)\widetilde{q}(z)=0. \tag{2.20}$$

Using $\tilde{g}_k=\sqrt{4\omega_0\omega_k}$ and $J(\omega)=\sum_k g_k^2\delta\left(\omega-\omega_k\right)$, we may write this as

$$\tilde{K}(z)\widetilde{q}(z)=0, \tag{2.21}$$

where $\tilde{K}(z)=z^2\left(1-\frac{\omega_0^2}{z^2}+4\omega_0\int_0^\infty d\omega\frac{J(\omega)}{\omega(\omega^2-z^2)}\right)$.

We can evaluate the integral in equation (2.21) using Cauchy's integral theorem, performing analytic continuation of the spectral density function, extending the integral to $-\infty$, closing the integral in the upper half of the complex plane. We can see from the form of the integrand that this procedure will be valid for spectral densities which are odd functions of ω, since the denominator is an odd function of ω and we require an even integrand. This results in

$$\widetilde{K}(z)=z^2-\omega_0^2-2i\pi\omega_0 J(z). \tag{2.22}$$

Rearranging and writing $z=\omega-i\epsilon$ yields

$$J(\omega)=\frac{1}{2\pi\omega_0}\lim_{\epsilon\to 0+}\mathrm{Im}\left[\tilde{K}\left(\omega-i\epsilon\right)\right]. \tag{2.23}$$

Now we repeat these steps for the case of the mapped Hamiltonian. We shall then compare the expression we obtain for the spectral density in that case with equation (2.23), in order to determine relations for the RC parameters in terms of the parameters appearing in the original Hamiltonian. The Hamiltonian is given by

$$\begin{aligned} H_q' &= \frac{1}{2}P_q^2+\frac{\omega_0^2}{2}q^2+\lambda\sqrt{4\Omega\omega_0}qx+\frac{1}{2}\Omega^2x^2+\frac{1}{2}p^2+x\sum_k\sqrt{4\Omega\omega_k}f_kX_k \\ &\quad+\sum_k\frac{P_k^2}{2}+\sum_k\frac{1}{2}\omega_k^2X_k^2+2\Omega x^2\sum_k\frac{f_k^2}{\omega_k}, \end{aligned} \tag{2.24}$$

or with the rescalings $\tilde{f}_k = \sqrt{4\Omega\omega_k} f_k$ and $\tilde{\lambda} = \sqrt{4\Omega\omega_0}\lambda$ we have that

$$H'_q = \frac{1}{2}P_q^2 + \frac{\omega_0^2}{2}q^2 + \tilde{\lambda}qx + \frac{\tilde{\lambda}^2}{2\Omega^2}q^2 + \frac{1}{2}\Omega^2 x^2 + \frac{1}{2}p^2 + x\sum_k \tilde{f}_k X_k + \sum_k \frac{P_k^2}{2} + \sum_k \frac{1}{2}\omega_k^2 X_k^2 + x^2 \sum_k \frac{\tilde{f}_k^2}{2\omega_k^2}. \tag{2.25}$$

Applying Hamilton's equations gives the three coupled equations

$$\ddot{q} = -\omega_0^2 q - \tilde{\lambda}x - \frac{\tilde{\lambda}^2}{\Omega^2}q, \tag{2.26}$$

$$\ddot{x} = -\tilde{\lambda}q - \Omega^2 x - \sum_k \tilde{f}_k X_k - x\sum_k \frac{\tilde{f}_k^2}{\omega_k^2}, \tag{2.27}$$

$$\ddot{X}_k = -x\tilde{f}_k - \omega_k^2 X_k. \tag{2.28}$$

Performing a Fourier transform, these equations become

$$\left(-z^2 + \omega_0^2 + \frac{\tilde{\lambda}^2}{\Omega^2}\right)\tilde{q}(z) + \tilde{\lambda}\tilde{x}(z) = 0, \tag{2.29}$$

$$\left(-z^2 + \Omega^2 + \sum_k \frac{\tilde{f}_k^2}{\omega_k^2}\right)\tilde{x}(z) + \tilde{\lambda}\tilde{q}(z) + \sum_k \tilde{f}_k \tilde{X}_k(z) = 0, \tag{2.30}$$

$$\left(-z^2 + \omega_k^2\right)\tilde{X}_k(z) + \tilde{f}_k\tilde{x}(z) = 0. \tag{2.31}$$

Rearranging equation (2.31) gives

$$\tilde{X}_k(z) = \frac{\tilde{f}_k\tilde{x}(z)}{z^2 - \omega_k^2}. \tag{2.32}$$

Substituting this into equation (2.30) yields

$$\tilde{x}(z) = \frac{-\tilde{\lambda}^2}{-z^2 + \Omega^2 + \sum_k \frac{-z^2\tilde{f}_k^2}{\omega_k^2(\omega_k^2 - z^2)}}\tilde{q}(z). \tag{2.33}$$

Equation (2.33) can now be used to eliminate the reaction coordinate and the bath coordinates from equation (2.29) to give

$$\left[-z^2 + \omega_0^2 + \frac{\tilde{\lambda}^2}{\Omega^2}\left(\frac{\mathcal{L}(z)}{\Omega^2 + \mathcal{L}(z)}\right)\right]\tilde{q}(z) = 0, \tag{2.34}$$

where we can label the pre-factor $\tilde{K}'(z)$ and where

$$\mathcal{L}(z) = -z^2\left(1+\sum_k \frac{\tilde{f}_k^2}{\omega_k^2\left(\omega_k^2-z^2\right)}\right) = -z^2\left(1+4\Omega\int_0^\infty d\omega \frac{J_{RC}(\omega)}{\omega(\omega^2-z^2)}\right). \tag{2.35}$$

We choose the coupling to the residual environment to be characterized by an Ohmic spectral density of the form $J_{RC}(\omega) = \gamma\omega\exp\left[-\frac{\omega}{\Lambda}\right]$, with frequency independent coupling strength γ and cutoff frequency Λ. The integral can be evaluated analogously to the unmapped case, and, when taking the limit $\Lambda \to \infty$, leads to the following expression for $\mathcal{L}(z)$,

$$\mathcal{L}(z) = -z^2 + 2i\pi\Omega\gamma z. \tag{2.36}$$

Now, since we require that the transformed Hamiltonian replicate the behaviour governed by the original Hamiltonian, we equate the expressions for the two spectral densities derived above. Substituting our expression for $\tilde{K}'(z)$ from equation (2.34) back into equation (2.23) yields

$$\begin{aligned} J(\omega) &= \frac{1}{2\pi\omega_0}\lim_{\epsilon\to 0+}\mathrm{Im}\left[\tilde{K}\left(\omega-i\epsilon\right)\right] \\ &= \left(\frac{1}{2\pi\omega_0}\right)\left(\frac{2\pi\Omega\gamma\tilde{\lambda}^2\omega}{\left(\Omega^2-\omega^2\right)^2+\left(2\pi\Omega\gamma\right)^2\omega^2}\right). \end{aligned} \tag{2.37}$$

Choosing $J(\omega)$ to be of Drude-Lorentz form,

$$J(\omega) = \alpha\frac{\omega_c\omega}{\omega^2+\omega_c^2}, \tag{2.38}$$

we obtain the following relations for the reaction coordinate natural frequency Ω and coupling strength λ, the parameters defining the mapping,

$$\Omega = \omega_c 2\pi\gamma \tag{2.39}$$

$$\lambda^2 = \frac{\pi\alpha\Omega}{2}. \tag{2.40}$$

Substituting from equations (2.39) and (2.40) back into equation (2.37) results in the following

expression for the spectral density

$$J(\omega) = \frac{\alpha\omega_c\omega}{\omega_c^2\left(1 - \frac{2\omega^2}{\Omega^2} + \frac{\omega^4}{\Omega^4}\right) + \omega^2}. \tag{2.41}$$

For low frequencies ω in the environment with respect to the cut off frequency ω_c and the RC frequency Ω, then under the condition that $\omega_c < \Omega$, this expression reduces to equation (2.38), the desired original Drude-Lorentz type spectral density. The parameter ω_c locates the exponential cut-off for the reservoir spectral density. If we tune γ such that the criteria $\omega_c < \Omega$ is met, then we are positioning the RC frequency in the range above the lower frequency environmental oscillators where the coupling to the system is strongest (this portion of the spectral density is represented now as part of the enlarged system which involves strong coupling between the TLS and the RC). The RC frequency itself is therefore located towards the tail of the spectral density where coupling to the residual reservoir is weaker, and we shall subsequently treat this accordingly through a Born-Markov master equation approach.

In this way, it can be noted that the RC formalism is designed to deal with environmental coupling regimes which differ from those for which the Polaron transformation is well suited to tackle, when combined with a second order time local master equation approach, see for example Ref. [18]. Indeed the Polaron technique alongside a perturbative master equation is equivalent to the non-interacting blip technique which is utilised by the authors in Ref. [7] as the basis for their discussion of transitions between localisation and delocalisation of the TLS energy eigenstates in the spin-boson model. There, the authors are concerned with low temperatures in the environment, or the limiting case of zero temperature, and important frequencies in the environmental oscillators which are fast relative to the system frequency scale. While their results can be captured well within the Polaron framework, the RC technique is less well-suited as it is designed for the opposite case of important environmental frequencies which are closer to the system frequency, embodied by the criteria that $\omega_c < \Omega$. The RC framework is less well suited for environmental temperatures which are very low with respect to the energy scale of the system. This latter issue is discussed in more detail in section 2.3.2 to follow, where we benchmark the RC framework against the exact solution for a simplified version of the

spin-boson problem considered in Ref. [7].

We are now in a position where all the parameters for the RC mapping have been established and we may work with the mapped Hamiltonian, equation (2.11), knowing it will yield equivalent behaviour for the dynamics of the central oscillator. In section 2.1.1 we will derive a master equation for the dynamics of the reduced density operator of the newly redefined system S', which now incorporates both the original central oscillator and the collective degree of freedom from the original environment encompassed in the RC.

2.1.1 Reaction Coordinate Master Equation for the Brownian oscillator

The goal now is to construct a master equation governing the dynamics of the reduced density operator $\rho_{S'}$ of the joint oscillator-RC system. We shall make use of the techniques discussed in section 1.2 to ensure the equation treats the coupling between the RC and the residual environment perturbatively, i.e. under the Born-Markov approximations, but keeps track of the coupling between the central oscillator and the RC exactly. We consider equation (2.11) and define

$$H_0 \equiv H_{S'} + \sum_k \omega_k r_k^\dagger r_k, \tag{2.42}$$

$$H_I^{eff} \equiv \left(b^\dagger + b\right) \sum_k f_k \left(r_k^\dagger + r_k\right) + \left(b^\dagger + b\right)^2 \sum_k \frac{f_k^2}{\omega_k}. \tag{2.43}$$

Let us write the interaction term as

$$H_I^{eff} = A \otimes B + \tilde{\lambda} A^2, \tag{2.44}$$

where

$$A = b^\dagger + b \tag{2.45}$$

$$B = \sum_k f_k \left(r_k^\dagger + r_k \right) \tag{2.46}$$

$$\tilde{\lambda} = \sum_k \frac{f_k^2}{\omega_k}. \tag{2.47}$$

Before making the Born-Markov approximations, the interaction picture master equation reads

$$\frac{d}{dt}\widetilde{\rho}_{S'}(t) = -i \ \mathrm{tr}_{E'} \left[\widetilde{H}_I(t), \widetilde{\rho}(0) \right] - \int_0^t d\tau \ \mathrm{tr}_{E'} \left[\widetilde{H}_I(t), \left[\widetilde{H}_I(t-\tau), \widetilde{\rho}(\tau) \right] \right], \tag{2.48}$$

where we have transformed H_I^{eff} into the interaction picture with respect to H_0

$$\tilde{H}_I(t) = e^{iH_0 t} H_I^{eff} e^{-iH_0 t} = \tilde{A}(t) \otimes \tilde{B}(t) + \tilde{\lambda} \tilde{A}^2(t). \tag{2.49}$$

Making the Born approximation, we assume the global density operator remains separable state all times,

$$\rho(t) \approx \rho_{S'}(t) \otimes \rho_{E'}. \tag{2.50}$$

We take the residual environment to be in a thermal state of the form

$$\rho_{E'} = \frac{\exp\left(-\beta \sum_k \omega_k r_k^\dagger r_k \right)}{\mathrm{tr}\left\{ \exp\left(-\beta \sum_k \omega_k r_k^\dagger r_k \right) \right\}}. \tag{2.51}$$

Substituting the expressions for $\tilde{H}_I(t)$ and $\rho(t)$ from equations (2.49) and (2.50) into equation (2.48) yields

$$\begin{aligned} \frac{d}{dt}\widetilde{\rho}_{S'}(t) &= -i\tilde{\lambda} \left[\widetilde{A}^2(t), \widetilde{\rho}_{S'}(0) \right] - \tilde{\lambda}^2 \int_0^t d\tau \left[\widetilde{A}^2(t), \left[\widetilde{A}^2(t-\tau), \widetilde{\rho}_{S'}(\tau) \right] \right] \\ &\quad - \int_0^t d\tau \left[\widetilde{A}(t), \left[\widetilde{A}(t-\tau), \widetilde{\rho}_{S'}(\tau) \right] \right] \Gamma^+(\tau) - \int_0^t d\tau \left[\widetilde{A}(t), \left\{ \widetilde{A}(t-\tau), \widetilde{\rho}_{S'}(\tau) \right\} \right] \Gamma^-(\tau), \end{aligned} \tag{2.52}$$

where we have defined the environment self-correlation functions $\Gamma^{\pm}$ as

$$\Gamma^{\pm} \equiv \frac{1}{2}\mathrm{tr}\left\{\left(\tilde{B}(\tau)B \pm \tilde{B}(-\tau)B\right)\rho_{E'}\right\}. \tag{2.53}$$

Noticing that

$$-i\tilde{\lambda}\left[\tilde{A}^2(t),\tilde{\rho}_{S'}(t)\right] = -i\tilde{\lambda}\left[\widetilde{A}^2(t),\widetilde{\rho}_{S'}(0)\right] - \tilde{\lambda}^2\int_0^t d\tau\left[\widetilde{A}^2(t),\left[\widetilde{A}^2(t-\tau),\widetilde{\rho}_{S'}(\tau)\right]\right], \tag{2.54}$$

we make the Markov approximation and replace τ with t in the argument for $\tilde{\rho}_{S'}$ and extend the integrals to infinity to give

$$\begin{aligned}\frac{d}{dt}\widetilde{\rho}_{S'}(t) &= -i\tilde{\lambda}\left[\widetilde{A}^2(t),\widetilde{\rho}_{S'}(t)\right] \\ &\quad -\int_0^\infty\int_0^\infty d\tau d\omega J_{RC}(\omega)\coth\left(\frac{\beta\omega}{2}\right)\cos(\omega\tau)\left[\widetilde{A}(t),\left[\widetilde{A}(t-\tau),\widetilde{\rho}_{S'}(t)\right]\right] \\ &\quad -i\int_0^\infty\int_0^\infty d\tau d\omega J_{RC}(\omega)\sin(\omega\tau)\left[\widetilde{A}(t),\left\{\widetilde{A}(t-\tau),\widetilde{\rho}_{S'}(t)\right\}\right],\end{aligned} \tag{2.55}$$

where we have used

$$\Gamma^{+}(\tau) = \int_0^\infty d\omega J_{RC}(\omega)\coth\left(\frac{\beta\omega}{2}\right)\cos(\omega\tau) \tag{2.56}$$

$$\Gamma^{-}(\tau) = i\int_0^\infty d\omega J_{RC}(\omega)\sin(\omega\tau). \tag{2.57}$$

Equation (2.55) is in the desired mater equation governing the dynamics of the enlarged system S', with weak coupling approximations applied to the interaction between the RC and the residual environment E'. We may simplify it a little further with a judicious application of the Sokhotski-Plemelj theorem which reads

$$\int_0^\infty d\omega f(\omega)\int_0^\infty d\tau e^{\pm i(\omega-\kappa)\tau} = \pi\int_0^\infty d\omega f(\omega)\delta(\omega-\kappa) \pm iP\left(\int_0^\infty d\omega\frac{f(\omega)}{\omega-\kappa}\right). \tag{2.58}$$

Here, P denotes that the Cauchy Principal Value is to be taken for the integral over ω, since there is a divergence at $\omega = \kappa$. We perform the integral over τ in the last term in equation (2.55) by parts and note that we require the imaginary part of the Sokhotski-Plemelj theorem. Selecting out only the terms dependent on τ we therefore find that

$$\int_0^\infty d\tau \sin(\omega\tau)\,\tilde{A}(t-\tau) \;=\; P\left(\frac{\tilde{A}(t)}{\omega}\right) + \int_0^\infty d\tau \frac{\cos(\omega\tau)}{\omega}\frac{\partial \tilde{A}(t-\tau)}{\partial\tau}. \tag{2.59}$$

Substituting these two terms back into the final term in equation (2.55) and performing the principal value part of the integral over ω we note that this yields a term which is equal in magnitude but opposite in sign to the first term in equation (2.55). Cancelling these two terms, therefore, and then transforming the remaining terms back into the Schrödinger picture, we obtain

$$\begin{aligned}\frac{d}{dt}\rho_{S'}(t) \;=\; & -i\left[H_{S'},\rho_{S'}(t)\right] - \int_0^\infty\int_0^\infty d\tau d\omega J_{RC}(\omega)\coth\left(\frac{\beta\omega}{2}\right)\cos(\omega\tau)\left[A,\left[\widetilde{A}(-\tau),\rho_{S'}(t)\right]\right] \\ & - \int_0^\infty\int_0^\infty d\tau d\omega J_{RC}(\omega)\frac{\cos(\omega\tau)}{\omega}\left[A,\left\{\left[\tilde{A}(-\tau),H_s\right],\widetilde{\rho}_{S'}(t)\right\}\right],\end{aligned} \tag{2.60}$$

where in the last term we have used the Heisenberg equation of motion $\frac{d\tilde{A}(t-\tau)}{d\tau} = i\left[H_S,\tilde{A}(t-\tau)\right]$.

Equation (2.60) is a time-local master equation for the evolution of the composite central oscillator and RC system. It will will keep track of any correlations between the central oscillator and the collective degree of freedom of the environment encompassed in the RC. Finally, for the purposes of numerical computation when it comes to solving for the dynamics, we obtain expressions for the interaction picture system operators A in terms of the eigenstates of $H_{S'}$, defined by $H_{S'}|\phi_n\rangle = \phi_n|\phi_n\rangle$. We can expand as follows

$$A = \sum_{j,k}|\phi_j\rangle\langle\phi_j|A|\phi_k\rangle\langle\phi_k| = \sum_{j,k}A_{j,k}|\phi_j\rangle\langle\phi_k|, \tag{2.61}$$

and move into the interaction picture

$$\begin{aligned}\tilde{A}(t) &= \exp\left[iH_{S'}t\right]\sum_{j,k}A_{j,k}|\phi_j\rangle\langle\phi_k|\exp\left[-iH_{S'}t\right] \\ &= \sum_{j,k}A_{j,k}\exp\left(i\xi_{j,k}t\right)|\phi_j\rangle\langle\phi_k|, \end{aligned} \tag{2.62}$$

where $\xi_{j,k}=\phi_j-\phi_k$. In order to write equation (2.60) in a more compact form, we define and evaluate the following integrals:

$$\begin{aligned}\hat{\chi} &\equiv \int_0^\infty\int_0^\infty d\tau d\omega J_{RC}(\omega)\coth\left(\frac{\beta\omega}{2}\right)\cos\left(\omega\tau\right)\widetilde{A}(-\tau) \\ &\approx \frac{\pi}{2}\sum_{j,k}J_{RC}\left(\xi_{j,k}\right)\coth\left(\frac{\beta\xi_{j,k}}{2}\right)A_{j,k}|\phi_j\rangle\langle\phi_k|, \end{aligned} \tag{2.63}$$

$$\begin{aligned}\hat{\Xi} &\equiv \int_0^\infty\int_0^\infty d\tau d\omega J_{RC}(\omega)\frac{\cos(\omega\tau)}{\omega}\left[H_{S'},A(-\tau)\right] \\ &\approx \frac{\pi}{2}\sum_{j,k}J_{RC}\left(\xi_{j,k}\right)A_{j,k}|\phi_j\rangle\langle\phi_k|, \end{aligned} \tag{2.64}$$

where we have neglected the Lamb shift terms in the same way as in Ref. [13]. This is justified in sections to follow, when we benchmark dynamics computed according to RC master equations against exact results and achieve excellent agreement. Using equations (2.63) and (2.64), we arrive at a compact form of the master equation for $\rho_{S'}$ given by

$$\frac{\partial\rho_{S'}(t)}{\partial t}=-i\left[H_{S'},\rho_{S'}(t)\right]-\left[A,\left[\hat{\chi},\rho_{S'}(t)\right]\right]+\left[A,\left\{\hat{\Xi},\rho_{S'}(t)\right\}\right]. \tag{2.65}$$

Let us, at this stage take stock. We have at our disposal two equations governing the dynamics of a quantum harmonic oscillator which is coupled to a bosonic environment: equations (1.50) and (2.65). The former is valid at weak interaction strengths, within the limits imposed by the Born-Markov approximations, and the latter is a strong coupling version which should take us beyond these limitations. Given some initial conditions for the system state (we have assumed thermal states for the environment), each of these equations can be solved using computational methods. We will go on to illustrate this in the sections which follow, showing that at weak

coupling both equations lead to dynamics which agree well with one another. At stronger coupling we shall see that they diverge.

First, however, we briefly introduce the RC master equation for the case of a spin as the central system of interest, in order that we may also compare with the dynamics obtained via equation (1.100), which gives the exact solution for the independent boson model.

2.2 Reaction coordinate mapping and master equation for the independent boson model

The RC formalism is applied in detail to the spin-boson model in Ref. [13]. The mapping and subsequent derivation of a master equation which treats the coupling between the TLS and the RC exactly, but the coupling between the RC and the residual environment to second order under the Born-Mark approximations is identical to that presented in Ref. [13] except that in the present case we wish to remove the tunneling term in the spin-boson Hamiltonian by setting $\Delta = 0$ in order that we may compare dynamics with the exact solution given in equation (1.100). The details of the derivation are also very similar to those discussed in detail in the previous sections for the harmonic oscillator.

We will therefore not repeat the working here. We just note that the resulting master equation for the reduced density operator for the joint TLS-RC system, $\rho_{S'}(t)$ is

$$\frac{\partial \rho_{S'}(t)}{\partial t} = -i\left[H_{S'}, \rho_{S'}(t)\right] - \left[A, \left[\hat{\chi}, \rho_{S'}(t)\right]\right] + \left[A, \left\{\hat{\Xi}, \rho_{S'}(t)\right\}\right], \tag{2.66}$$

Here $H_{S'}$ represents the joint TLS and RC Hamiltonian, incorporating the self-energies of the TLS and RC as well as the interaction term coupling them, and reads as

$$H_{S'} \equiv \frac{\epsilon}{2}\sigma_z + \lambda\sigma_z\left(a^\dagger + a\right) + \Omega a^\dagger a. \tag{2.67}$$

Here Ω is the natural frequency of the RC, the operators a and $a^\dagger$ respectively annihilate and

create excitations of the RC, λ is a parameter determining the coupling strength between the RC and the TLS, and $A \equiv a + a^\dagger$. The joint TLS-RC operators $\hat{\chi}$ and $\hat{\Xi}$ have the same forms as that given in equations (2.63) and (2.64).

We are now in a position to compare the dynamics predicted with the strong coupling theory of the RC formalism with those of the weak coupling Born-Markov approach for both the harmonic oscillator and the two-level system.

2.3 Dynamics at strong reservoir coupling

2.3.1 Dynamics of the damped harmonic oscillator

We will look at the expectation values for the position and momentum of the model we have presented thus far of a quantum harmonic oscillator, damped by its interaction with a surrounding environment. We will compare predictions made by the RC treatment with both a weak coupling theory, generated from a standard Born-Markov master equation, and an exact solution which can be found in Ref. [19].

The weak coupling solutions can be obtained via a manipulation of the master equation derived in section 1.3.1, which for clarity we repeat here:

$$\frac{d}{dt}\rho(t) = -i\left[H_S + \frac{1}{2}m\tilde{\omega}_0^2 x^2, \rho(t)\right] - i\gamma\left[x, \{p, \rho(t)\}\right] - D\left[x, [x, \rho(t)]\right] - f\left[x, [p, \rho(t)]\right], \quad (2.68)$$

where the self-Halmiltonian of the system is given by

$$H_S = \frac{1}{2m}p^2 + \frac{1}{2}m\omega_0^2 x^2, \quad (2.69)$$

the coefficients in front of each commutator bracket are

$$\tilde{\omega}_0 = -\frac{2}{m}\int_0^\infty d\tau\eta(\tau)\cos(\omega_0\tau), \tag{2.70}$$

$$\gamma = \frac{1}{m\omega_0}\int_0^\infty d\tau\eta(\tau)\sin(\omega_0\tau), \tag{2.71}$$

$$D = \int_0^\infty d\tau\eta\nu(\tau)\cos(\omega_0\tau), \tag{2.72}$$

$$f = -\frac{1}{m\omega_0}\int_0^\infty d\tau\nu(\tau)\sin(\omega_0\tau), \tag{2.73}$$

and where the noise and dissipation kernels are defined as

$$\nu(\tau) = \int_0^\infty d\omega J(\omega)\coth\left(\frac{\beta\omega}{2}\right)\cos(\omega\tau), \tag{2.74}$$

$$\eta(\tau) = \int_0^\infty d\omega J(\omega)\sin(\omega\tau). \tag{2.75}$$

The expectation value of the momentum operator obeys $\frac{d}{dt}\langle p\rangle(t) = \frac{d}{dt}\mathrm{Tr}\left(\rho p\right) = \mathrm{Tr}\left[\left(\frac{d}{dt}\rho\right)p\right]$. Multiplying equation (2.68) on the right by p, performing the trace operation and making use of the relations

$$[x,p] = i\mathbb{1}, \tag{2.76}$$

$$\left[x^2,p\right] = 2ix, \tag{2.77}$$

$$\left[x,p^2\right] = 2ip, \tag{2.78}$$

yields an equation of motion for average momentum given by

$$\frac{d}{dt}\langle p\rangle = -m\left(\omega_0^2+\tilde{\omega}_0^2\right)\langle x\rangle - 2\gamma\langle p\rangle. \tag{2.79}$$

An equation of motion for the expectation value of the position operator can be obtained in

similar fashion, resulting in

$$\frac{d}{dt}\langle x\rangle = \frac{1}{m}\langle p\rangle. \tag{2.80}$$

Solving equations (2.79) and (2.80) provides us with a weak coupling theory with which to compare results obtained through the RC treatment.

As for an exact solution, we make use of results already obtained and elegantly explained in Ref. [19]. They obtain the dynamics for certain system and reservoir expectation values via an exact diagonalisation of the full Hamiltonian describing the system and reservoir degrees of freedom. Though a little involved, this is possible in the case of a quantum harmonic oscillator coupled to a reservoir of oscillators and thus is why this model serves well as a benchmark for the RC treatment. We will make use of equation (48) in that article which we repeat here for the purposes of self-containment:

$$\langle x(t)\rangle = \langle\langle\cos(\omega t)\rangle\rangle\langle x(0)\rangle + \frac{1}{m}\langle\langle\omega^{-1}\sin(\omega t)\rangle\rangle\langle p(0)\rangle, \tag{2.81}$$

$$\langle p(t)\rangle = \langle\langle\cos(\omega t)\rangle\rangle\langle p(0)\rangle - m\langle\langle\omega\sin(\omega t)\rangle\rangle\langle x(0)\rangle. \tag{2.82}$$

The double angled brackets signify an average over frequency with respect to a probability distribution given in equation (18) in Ref. [19] by

$$\pi(\omega) = |\alpha(\omega)|^2 \frac{4\omega_0\omega}{(\omega_0+\omega)^2}. \tag{2.83}$$

The natural frequency of the oscillator is given by ω_0 and its mass by m. The bath contains a distribution of frequencies denoted by ω. The function $\alpha(\omega)$ is given in the appendix of Ref. [19] in equations (A17) and (A.18) as

$$|\alpha(\omega)|^2 = \frac{(\omega_0+\omega)^2}{\omega_0^2\,|V(\omega)|^2}\left(\frac{1}{Y^2(\omega)+\pi^2}\right). \tag{2.84}$$

The function $Y(\omega)$ is given in equation (A.15)

$$Y(\omega) = \frac{1}{|V(\omega)|^2}\left[\frac{2\left(\omega^2-\omega_0^2\right)}{\omega_0} + P\int_0^\infty d\omega' \frac{|V(\omega')|^2}{\omega'-\omega} - \int_0^\infty d\omega' \frac{|V(\omega')|^2}{\omega'+\omega}\right], \tag{2.85}$$

and $\left|V(\omega)^2\right|$ is the spectral density describing the coupling to the environment. P denotes that the Cauchy Principal Value is to be taken on integration. To summarise at this stage: we wish to compute the dynamics for position and momentum expectation values of the reduced system with global Hamiltonian given by equations (2.8), (2.9) and (2.10). We have derived a treatment according to the Reaction Coordinate formalism and we will compare this with dynamics at weak coupling according to equations (2.79) and (2.80) and an exact solution given by equations (2.81) and (2.82).

The reaction coordinate treatment involves solving equation (2.65) using computational methods to obtain the dynamics of the enlarged system S'. We may then calculate the expectation value of position and momentum operators ($x^S \otimes I^{RC}$ and $p^S \otimes I^{RC}$). Performing the partial trace over the RC degree of freedom will give the average position and momentum dynamics for S. Figure 2.2 shows the results of a reaction coordinate treatment, a weak coupling master equation treatment and the exact solution in a strong coupling regime. The solutions depicted are for $\langle x_0\rangle = \langle p_0\rangle = 1$. This corresponds to an initial coherent state for the system S:

$$|\alpha\rangle \equiv D(\alpha)|0\rangle, \tag{2.86}$$

where $\alpha = \sqrt{\frac{m\omega_0}{2}} + i\sqrt{\frac{1}{2m\omega_0}}$ and the displacement operator is given by $D(\alpha) \equiv \exp\left(\alpha a^\dagger - \alpha^* a\right)$. Note that this state corresponds to one where the expectation values for initial position and

momentum are equal to 1, $\langle x_0\rangle = \langle p_0\rangle = 1$:

$$\begin{aligned}
\langle\alpha|x|\alpha\rangle &= \langle 0|D^\dagger(\alpha)xD(\alpha)|0\rangle \\
&= \sqrt{\frac{1}{2m\omega_0}}\langle 0|D^\dagger(\alpha)\left(a+a^\dagger\right)D(\alpha)|0\rangle \\
&= \sqrt{\frac{1}{2m\omega_0}}\left[\langle 0|\left(a+\alpha\right)|0\rangle + \langle 0|\left(a+\alpha*\right)|0\rangle\right] \\
&= \sqrt{\frac{2}{m\omega_0}}\mathrm{Re}\alpha = \sqrt{\frac{2}{m\omega_0}}\sqrt{\frac{m\omega_0}{2}} = 1. \qquad (2.87)\\
\langle\alpha|p|\alpha\rangle &= \langle 0|D^\dagger(\alpha)pD(\alpha)|0\rangle \\
&= -i\sqrt{\frac{m\omega_0}{2}}\langle 0|D^\dagger(\alpha)\left(a-a^\dagger\right)D(\alpha)|0\rangle \\
&= \sqrt{2m\omega_0}\mathrm{Im}\alpha = \sqrt{2m\omega_0}\frac{1}{\sqrt{2m\omega_0}} = 1. \qquad (2.88)
\end{aligned}$$

We have made use of the relations $D^\dagger(\alpha)aD(\alpha) = a+\alpha$ and $D^\dagger(\alpha)a^\dagger D(\alpha) = a^\dagger + \alpha^*$. We have truncated the system and reaction coordinate oscillators at $n = 10$. The spectral density considered is given by

$$J(\omega) = \alpha_0\frac{\omega_c\omega}{\omega^2+\omega_c^2}. \qquad (2.89)$$

We see that the RC treatment yields excellent agreement with the exact solution in a regime where the weak coupling theory fails to capture the dynamics correctly. Furthermore we may verify that the RC treatment agrees with the weak coupling theory in regimes where it does yield accurate results. We show this in figure 2.3.

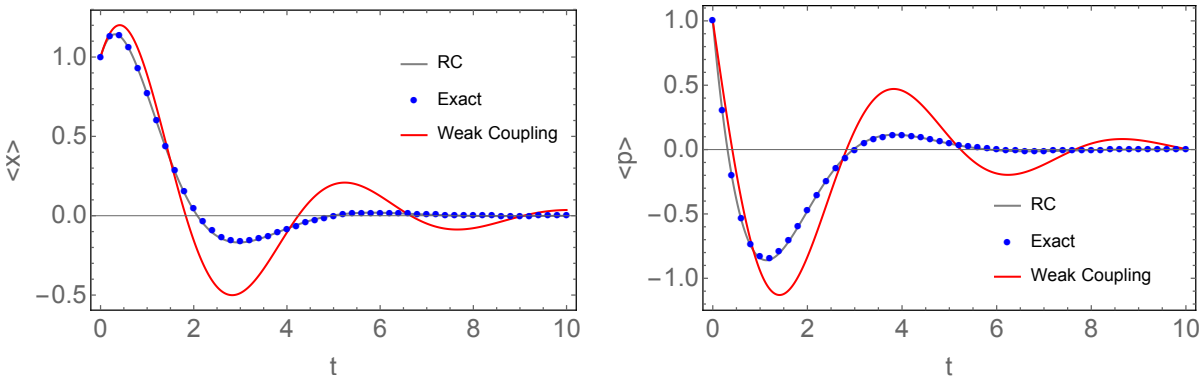

(a) (b)

Figure 2.2: A comparison of results from a reaction coordinate treatment of a damped harmonic oscillator (grey line), with an exact solution according to Ref. [19] (blue dots) and with a weak coupling master equation (red line). (a) The expectation value for the position operator $\langle x \rangle$; (b) the expectation value for the momentum operator $\langle p \rangle$. Parameters: $\alpha_0 = 1$, $\omega_0 = 2$, $\omega_c = 3$, $\beta = 1.5$. The weak coupling treatment fails to capture the dynamics correctly for this value of α_0, but the reaction coordinate treatment matches well with the exact results.

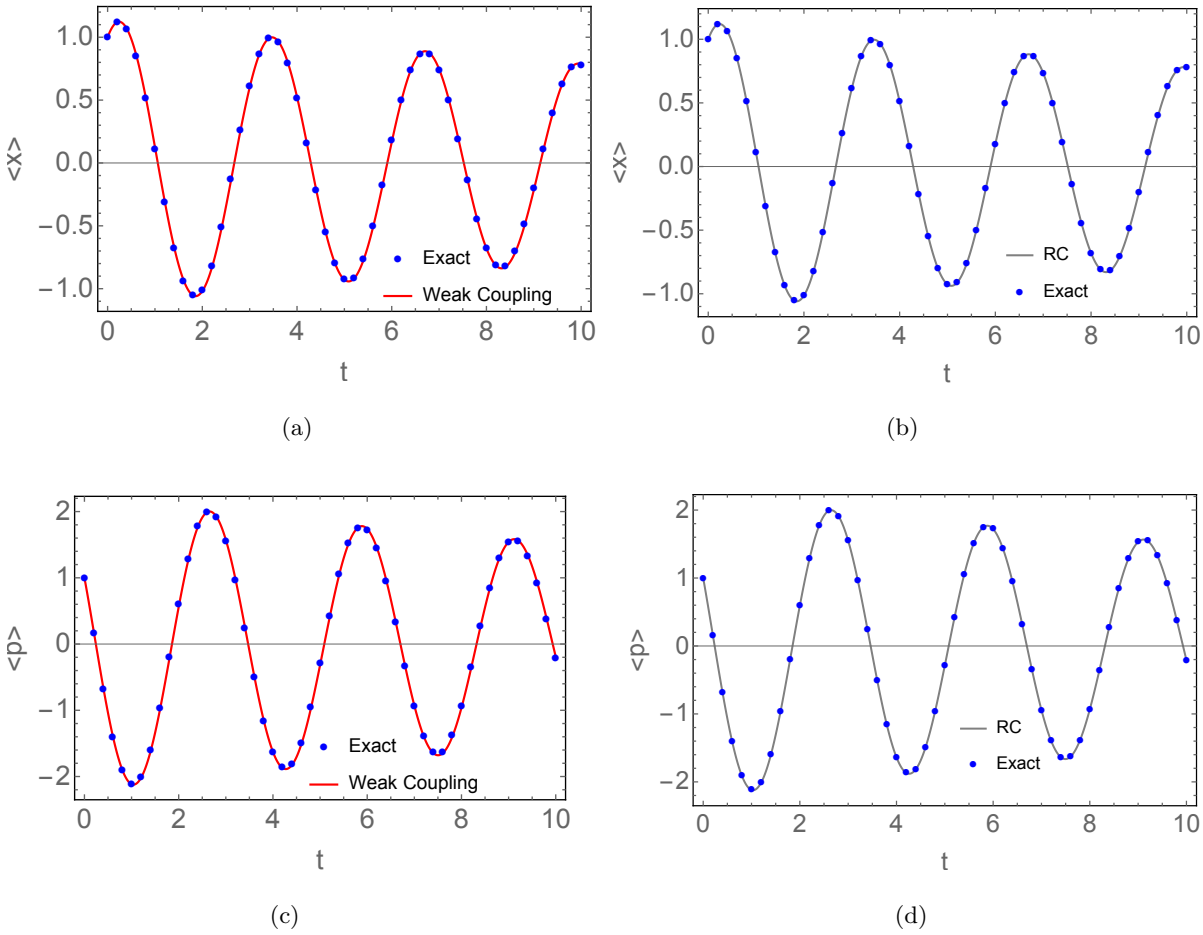

Figure 2.3: (a) A comparison of the expectation value for the position operator $\langle x \rangle$ computed from a weak coupling damped harmonic oscillator master equation (*red line*) with the exact solution from equation (2.81) (*blue dots*). (b) $\langle x \rangle$ computed according to the RC master equation (*grey line*) and the exact solution (*blue dots*). (c) and (d) show the case for the expectation value of the momentum operator $\langle p \rangle$. Parameters: $\alpha_0 = 0.1$, $\omega_0 = 2$, $\omega_c = 3$, $\beta = 1.5$. In this regime of weaker coupling, a standard Born-Markov treatment, the reaction coordinate treatment and the exact resuls all converge.

2.3.2 Dynamics of the spin-boson model

We shall look, here, at the dynamics of the spin-boson model with the simplification of setting the tunnelling term $\Delta \to 0$. As previously discussed, this enables us to write down an exact analytical expression for the global density operator as a function of time and in the case of an environment initialised in a thermal state we obtain an exact equation for the reduced density

operator of the spin as a function of time given by equation (1.100). The temperature of the environment enters through the decoherence function, a function which describes the decay of the off diagonal elements of the reduced spin density operator, given in equation (1.99). We will also consider the dynamics predicted by an RC treatment, namely those governed by a solution to equation (2.66).

Let us consider two alternative spectral densities, describing the coupling between the system and the environment: an underdamped spectral density of the form

$$J_{UD}(\omega) = \frac{\alpha_{UD}\Gamma\omega_0^2\omega}{(\omega_0^2-\omega^2)^2+\Gamma^2\omega^2}, \tag{2.90}$$

and an overdamped spectral density given by

$$J_{OD}(\omega) = \frac{\alpha_{OD}\omega_c\omega}{\omega^2+\omega_c^2}. \tag{2.91}$$

These forms of spectral density are studied in Ref. [14] in relation to non-Markovian effects in excitonic energy transfer in molecular dimers. Each of these is plotted in figure 2.4. The underdamped case has a peak centered at ω_0 and width determined by Γ, with the dimensional coupling parameter α_{UD} employed to tune the coupling strength. In the overdamped case, the coupling strength is tuned via α_{OD} and the spectrum is broader with a Lorentzian cut off determined by ω_c.

Performing the mapping results in the following relations for the underdamped spectral density, when we take the limit $\Lambda \to \infty$:

$$\Omega = \omega_0, \tag{2.92}$$

$$\lambda = \sqrt{\frac{\pi\alpha_{UD}\omega_0}{2}}, \tag{2.93}$$

$$\gamma = \frac{\Gamma}{2\pi\omega_0}. \tag{2.94}$$

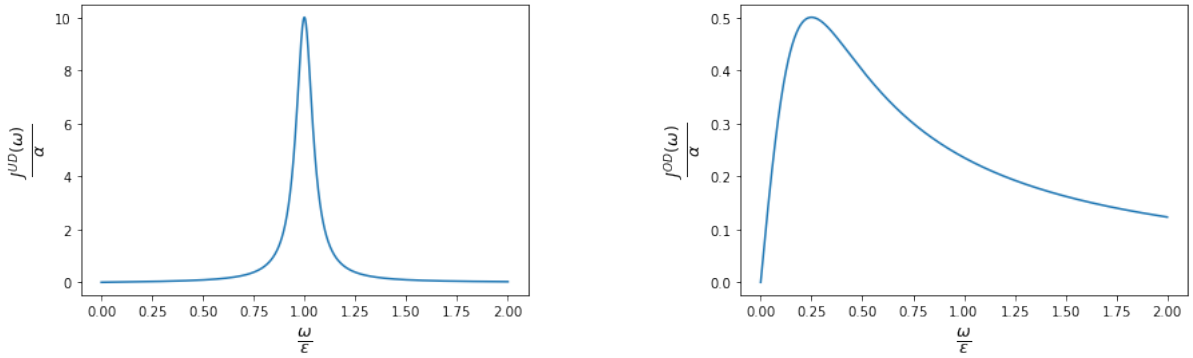

(a) Underdamped spectral density

(b) Overdamped spectral densty

Figure 2.4: Examples of underdamped and overdamped spectral densities. Parameters: (a) $\alpha = 3/\pi$, $\Gamma = 0.1$, $\omega_0 = 1$ (b) $\alpha = 3/\pi$, $\omega_c = 0.2$.

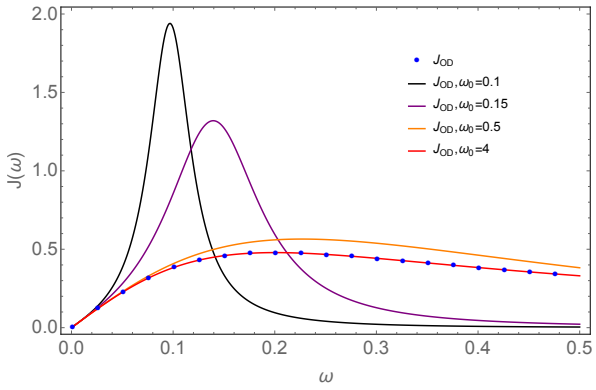

Figure 2.5: The overdamped spectral density given by equation (2.91) can be obtained from the underdamped spectral density by tuning the appropriate parameters, namely by fixing $\Gamma = \frac{\omega_0^2}{\omega_c}$ and increasing ω_0 such that good agreement between J_{OD} and J_{UD} is achieved at large values of ω_0. Parameters: $\alpha = 3/\pi$, $\omega_c = 0.2$.

In the previous sections we determined relations for the overdamped spectral density. In that case we were left with a free parameter to tune in order to obtain close agreement between the mapped dynamics at the exact solution. However, we note in figure 2.5 that a smooth transition between the two forms of spectral density can be achieved by careful tuning of parameters, so to eliminate any ambiguity we use equations (2.92 - 2.94) to study both forms of coupling.

In figure 2.6, we show how it is possible to achieve close agreement between the behaviour predicted by the RC treatment using equation (2.66) and the exact solution given by equation (1.100). The plots depict the decoherence of the off-diagonal term ρ_{01} in the TLS density

operator ρ_S for two different initial states: $|+\rangle = \frac{1}{\sqrt{2}}(|0\rangle + |1\rangle)$ and $|-\rangle = \frac{1}{\sqrt{2}}(|0\rangle - |1\rangle)$. In the RC case, one needs to perform a partial trace over the collective coordinate degree of freedom to eliminate the RC from $\rho_{S'}$. Close agreement is seen in both the weak coupling and strong coupling regimes, for both the underdamped and overdamped forms of environmental spectral density.

We can also verify the behaviour of a joint system-environment observable, namely the expectation value for the interaction energy $\langle H_{int}\rangle(t) = \mathrm{tr}[\rho(t)\sigma_z \sum_k g_k(b_k^\dagger + b_k)]$. It is most straightforward to evaluate this in the interaction picture. In section 1.4.2 we evaluated expressions for the TLS density operator matrix elements in the interaction picture using an exact expression for the time evolution operator $\tilde{U}^\dagger(t)$ and obtained equations (1.93-1.95). If we do not perform the trace of the environment degrees of freedom, we can write down a similar expression for the global state:

$$\begin{aligned}
\tilde{\rho}(t) &= \tilde{U}(t)\rho(0)\tilde{U}^\dagger(t) \\
&= \left(|0\rangle\langle 0| \prod_k D\left(\alpha_k\right) + |1\rangle\langle 1| \prod_k D\left(-\alpha_k\right)\right) \rho_S \otimes \rho_B^{th} \left(|0\rangle\langle 0| \prod_k D\left(-\alpha_k\right) + |1\rangle\langle 1| \prod_k D\left(+\alpha_k\right)\right) \\
&= \rho_S^{00}|0\rangle\langle 0| \otimes \prod_k D\left(+\alpha_k\right) \rho_B^{th} \prod_k D\left(-\alpha_k\right) + \rho_S^{01}|0\rangle\langle 1| \otimes \prod_k D\left(+\alpha_k\right) \rho_B^{th} \prod_k D\left(+\alpha_k\right) \\
&+ \rho_S^{00}|1\rangle\langle 0| \otimes \prod_k D\left(-\alpha_k\right) \rho_B^{th} \prod_k D\left(-\alpha_k\right) + \rho_S^{11}|1\rangle\langle 1| \otimes \prod_k D\left(-\alpha_k\right) \rho_B^{th} \prod_k D\left(+\alpha_k\right).
\end{aligned} \tag{2.95}$$

Here we have assumed we initialise the global system in a product state with the environment at thermal equilbrium at a temperature β: $\rho_B^{th} \equiv \frac{1}{Z_B} e^{-\beta H_B}$.

In the interaction picture, the interaction energy becomes $\tilde{H}_{int} = \sigma_z \sum_k g_k(b_k^\dagger e^{i\omega_k t} + b_k e^{-i\omega_k t})$. Combining this with equation (2.95), we can evaluate $\langle H_{int}\rangle(t) = \mathrm{tr}\left[\tilde{H}_{int}\tilde{\rho}(t)\right]$, which, after some algebraic manipulations, results in the following exact analytical expression

$$\langle H_{int}\rangle(t) = 2\int_0^\infty d\omega \frac{J(\omega)}{\omega}[\cos(\omega t) - 1]. \tag{2.96}$$

It is also possible to evaluate the interaction energy within the RC framework, by computing $\mathrm{tr}[\rho_{S'}(t)\lambda\sigma_z(a^\dagger + a)]$, where we obtain $\rho_{S'}(t)$ by numerically solving equation (2.66). In figure 2.7, we show how the RC framework yields an excellent approximation of the interaction energy in both weak and strong coupling regimes. In this case, the initial TLS state is the $|+\rangle$ state, however the dynamics of the interaction energy are independent of this initial state. Indeed, the exact expression for $\langle H_{int}\rangle$ given in equation (2.96) is independent of any parameters in the initial TLS state and depends only on the form of the spectral density. Here we show the results for the overdamped case, but equally good agreement is also seen when we tune to the underdamped situation.

We stress that computing a joint system-environment observable is not a straightforward task in open quantum systems which are not exactly solvable. The standard approach of deriving a weak coupling Born-Markov master equation always traces out any information on the environment, which, in any case is assumed to remain static in time and in a separable state with the system at all times. An advantage of the RC treatment, in addition to allowing us to go to stronger coupling regimes, is that we may keep track of some environment dynamics, approximating them through the behaviour of the collective RC. This enables computation of joint system-environment observables, such as the interaction energy, which we shall see later on is essential in thermodynamic settings, for example in extending analyses of heat engines to the strong coupling regime.

We will finish this section with a caveat: that care still needs to be taken with applying the RC mapping to solve a strongly coupled situation. At low temperatures, the RC method agrees less well with the exact solution. We depict this in figure 2.8. The disparity is apparent in both the weak and stronger coupling regimes, for both spectral densities variations (although we only show the overdamped case here). The RC treatment captures qualitatively the correct behaviour but over estimates the damping of the oscillations in the real part of the coherence of the TLS, and this is more pronounced as the coupling is turned up.

A hint as to the reason for this breakdown can be found in the fact that even at weak coupling a disparity is seen. At strong coupling, it is clear that a weak coupling treatment of an open

quantum system will fail because an appreciable interaction between system and environment will invalidate the assumption that the environment remains unchanged and uncorrelated from the system at all times. But even at weak coupling, in a low temperature regime, one can imagine that small disturbances to the environment may remain longer lived than they would at higher temperatures when the environment rethermalises quickly on the scale of the system dynamics.

We can check this by looking at the self-correlation functions of the residual environment E', given by

$$D^+(\tau) = \int_0^\infty J_{RC}(\omega)\coth(\frac{\beta\omega}{2})\cos(\omega\tau), \tag{2.97}$$

$$D^-(\tau) = \mathrm{i}\int_0^\infty J_{RC}(\omega)\sin(\omega\tau). \tag{2.98}$$

Inserting $J_{RC}(\omega) = \gamma\omega\exp(\frac{-\omega}{\Lambda})$ for the spectral density in the RC picture, we can simplify these expressions and investigate how they behave for different residual environment temperatures (which we always take to be the same temperature as the environment in the original picture). The expression for D^- becomes

$$D^-(\tau) = \mathrm{i}\int_0^\infty \gamma\omega\exp(\frac{-\omega}{\Lambda})\sin(\omega\tau) = \frac{2\gamma\Lambda^3\tau}{(1+\Lambda^2\tau^2)^2}, \tag{2.99}$$

which in the limit $\Lambda \to \infty$ tends to zero. The expression for D^+ may be separated into vacuum and thermal contributions of the form

$$D^+(\tau) = D^+_{vac}(\tau) + D^+_{th}(\tau), \tag{2.100}$$

$$D^+_{vac}(\tau) = \int_0^\infty \gamma\omega\exp(\frac{-\omega}{\Lambda})\cos(\omega\tau), \tag{2.101}$$

$$D^-_{th}(\tau) = \int_0^\infty \gamma\omega\exp(\frac{-\omega}{\Lambda})\left[\coth(\frac{\beta\omega}{2}) - 1\right]\cos(\omega\tau). \tag{2.102}$$

In the same infinite cut-off limit $\Lambda \to \infty$ the expression for D^+_{vac} tends to $\frac{-\gamma}{\tau^2}$ and the expression for D^+_{th} tends to $\gamma(\frac{1}{\tau^2} - \frac{\pi^2\mathrm{cosech}^2(\frac{\pi\tau}{\beta})}{\beta^2})$. The vacuum part therefore cancels out and we are inter-

ested in the behaviour of the expression $-\frac{\pi^2 \text{cosech}^2(\frac{\pi\tau}{\beta})}{\beta^2}$. We plot the modulus of this expression in figure 2.9 for different inverse temperatures. As $\beta \to \infty$ this expression tends to $-\frac{1}{\tau^2}$ and as the temperature increases the correlation function becomes more and more delta-function-like.

The Born-Markov approximations are valid in the limit of short lived environment self-correlation functions and as the temperature decreases and these become longer lived, these same approximations made with regards to the mapped environment will cause the RC master equation to yield results which correspond less well to the exact solution for the independent boson model.

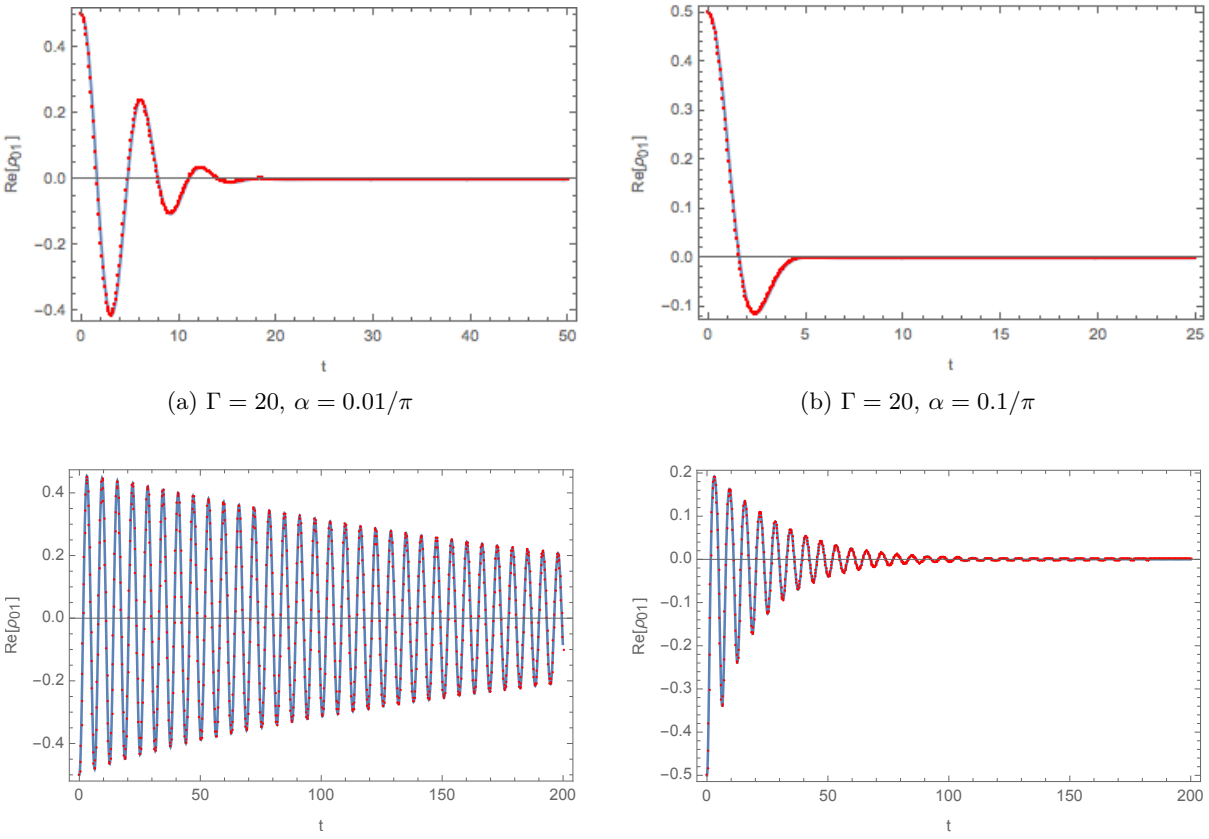

(a) $\Gamma = 20$, $\alpha = 0.01/\pi$

(b) $\Gamma = 20$, $\alpha = 0.1/\pi$

(c) $\Gamma = 0.1$, $\alpha = 0.01/\pi$

(d) $\Gamma = 0.1$, $\alpha = 0.01/\pi$

Figure 2.6: Real part of the coherence ρ_{01} of the TLS density operator undergoing pure dephasing according to the independent boson model. The red dots are obtained using the RC method and the blue curve is computed from the exact solution. The TLS is initialized in the $|+\rangle$ state for the overdamped case in (a) and (b), and the $|-\rangle$ state for the underdamped case in (c) and (d). (a) and (c) display the case for weak coupling, while (b) and (d) the strong coupling behaviour. Parameters: $\epsilon = 1$, $\omega_0 = 1$, $\beta = 0.95$. We see that the RC solution agrees well with the exact dynamics and both weak and strong system-reservoir coupling.

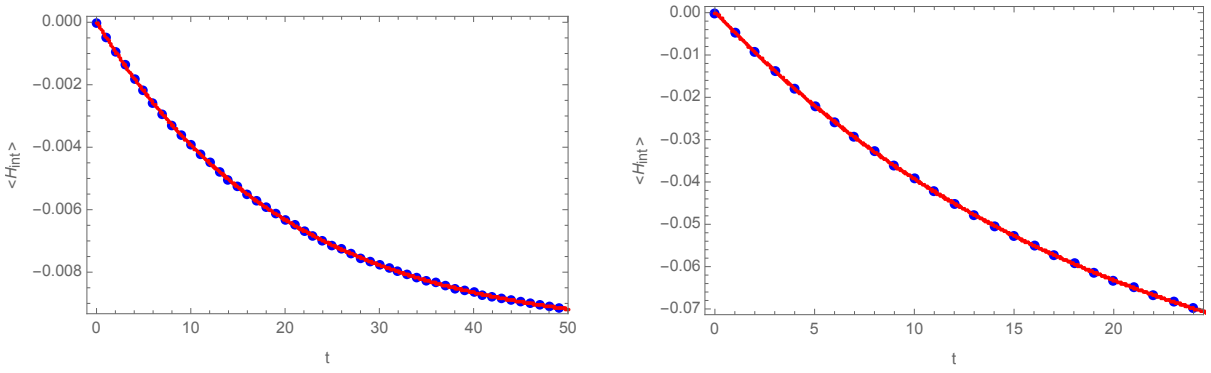

(a) $\alpha = 0.01/\pi$ (b) $\alpha = 0.1/\pi$

Figure 2.7: Interaction energy computed exactly, red curve, as well as within the RC framework, blue dots. Parameters: $\epsilon = 1$, $\omega_0 = 1$, $\Gamma = 20$, $\beta = 0.95$. We see that the interaction energy computed according to the RC framework agrees well with the exact result.

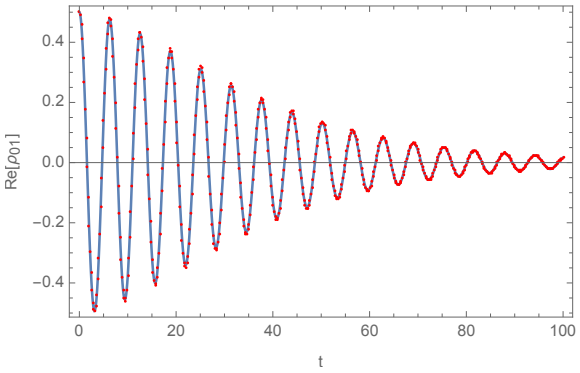

(a) $\alpha = 0.01/\pi$, $\beta = 20$.

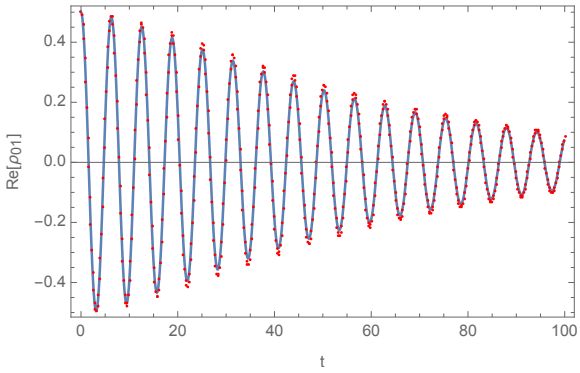

(b) $\alpha = 0.01/\pi$, $\beta = 40$

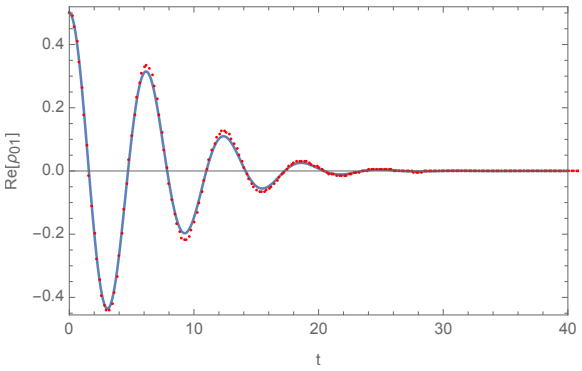

(c) $\alpha = 0.1/\pi$, $\beta = 20$.

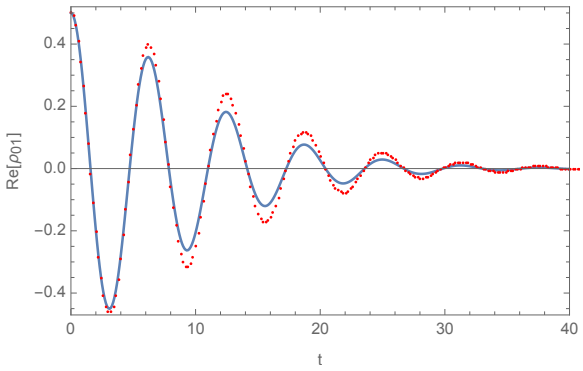

(d) $\alpha = 0.1/\pi$, $\beta = 40$.

Figure 2.8: Real part of the coherence ρ_{01} of the TLS density operator undergoing pure dephasing according to the independent boson model at cold temperatures. The red dots are obtained using the RC method and the blue curve is computed from the exact solution. The TLS is initialized in the $|+\rangle$ state and (a), (b) show the case for weak coupling, while (c), (d) show the strong coupling case. Parameters: $\epsilon = 1$, $\omega_0 = 1$, $\Gamma = 20$. At very low temperatures, we do not obtain as good an agreement between results computed according the RC treatment and the exact result.

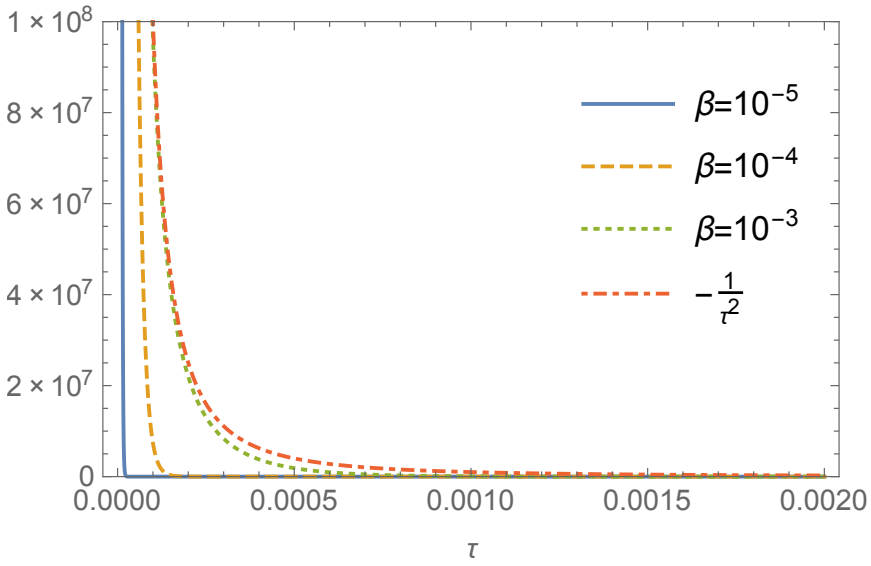

Figure 2.9: The residual environment self-correlation functions versus time τ for different inverse temperatures β. At very low temperatures, the self-correlation functions are lower lived and less delta function like. For a Markovian approximation to be valid on the environment, one requires that the self-correlation functions are close to delta functions.

Chapter 3

Quantum heat engines at strong coupling

3.1 Introduction

The theory of thermodynamics emerged in the early nineteenth century as a result of efforts within the scientific community to evaluate the performance of steam engines, designed for the purpose of converting a source of energy in terms of heat flow into useful energetic output in terms of mechanical work. Sadi Carnot's result [20] that the second law of thermodynamics may be understood in terms of an ultimate bound on the efficiency of any device which converts heat into work serves as a testament to the seminal role played by the study of heat engines in the formulation of the classical theory thermodynamics as we understand it today, exemplified by its ever prominent role in foundational texts on the subject [21]. With eloquence befitting his status as a pioneer in the development of one of the pillars of classical physics he motivates the study of heat engines in 1824 by writing:

> "C'est à la chaleur que doivent être attribués les grands mouvements qui frappent nos regards sur la terre... les agitations de l'atmosphère, l'ascension des nuages,

> la chute des pluies et des autres météores, les courants d'eau... les tremblements de terre, les éruptions volcaniques... C'est dans cet immense réservoir que nous pouvons puiser la force mouvante nécessaire à nos besoins; la nature... nous a donné la faculté de faire naître en tous temps et en tous lieux la chaleur et la puissance motrice qui en est la suite. Développer cette puissance, l'approprier à notre usage, tel est l'objet des machines à feu."

"Heat is the cause of all that we find striking on this planet: rumblings in the atmosphere, cloud formation, rainfall and other meteorological events, the flow of water, earthquakes, volcanic eruptions," he writes. "We have the ability to extract the mechanical work sufficient for our needs from this immense reservoir and moreover, nature has given us the power to create heat and consequently its motive power anywhere and at any time we like. Developing this power and appropriating it to our needs, such is the goal of heat engines."

It is remarkable that two centuries later, in many regards motivations for studying classical heat engines remain unchanged, although authors of papers published on this topic are perhaps suitably more modest in their eloquence on the subject. The mitigation of friction and improvement of engine efficiency are still at the forefront of theoretical research today [22, 23], with the ultimate goal of extracting more useful work output to meet our needs for the price of less heat energy.

As technology advances apace, devices of the twenty-first century have been decreasing in size. Quantum technology is already present in many modern day devices and with the advent of nanoscale devices like the quantum computers of the near future, it is generally well-accepted within the research community that nanoscale heat engines will be required to power or, when run in reverse, to efficiently dissipate the heat these devices generate into the environment at the price of some invested work cost. In this regard, there are similar motivations for studying a quantum version of the classical heat engine models studied by Carnot and his contemporaries: how can we engineer these devices to be as efficient as possible? How can we maximise their power output or refrigeration power?

On the other hand, there is, in addition to the practical motivations discussed above, a more fundamental reason for studying quantum versions of heat engines. Just as they served as a seminal influence on the formulation of the classical theory of thermodynamics, they can serve as a means for investigating a quantum version of thermodynamics. Classical thermodynamics emerged as a phenomenological set of laws governing the energetic exchanges between systems whose constituent particle number tends to infinity. As systems scale down, in the quantum setting, very often one deals with just a small number of particles, sometimes even just one. As fervour within the research community has intensified in the field of quantum thermodynamics over the recent decades, it was not expected that thermodynamic laws would, a priori, apply in this setting, with perhaps new thermodynamic effects emerging at the quantum scale. Remarkably, however, in settings which reflect the spirit of classical thermodynamics, but with small quantum systems as the working fluid, it transpires that the laws of thermodynamics do indeed constrain the operation of heat engines [24, 25, 26, 27, 28].

That is not to say that novel quantum thermodynamic effects have not been seen. It is well known that real classical heat engines, operating in finite time rather than the idealised reversible conditions assumed in the Carnot setting, suffer from friction and heat leaks. In finite time quantum heat engines, an entirely new type of friction has been discovered which is purely quantum mechanical in its nature [29, 30, 31], and research into how to mitigate these losses has ensued [32, 33, 34]. It has even been shown that in certain situations improved engine performance can be achieved through clever use of certain quantum resources [35, 36], and in some cases even violate classical thermodynamic bounds [37, 38]. However, these treatments usually make use of a setting beyond which the laws of thermodynamics would typically apply, for example non-thermal heat reservoirs [37, 38] or systems out of thermal equilibrium [39].

Much of the research to date on quantum mechanical models of heat engines has been focused on the weak coupling regime [40, 41, 42, 27, 43, 37, 44]. The reasons for this restriction are twofold. The analysis of the engine cycle is greatly simplified when one can treat the strokes of the engine during which it is coupled to a heat reservoir using the Lindblad theory of weak coupling master equations under the Born-Markov assumptions. The second reason follows

from the first: under a Born-Markov treatment the working quantum system and heat reservoir quantum states remain separable at all times, making distinguishing energy flows in terms of heat and work less problematic [45]. Developing an understanding of whether and how thermodynamic treatments may be modified to apply beyond this regime is both of fundamental and practical importance. Nanoscale devices are already able to operate in the strong coupling regime [46, 47, 48, 49, 50, 9, 51] and quantum heat machines have been proposed which have exciting practical applications, such as in laser cooling [52, 53].

Identifying consistent definitions of heat, work, and internal energy in the strong coupling regime has been the subject of recent research [54, 45, 55, 56], as well as whether the second law can be formulated in a regime beyond weak coupling via the means of fluctuation relations [57, 58, 59] or bounds on entropy production [60, 61, 62, 63]. Yet a consistent approach to tackling thermodynamic cycles when strong system-reservoir interactions are present is still lacking, despite some recent efforts involving continuously coupled engines [64, 15, 65] or single stroke work extraction processes from a single reservoir [66].

In this chapter, we turn our attention therefore to heat engine analysis in the strong coupling regime. We will look at how non-negligible system-reservoir interactions affect the operation of the traditional theoretical reversible equilibrium heat engine which operates in an infinite time cycle. In chapter 4 we will turn our attention to the non-equilibrium and finite time case. The work presented in this chapter was published in Ref [16].

3.2 Equilibrium quantum heat engine

Quantum, as well as classical, heat engines come in many different flavours and can be classified according to their different ordering of strokes which involve an interaction between the working system and strokes which involve the extraction of work. Broadly speaking there are three different classifications: four-stroke, two-stroke and continuous engines. We will focus here on a quantum heat engine operating in a four-stroke Otto cycle. We make this choice for several reasons. Firstly, there have been several previous studies of quantum Otto cycles in the

weak coupling regime [41, 42, 27, 43, 37, 44] with various results ranging from those analogous to classical thermodynamic bounds [27], to interesting violations thereof [37]. A comparison between the strong coupling version of this cycle and its weakly coupled counterpart is clearly therefore topically relevant at present. The second reason for our choice is that the Otto cycle makes a clear distinction between separate strokes where either work is extracted from (or done on) the system, or where energy is exchanged between the system and the reservoirs. In such a way, we can circumvent any debate concerning the definition of heat and work in the quantum regime, since our intention is to focus our discussion on the effects of strong coupling on such cycles, rather than any issues concerning such definitions.

3.2.1 Otto cycle model

The working fluid for our heat engine will be a two-level quantum system (TLS) with ground and excited states $|g\rangle$ and $|e\rangle$, eigenstates of a self-Hamiltonian H_S. We label as μ the energy gap between these two states. The thermodynamic Otto cycle for the TLS is schematically depicted in Figure 3.1. It consists of the following four strokes:

- *Hot isochore* $A' \to B$: At point A' the system is coupled to a hot reservoir R_h, which is at thermal equilibrium at temperature T_h. The global state of system plus reservoir equilibrates and reaches a steady state at point B. During the stroke H_S remains fixed with energy gap labelled μ_h. In standard treatments of the cycle, this would be where the stroke ends but this is because it is common to ignore the final step where the system is decoupled from the reservoir ($B \to B'$). We choose to make this step explicit in our treatment because, at non-negligible system-reservoir interaction strength, there is an energetic cost associated with it which needs to be evaluated.

- *Isentropic expansion* $B' \to C$: The energy gap between the two eigenstates of H_S is changed from μ_h to μ_c with $\mu_c < \mu_h$, while the system remains closed. At point C, the system is coupled to a cold reservoir R_c, which is at thermal equilibrium at temperature T_c. This finishes the stroke at point C'.

- *Cold isochore* $C' \to D$: The global state of system plus reservoir equilibrates and reaches a steady state at point D while H_S remains fixed with energy splitting μ_c. The system is then decoupled from the cold reservoir to reach point D'.

- *Isentropic compression* $D' \to A$: The energy gap between the two eigenstates of H_S is changed back from μ_c to μ_h, while the system remains closed. The system is then coupled to the hot reservoir, reaching point A', and the cycle begins again.

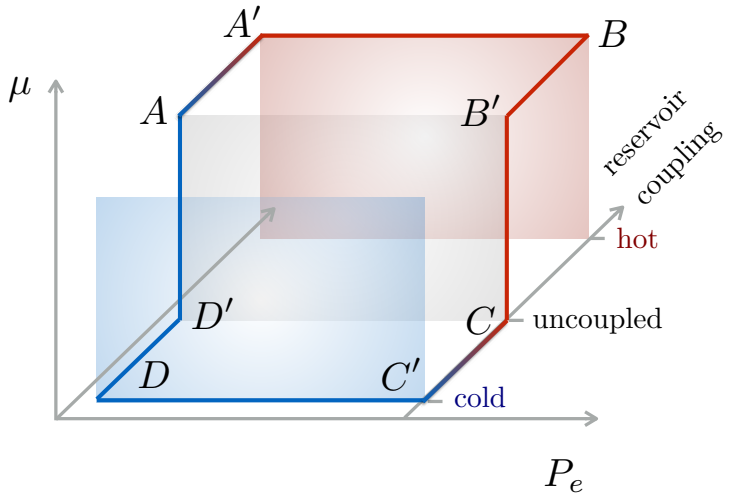

Figure 3.1: The Otto cycle for a two-level quantum system as a working fluid, with ground state $|g\rangle$ and excited state $|e\rangle$. We plot on the vertical axis the energy gap between the ground and excited state, labeled μ, and on the horizontal axis the population of the excited state P_e. The third axis running into the page schematically represents the three possible configurations of the system: uncoupled from any reservoirs, coupled the hot reservoir at temperature T_h or coupled to the cold reservoir at temperature T_c. The standard four strokes of the cycle are hot isochoric thermalisation $A' \to B$, isentropic expansion $B' \to C$, cold isochoric thermalisation $C' \to D$, and isentropic compression $D' \to A$. Here, we expand the cycle to explicitly include steps where the system-reservoir interactions are switched on or off: coupling to the hot reservoir $A \to A'$, decoupling from the hot reservoir $B \to B'$, coupling to the cold reservoir $C \to C'$, and decoupling from the cold reservoir $D \to D'$. This figure is reproduced from Ref. [16].

We model each reservoir as a system of harmonic oscillators, each of which is coupled to the central working TLS (when the interaction is on) but which do not interact with each other. This model of a central spin interacting with a bath of harmonic oscillators is typically referred to as the spin-boson model. It serves as a paradigmatic model in the study of dissipation in open quantum systems [7]. Examples of its application range from decoherence in biological systems [8] to semiconductor quantum dots [67, 68]. Setting $\hbar = 1$ throughout, we write the

TLS internal energy as

$$H_S(t) = \frac{\mu(t)}{2} I + \frac{\epsilon(t)}{2}\sigma_z + \frac{\Delta(t)}{2}\sigma_x, \tag{3.1}$$

where $\epsilon(t)$ represents the TLS bias, $\Delta(t)$ the tunnelling matrix element, $\sigma_{x,z}$ denote the usual Pauli matrices, and I is the identity. The eigenstates of H_S are associated with eigenvalues 0 and $\mu(t)$, where

$$\mu(t) = \sqrt{\epsilon^2(t) + \Delta^2(t)}. \tag{3.2}$$

The first term in Eq. (3.1), proportional to the identity, serves therefore to provide a time-dependent shift of the system energy scale such that the ground state energy is always set to zero. Because the cycle is periodic and energy conserved, the work output and total heat dissipated into each reservoir is unaffected by its presence. We use it to arrive at an unambiguous definition of positive work as that done on the system during the relevant isentropic strokes. Negative work is therefore work extracted from the system. The remaining terms are typical in spin-boson models employed for the analysis of, for example, quantum dots, superconducting circuits or spins in magnetic fields [48, 49, 50, 9, 69, 70].

We now proceed by assuming that the TLS couples to each harmonic oscillator of a reservoir via its position x_k. If there are k oscillators, each with a different natural frequency ω_k and mass m_k, we may write down the following general form for the kinetic and potential energy of a reservoir:

$$H_{SR} = \sum_k \frac{{p_k}^2}{2m_k} + \frac{m_k {\omega_k}^2}{2}\left(x_k - \frac{d_k}{m_k {\omega_k}^2}\sigma_z\right)^2. \tag{3.3}$$

Here, p_k is the momentum of oscillator k, d_k denotes the coupling parameters for the interaction between the TLS and this bosonic field and σ_z is the usual Pauli operator acting on the TLS subspace. We may decompose Eq. (3.3) into more familiar reservoir Hamiltonian and interaction terms by defining creation and annihilation operators $b_k^\dagger$ and b_k for excitations in each harmonic oscillator. These must satisfy $x_k = (1/2m_k\omega_k)^{1/2}(b_k^\dagger + b_k)$ and $p_k = i(m_k\omega_k/2)^{1/2}(b_k^\dagger - b_k)$. Using labels h and c to distinguish between the hot and cold reservoirs R_h and R_c, and defining creation and annihilation operators $c_k^\dagger$ and c_k in the same way for the cold reservoir, the self-Hamiltonians

for the reservoirs are then given by

$$H_{R_h} = \sum_k \omega_k^h (b_k^\dagger b_k + 1/2), \tag{3.4}$$

$$H_{R_c} = \sum_q \omega_q^c (c_q^\dagger c_q + 1/2). \tag{3.5}$$

The interaction terms describing the coupling between the TLS and each reservoir, with all constants incorporated into $f_k^h \equiv \frac{d_k}{\sqrt{m_k^h \omega_k^h}}$ and $f_q^c \equiv \frac{d_q}{\sqrt{m_q^c \omega_q^c}}$, may then be written

$$H_{I_h} = -\sigma_z \sum_k f_k^h (b_k^\dagger + b_k) + \sum_k \left(f_k^h\right)^2 / \omega_k^h, \tag{3.6}$$

$$H_{I_c} = -\sigma_z \sum_q f_q^c (c_q^\dagger + c_q) + \sum_q \left(f_q^c\right)^2 / \omega_q^c. \tag{3.7}$$

Summing equations (3.1), (3.4), (3.5), (3.6) and (3.7) gives the full Hamiltonian incorporating the self-energy of the TLS and each reservoir as well as all interaction energy terms:

$$H(t) = H_S(t) + H_{R_h} + H_{R_c} + H_{I_h} + H_{I_c}. \tag{3.8}$$

In practice, only one set of either hot or cold reservoir terms will be present at a time, according to which isochore stroke is being treated. In the following, we shall omit terms in the reservoir and interaction Hamiltonians proportional to the identity as they do not contribute when evaluating a complete engine cycle, nor help in defining sign conventions as was the case for $H_S(t)$.

3.2.2 A brief aside on applying the reaction coordinate formalism to a heat engine

The RC formalism for treating non-negligible system-reservoir interactions was discussed in depth in chapter 2. But let us briefly review the salient features in order to make the treatment of this heat engine self-contained. Recall that we apply a unitary mapping of the full system-reservoir Hamiltonian, which results in an enlarged system S', consisting of the TLS and the

RC, a single collective degree of freedom of the environment, which interact strongly. There are then terms which describe the weak interaction between the RC and a redefined residual environment E'.

Restricting ourselves to a single reservoir for the time being for simplicity, and therefore dropping the h or c labels, the Hamiltonian in the original picture is given by

$$H = \frac{\mu(t)}{2} I + \frac{\epsilon(t)}{2}\sigma_z + \frac{\Delta(t)}{2}\sigma_x + \sum_k \omega_k b_k^\dagger b_k - \sigma_z \sum_k g_k (b_k^\dagger + b_k), \tag{3.9}$$

where we have ignored terms in the reservoir and interaction Hamiltonians which are proportional to the identity as previously stated. We characterise the system-reservoir interaction by means of the reservoir spectral density [7] defined as

$$J(\omega) \equiv \sum_k g_k^2 \delta(\omega - \omega_k). \tag{3.10}$$

In practice, we make the model tractable by taking the continuum limit for the bath oscillators, and by employing the following functional form of the spectral density for each reservoir,

$$J(\omega) = \frac{\alpha \omega \omega_c}{\omega^2 + \omega_c^2}, \tag{3.11}$$

where α is the coupling strength and ω_c is a cutoff frequency.

We define a creation operator acting on the RC subspace $a^\dagger = (1/\lambda)\sum_k g_k b_k^\dagger$, satisfying bosonic commutation relations, with $\lambda = \sqrt{\sum_k g_k^2}$. The interaction term in equation (3.9) may now be rewritten as

$$H_I = -\sigma_z \sum_k g_k (b_k^\dagger + b_k) = -\lambda \sigma_z (a^\dagger + a). \tag{3.12}$$

The reservoir Hamiltonian is rewritten as

$$H_R = \sum_k \omega_k b_k^\dagger b_k = \Omega a^\dagger a + \sum_k f_k (a^\dagger + a)(r_k^\dagger + r_k) + \sum_k \nu_k r_k^\dagger r_k. \tag{3.13}$$

The TLS terms in the Hamiltonian remain unchanged. The full Hamiltonian therefore maps to

$$\tilde{H}(t) = \frac{\mu(t)}{2} I + \frac{\epsilon(t)}{2}\sigma_z + \frac{\Delta(t)}{2}\sigma_x - \lambda\sigma_z(a^\dagger + a) + \Omega a^\dagger a + \sum_k f_k(a^\dagger + a)(r_k^\dagger + r_k) + \sum_k \nu_k r_k^\dagger r_k. \tag{3.14}$$

Here, the RC has natural frequency Ω, it couples to the system with strength λ, and to the residual environment via g_k, whose oscillator excitations at natural frequency ν_k are created (annihilated) by $r_k^\dagger$ (r_k).

The procedure for finding a functional form in the continuum limit for the spectral density function $\tilde{J}(\omega) \equiv \sum_k f_k^2 \delta(\nu - \nu_k)$ characterising the coupling between the enlarged system S' and the residual bath E', as well as the parameters Ω and λ, has been discussed previously in chapter 2. It results in the following definitions

$$\Omega = 2\pi\gamma\omega_c, \tag{3.15}$$

$$\lambda = \sqrt{\frac{\pi\alpha\Omega}{2}}, \tag{3.16}$$

$$\tilde{J}(\omega) = \gamma e^{-\omega/\Lambda}. \tag{3.17}$$

γ is a free parameter and we choose to set $\gamma = \frac{\sqrt{\epsilon^2+\Delta^2}}{2\pi\omega_c}$ as in Ref. [13]. The cutoff frequency Λ is eventually taken to infinity and this results in the original form of the spin-boson spectral density being represented accurately post mapping.

We may now employ the same strategy as that outlined in chapter 2 whereby a standard Born-Markov treatment [1] of the enlarged open quantum system S' yields a second order master equation which captures strong coupling between the TLS and the RC exactly, while only the weakly coupled residual environment is traced out. We may solve this numerically to obtain the dynamics of S' (and subsequently the TLS if we trace out the RC degrees of freedom). We truncate the number of RC basis states, labelled n here, at a size sufficient to ensure convergence in the metrics of the engine (work, heat, efficiency). In a standard treatment of the isochoric strokes, non-Markovian and strong reservoir coupling effects preclude second order

(i.e. Born-Markov) expansions in the original unmapped representation but we have seen how this combination of Hamiltonian mapping and second order master equation is capable of very accurately capturing both the TLS dynamics and steady-states over a wide range of parameters. Furthermore, the mapping also renders properties of the reservoir accessible through the RC itself. As such, we are able to track system-reservoir correlations, which are very often not accessible through other open systems approaches. We shall see how this is crucial in studying the heat engine at strong coupling in the following sections. It enables a tractable analysis of the Otto cycle to be formulated in terms of the full system-reservoir Hamiltonian, including interactions and the resulting correlations.

Particularly important in the context of the heat engine treatment is the global equilibrium state of the correlated TLS and reservoir at the end of each isochore. We can approximate this using the steady state solution of the master equation governing the dynamics of S', which is given by a thermal state of the mapped system Hamiltonian

$$\tilde{H}_{S'} \equiv \frac{\mu(t)}{2} I + \frac{\epsilon(t)}{2}\sigma_z + \frac{\Delta(t)}{2}\sigma_x - \lambda\sigma_z(a^\dagger + a) + \Omega a^\dagger a, \tag{3.18}$$

as

$$\tilde{\rho}_{S'} = \frac{\exp\left(-\beta\tilde{H}_{S'}\right)}{\mathrm{tr}\left[\exp\left(-\beta\tilde{H}_{S'}\right)\right]}, \tag{3.19}$$

where $\beta = 1/k_B T$ is the inverse temperature of the reservoir to which the system is coupled for that particular isochore. The global state is then approximately given by

$$\tilde{\rho} \approx \tilde{\rho}_{S'} \otimes \tilde{\rho}_{E'} \tag{3.20}$$

where

$$\tilde{\rho}_{E'} = \frac{\exp(-\beta\tilde{H}_{E'})}{\mathrm{tr}[\exp(-\beta\tilde{H}_{E'})]}, \tag{3.21}$$

is a Gibbs thermal state of the residual environment with $\tilde{H}_{E'} = \sum_k \nu_k r_k^\dagger r_k$. The reduced state of the TLS can be obtained by performing a partial trace over the RC degrees of freedom such

that $\rho_S = \mathrm{tr}_{RC+E'}[\tilde{\rho}] = \mathrm{tr}_{RC}[\tilde{\rho}_{S'}]$. In general this does not take the form of a canonical Gibbs thermal state since there are correlations between the system and reservoir accrued via their non-negligible interactions. Eqs. (3.19) and (3.20) are central to the analysis of the generalised Otto cycle beyond weak coupling assumptions, which follows this section.

To illustrate this, we consider the energy expectation with respect to the full Hamiltonian

$$\langle H \rangle = \mathrm{tr}[H\rho], \tag{3.22}$$

where H is given by Eq. (3.9) and $\rho = \exp(-\beta H)/\mathrm{tr}[\exp(-\beta H)]$ is a thermal state of the interacting system and reservoir in the original representation. Such a calculation is necessary at points B and D of the cycle as described in section 3.2.1 as a key ingredient in calculating work and heat around the cycle. Eq. (3.22) is difficult to evaluate if a factorisation assumption between the system and reservoir is not made. However, under the RC treatment it becomes

$$\langle H \rangle = \mathrm{tr}[\tilde{H}\tilde{\rho}] \approx \mathrm{tr}[\tilde{H}_{S'}\tilde{\rho}_{S'}] + \mathrm{tr}[\tilde{H}_{E'}\tilde{\rho}_{E'}], \tag{3.23}$$

where we have used Eq. (3.20) for the mapped density operator and the fact that $\mathrm{tr}[\sum_k f_k(a^\dagger + a)(r_k^\dagger + r_k)\tilde{\rho}_{E'}] = 0$. The average energy of the interacting system and reservoir therefore simplifies into a sum of thermal expectations for the enlarged mapped system Hamiltonian and the residual bath. The natural boundary this method draws between the system and reservoir is also intuitively appealing as it provides a link to standard thermodynamics but at finite coupling strength: the residual environment provides a well defined temperature, serving as the textbook static thermal reservoir employed in traditional thermodynamic treatments of heat engines as a reference for energy absorption and dissipation even at strong coupling.

3.2.3 Generalised Otto Cycle Analysis

We now present a detailed analysis of the Otto cycle by considering energetic changes with respect to the full system-reservoir Hamiltonian H and global state, which we will label χ. Doing

so allows us to go beyond weak system-reservoir coupling and vanishing correlations. Using the RC formalism, we will derive expressions which may be evaluated for arbitrary interaction strength but will simplify to standard weak coupling forms when the assumption of fully factorising TLS-reservoir states is permitted. Let us now go through the cycle stroke by stroke, as described in section 3.2.1.

Hot isochore

The cycle is periodic and we are treating here the equilibrium version of the cycle, where the isochoric strokes are run for a theoretical infinite time such that full equilibration can occur. Therefore we may choose any starting point for our treatment without loss of generality. We consider starting at point A' in figure. 3.1. The interaction between the system and the hot reservoir has just been switched on. We assume this happens instantaneously. The interaction with the cold reservoir is not present and the Hamiltonian along the isochore is given by

$$H = H_S^{A'} + H_{R_h} + H_{R_c} + H_{I_h}, \tag{3.24}$$

where

$$H_S^{A'} = \frac{\mu_h}{2} I + \frac{\epsilon_h}{2}\sigma_z + \frac{\Delta_h}{2}\sigma_x, \tag{3.25}$$

with superscripts labelling the points around the cycle. We have $H_S^B = H_S^{A'}$ since the stroke involves no source of external work. At the end of the stroke (point B) the full state of the system and both reservoirs χ^B has relaxed to equilibrium such that it might be written as

$$\chi^B = \rho_h \otimes \rho_{R_c}. \tag{3.26}$$

Here

$$\rho_h = \frac{\exp\left[-\beta_h\left(H_S^B + H_{R_h} + H_{I_h}\right)\right]}{\mathrm{tr}\left\{\exp\left[-\beta_h\left(H_S^B + H_{R_h} + H_{I_h}\right)\right]\right\}} \tag{3.27}$$

is the equilibrium state of the interacting TLS and hot reservoir and ρ_{R_c} represents the state of the uncoupled cold reservoir. We write this in factorised form making the assumption that

there are no correlations between the system and the cold reservoir at this stage in the cycle. This implies that while a reservoir is uncoupled from the TLS it returns to its uncorrelated thermal Gibbs state at the appropriate temperature. One could imagine that we have access to two further large infinite thermal reservoirs for the purpose of returning the uncoupled ones to their thermal states.

For a non-negligible interaction term H_{I_h}, the density matrix of the system and hot reservoir ρ_h is difficult to evaluate using standard open quantum systems techniques. Employing the RC formalism, and in particular Eq. (3.20), we may write

$$\rho_h \approx \frac{\exp(-\beta_h \tilde{H}^B_{S'})}{\mathrm{tr}[\exp(-\beta_h \tilde{H}^B_{S'})]} \otimes \tilde{\rho}_{E'_h} = \tilde{\rho}_{S'_h} \otimes \tilde{\rho}_{E'_h}, \tag{3.28}$$

which is more tractable since we have reduced the full environment of the hot reservoir to an effective single oscillator correlated with the TLS. The residual environment is now uncorrelated with the enlarged system and remains factorisable: $\tilde{\rho}_{E'_h}$ is a thermal state of the hot reservoir residual environment (self Hamiltonian $\tilde{H}_{E'_h}$) at inverse temperature $\beta_h = 1/k_B T_h$. The Hamiltonian for the enlarged system S' appearing in this equation is given by

$$\tilde{H}^B_{S'} = H^B_S - \lambda_h \sigma_z (a^\dagger_h + a_h) + \Omega_h a^\dagger_h a_h, \tag{3.29}$$

which includes a RC for the hot reservoir, with natural frequency Ω_h and creation (annihilation) operators $a^\dagger_h$ (a_h).

We wish to evaluate the average energy at the end of the stroke, point B, as this is the quantity needed for a final calculation of the heat dissipated and work extracted around the full cycle. This is done by taking the trace of the Hamiltonian with the full state $\chi^B = \rho_h \otimes \rho_{R_c}$:

$$\begin{aligned} \langle H \rangle^B &= \mathrm{tr}\left[\left(H^B_S + H_{R_h} + H_{R_c} + H_{I_h}\right) \rho_h \otimes \rho_{R_c}\right] \\ &= \mathrm{tr}\left[\tilde{H}^B_{S'} \tilde{\rho}_{S'_h}\right] + \mathrm{tr}\left[\tilde{H}_{E'_h} \tilde{\rho}_{E'_h}\right] + \mathrm{tr}\left[H_{R_c} \rho_{R_c}\right]. \end{aligned} \tag{3.30}$$

In the second line we have used Eq. (3.28), as in the example of Eq. (3.23). We can distinguish

correlated contributions in the first term in the second line of Eq. (3.30) from uncorrelated contributions in the second term, which depend only on the residual thermal bath and will cancel out in the full cycle analysis. The presence of the residual thermal bath is still important, however, as it provides a reference against which we can define energy absorption along the hot isochore. The third term in Eq. (3.30) is the internal energy of the cold reservoir and we recall that we assume both reservoirs re-thermalise when uncoupled from the system. In this way, each reservoir is initially in a thermal equilibrium state at a well-defined temperature whenever the coupling with the TLS is turned on. Correlations are then generated along the subsequent isochore. ρ_{R_c} is therefore taken to be a Gibbs thermal state at inverse temperature $\beta_c = 1/k_B T_c$ at this point:

$$\rho_{R_c} = \rho_{th_c} = \frac{\exp(-\beta_c H_{R_c})}{\mathrm{tr}[\exp(-\beta_c H_{R_c})]}. \tag{3.31}$$

In the standard treatments of the cycle, one assumes that the interaction is weak enough that one may treat the isochores according to a Born-Markov master equation. One therefore makes the approximation that the full state remains separable at all times with each reservoir in a thermal state at its given temperature. In other words, the state ρ_h is given by a tensor product of the system state ρ_{S_h} and the hot reservoir state ρ_{th_h}. Each state is of canonical Gibbs form with respect to the relevant self-Hamiltonian. For the TLS, this yields

$$\rho_{S_h} = \frac{\exp\left(-\beta_h H_S^B\right)}{\mathrm{tr}\left[\exp\left(-\beta_h H_S^B\right)\right]}, \tag{3.32}$$

with H_S^B defined in Eq. (3.25), and for the hot reservoir we have

$$\rho_{th_h} = \frac{\exp(-\beta_h H_{R_h})}{\mathrm{tr}[\exp(-\beta_h H_{R_h})]}. \tag{3.33}$$

We note that both of these states are diagonal with respect to their respective self-Hamiltonians and therefore contain no coherence in the relevant energy eigenbases. Using equations (3.1) and (3.2) for the system Hamiltonian, the expression for the average energy at weak coupling then

simplifies to

$$\langle H\rangle^{B}_{weak} = \frac{\mu_h}{2}\left[1-\tanh\left(\frac{\mu_h}{2k_BT_h}\right)\right] + \langle H_{R_h}\rangle_{th} + \langle H_{R_c}\rangle_{th}, \tag{3.34}$$

where we denote the reservoir thermal expectations by $\langle H_{R_i}\rangle_{th} = \mathrm{tr}[H_{R_i}\rho_{th_i}]$, for $i = h, c$. We see, in this way, that standard weak coupling results can be recovered from the RC version when further separability assumptions, relying on negligible coupling, are made.

We then turn off the interaction between the TLS and the hot reservoir. We need to consider explicitly any cost associated with this step. To do so we define the point after decoupling as B' and denote the corresponding Hamiltonian as

$$H^{B'} = H^{B}_{S} + H_{R_h} + H_{R_c}. \tag{3.35}$$

The average energy of the total system $\chi_{B'}$ is then given by

$$\langle H\rangle^{B'} = \mathrm{tr}\left[\left(H^{B}_{S} + H_{R_h} + H_{R_c}\right)\chi^{B'}\right]. \tag{3.36}$$

We assume H_{I_h} is switched off instantaneously. The full state has no time to change between points B and B', $\chi^{B'} = \chi^{B} = \rho_h \otimes \rho_{th_c}$, and the work associated with this step is given by the change in average energy

$$\langle H\rangle^{B'} - \langle H\rangle^{B} = -\mathrm{tr}\left[H_{I_h}\rho_h\right]. \tag{3.37}$$

In a weak coupling treatment $\rho_h = \rho_{S_h}\otimes\rho_{th_h}$ and equation (3.37) for the energetic cost associated with decoupling from the environment evaluates exactly to zero because $\mathrm{tr}\left[H_{I_h}\rho_h\right] = 0$ when the reservoir state is diagonal with respect to its self-Hamiltonian. At finite coupling, however, the RC approach yields the state given by equation (3.28) and we obtain

$$\langle H\rangle^{B'} - \langle H\rangle^{B} = \lambda_h \mathrm{tr}\left[\sigma_z(a^{\dagger}_h + a_h)\tilde{\rho}_{S'_h}\right], \tag{3.38}$$

which is generally non-zero. This work contribution associated with decoupling must be included

in the cycle analysis. If this contribution were negative, then we would gain a certain amount of extracted work from the engine at this point. However, we shall see that it is positive in the examples considered in section 3.2.6, and thus represents a penalty in the amount of work extracted from the engine.

It is possible to mitigate some of this cost by performing a modified version of the Otto cycle. For ease of presentation we will hold back our treatment of that version until section 3.2.5 which involves considering the case of an adiabatic interaction switch off. For the time being, we proceed with the next stroke of the cycle.

Isentropic expansion

No interaction between the TLS and either reservoir is now present. The energy gap in H_S is changed such that $\mu_h \to \mu_c$ by tuning the parameters $\epsilon_h \to \epsilon_c$, $\Delta_h \to \Delta_c$. The TLS Hamiltonian at the end of the stroke (point C) is given by

$$H_S^C = \frac{\mu_c}{2} I + \frac{\epsilon_c}{2}\sigma_z + \frac{\Delta_c}{2}\sigma_x. \tag{3.39}$$

Once again, we seek to evaluate the average energy along the stroke as

$$\langle H(t)\rangle = \mathrm{tr}\left[\left(H_S(t) + H_{R_h} + H_{R_c}\right)\chi(t)\right]. \tag{3.40}$$

The evolution of the global state, and in particular of the TLS component, depends in general on the details of the time-dependent protocol for tuning the TLS parameters. In the usual treatment of the Otto cycle, it is assumed that these parameters are changed very slowly. In this limit, the quantum adiabatic theorem holds [71]. This result is well understood but for clarity we will re-derive it in the present context of our heat engine.

We begin by defining a unitary transformation

$$V(t) = \exp\left[-i\sigma_y\theta(t)/2\right], \tag{3.41}$$

with $\theta(t) = \tan^{-1}[\Delta(t)/\epsilon(t)]$. Now, we consider the Hamiltonian H' in the frame defined by $V(t)$:

$$\begin{aligned} H'(t) &= V^\dagger(t)H(t)V(t) + i\dot{V}^\dagger(t)V(t) \\ &= \frac{\mu(t)}{2}(I+\sigma_z) - \frac{\dot{\theta}(t)}{2}\sigma_y + H_{R_h} + H_{R_c}. \end{aligned} \tag{3.42}$$

If $\epsilon(t)$ and $\Delta(t)$ are tuned with the same time dependence then $\dot{\theta}(t) = 0$. Otherwise, if these parameters are tuned slowly enough such that $\dot{\theta}(t) \ll \mu(t)$ then the transformation defined by $V(t)$ approximately diagonalises the system Hamiltonian $H_S(t)$ at any instant in time (it remains proportional to σ_z). We may transform the global state into the basis defined by $V(t)$ as well to yield $\chi'(t) \equiv V^\dagger(t)\chi(t)V(t)$. In this basis, the average energy at any point along the stroke, is given by

$$\langle H(t)\rangle = \frac{\mu(t)}{2}\left\{1 + \mathrm{tr}\left[\sigma_z\chi'(t)\right]\right\} + \mathrm{tr}\left[(H_{R_h} + H_{R_c})\chi'(t)\right], \tag{3.43}$$

where we have dropped the term in $\dot{\theta}(t)$ maintaining the assumption that the parameters are tuned slowly enough such that $\dot{\theta}(t) \ll \mu(t)$. Now we proceed to evaluate the right hand side of Eq. (3.43) and the purpose of rotating into the frame in which $H_S(t)$ remains diagonal becomes clear. Let us define a time evolution operator in the transformed frame as $U'(t) \equiv T\exp\left[-i\int_0^t H'_S(\tau)d\tau\right]$, with T denoting the time-ordered exponential. Now we substitute $\chi'(t) \equiv U'(t)\chi'(0)U'^\dagger(t)$ into Eq. (3.43) and show that the term $\mathrm{tr}\left[\sigma_z\chi'(t)\right]$ remains constant:

$$\begin{aligned} \mathrm{tr}\left[\sigma_z\chi'(t)\right] &= \mathrm{tr}\left[\sigma_z U'(t)\chi'(0)U'^\dagger(t)\right] \\ &= \mathrm{tr}\left[U'^\dagger(t)\sigma_z U'(t)\chi'(0)\right], \end{aligned} \tag{3.44}$$

where we have used the cyclic property of the trace. In the adiabatic limit ($\dot{\theta} \ll 1$), $H'_S(t) \approx (\mu(t)/2)(I+\sigma_z)$, such that the time evolution operator commutes with σ_z, and so $U'^\dagger(t)\sigma_z U'(t) = \sigma_z$. This leaves us with $\mathrm{tr}\left[\sigma_z\chi'(t)\right] = \mathrm{tr}\left[\sigma_z\chi'(0)\right]$, i.e. this term remains constant along the

stroke. The average energy along the stroke is then

$$\begin{aligned}\langle H(t)\rangle &= \frac{\mu(t)}{2}\left\{1+\mathrm{tr}\left[\sigma_z\chi(0)\right]\right\}+\mathrm{tr}\left[(H_{R_h}+H_{R_c})\chi'(t)\right]\\ &= \frac{\mu(t)}{\mu(0)}\langle H_S(0)\rangle+\mathrm{tr}\left[(H_{R_h}+H_{R_c})\chi(t)\right].\end{aligned} \tag{3.45}$$

There is no dependency in the reservoirs Hamiltonians along the stroke, and so their energy expectation values are unchanging. The energy of the global system at the end of the stroke reads

$$\begin{aligned}\langle H\rangle^C &= \mathrm{tr}\left[\left(H_S^C+H_{R_h}+H_{R_c}\right)\chi^C\right]\\ &= \frac{\mu_c}{\mu_h}\mathrm{tr}\left[H_S^B\rho_h\right]+\mathrm{tr}\left[H_{R_h}\rho_h\right]+\langle H_{R_c}\rangle_{th}.\end{aligned} \tag{3.46}$$

The average energy along the stroke scales linearly with $\mu(t)$ and the difference in energy between the start and end points of the stroke gives the work extracted:

$$\langle H\rangle^C-\langle H\rangle^{B'}=\left(\frac{\mu_c}{\mu_h}-1\right)\mathrm{tr}\left[H_S^B\rho_h\right]. \tag{3.47}$$

In the weak coupling limit this reduces to

$$\langle H\rangle^C_{weak}-\langle H\rangle^{B'}_{weak}=\left(\frac{\mu_c}{2}-\frac{\mu_h}{2}\right)\left[1-\tanh\left(\frac{\mu_h}{2k_BT_h}\right)\right], \tag{3.48}$$

where $\mu_h>\mu_c$.

The interaction between the system and the cold reservoir is now switched on instantaneously, taking us to point C'. Again we wish to account for any energetic costs this entails and so evaluate the average energy:

$$\langle H\rangle^{C'}=\mathrm{tr}\left[\left(H_S^C+H_{R_h}+H_{R_c}+H_{I_c}\right)\chi^{C'}\right], \tag{3.49}$$

with $\chi^{C'}=\chi^C$ because the switch on is done instantaneously. As previously stated, we assume that the hot and cold reservoirs relax to equilibrium at temperatures T_h and T_c, respectively,

when uncoupled from the TLS. This means that when the interaction is turned on, the system is coupling to a reservoir in a thermal equilibrium state. Hence, the work associated with coupling to the cold reservoir, $\langle H\rangle^{C'} - \langle H\rangle^{C}$, evaluates to zero in both the weak coupling and RC treatments as the cold reservoir state ρ_{R_c} is a thermal state.

Cold isochore

This stroke proceeds analogously to the hot isochore. The global state relaxes to equilibrium with the cold reservoir interaction present. The full state at the end of the stroke (point D) is given by

$$\chi^{D} = \rho_c \otimes \rho_{th_h} \tag{3.50}$$

Here

$$\rho_c = \frac{\exp\left[-\beta_c\left(H_S^D + H_{R_c} + H_{I_c}\right)\right]}{\mathrm{tr}\left\{\exp\left[-\beta_c\left(H_S^D + H_{R_c} + H_{I_c}\right)\right]\right\}} \tag{3.51}$$

is a thermal state of the interacting TLS and cold reservoir. We have assumed that the hot reservoir has re-thermalised along the stroke, see Eq. (3.33).

We apply the RC treatment to account for the interacting system and cold reservoir once again and accordingly write down the average energy at point D:

$$\begin{aligned}\langle H\rangle^{D} &= \mathrm{tr}\left[\left(H_S^C + H_{R_h} + H_{R_c} + H_{I_c}\right)\rho_c\rho_{th_h}\right] \\ &= \mathrm{tr}\left[\tilde{H}_{S'}^C\tilde{\rho}_{S'_c}\right] + \mathrm{tr}\left[\tilde{H}_{E'_c}\tilde{\rho}_{E'_c}\right] + \langle H_{R_h}\rangle_{th},\end{aligned} \tag{3.52}$$

with

$$\rho_c = \frac{\exp(-\beta_c\tilde{H}_{S'}^C)}{\mathrm{tr}[\exp(-\beta_c\tilde{H}_{S'}^C)]} \otimes \tilde{\rho}_{E'_c} = \tilde{\rho}_{S'_c} \otimes \tilde{\rho}_{E'_c}, \tag{3.53}$$

where

$$\tilde{H}_{S'}^C = H_S^C - \lambda_c\sigma_z(a_c^\dagger + a_c) + \Omega_c a_c^\dagger a_c \tag{3.54}$$

is the RC mapped Hamiltonian for the system and cold reservoir. Here, $\tilde{\rho}_{E'_c}$ is a thermal state of the cold reservoir residual environment (with Hamiltonian $\tilde{H}_{E'_c}$) at inverse temperature β_c.

In the weak coupling treatment, the state again reduces to the product of three thermal states for the system and the two reservoirs, such that the average energy simplifies to

$$\langle H\rangle^{D}_{weak} = \frac{\mu_c}{2}\left[1-\tanh\left(\frac{\mu_c}{2k_BT_c}\right)\right] + \langle H_{R_h}\rangle_{th} + \langle H_{R_c}\rangle_{th}. \tag{3.55}$$

The interaction between the system and the cold reservoir is now switched off and we reach point D'. With no interaction terms in the Hamiltonian, the average energy reads

$$\langle H\rangle^{D'} = \mathrm{tr}\left[\left(H_S^C + H_{R_h} + H_{R_c}\right)\chi^{D'}\right]. \tag{3.56}$$

If the interaction is switched off instantaneously then $\chi^{D'} = \chi^{D} = \rho_c \otimes \rho_{th_h}$, and the work cost is

$$\langle H\rangle^{D'} - \langle H\rangle^{D} = -\mathrm{tr}\left[H_{I_c}\rho_c\right]. \tag{3.57}$$

In the weak coupling treatment, the cold reservoir remains in a thermal state and factorises out of the expression for ρ_c. The cost again, therefore, evaluates to zero. At strong coupling, however, we obtain

$$\langle H\rangle^{D'} - \langle H\rangle^{D} = \lambda_c \mathrm{tr}\left[\sigma_z(a_c^\dagger + a_c)\tilde{\rho}_{S_c'}\right], \tag{3.58}$$

within the RC approach, which is generally non-zero. In section 3.2.5 we consider the alternative treatment of mitigating this work penalty by adiabatic decoupling.

Isentropic compression

This stroke is analogous to the isentropic expansion stroke, with the system parameters changed back to their original values. At point A the TLS Hamiltonian therefore reads

$$H_S^A = \frac{\mu_h}{2}I + \frac{\epsilon_h}{2}\sigma_z + \frac{\Delta_h}{2}\sigma_x. \tag{3.59}$$

Again, we consider the adiabatic limit such that the average energy at point A is given by

$$\begin{aligned}\langle H\rangle^A &= \mathrm{tr}\left[\left(H_S^A + H_{R_h} + H_{R_c}\right)\chi^A\right] \\ &= \frac{\mu_h}{\mu_c}\mathrm{tr}\left[H_S^C\rho_c\right] + \mathrm{tr}\left[H_{R_c}\rho_c\right] + \langle H_{R_h}\rangle_{th}.\end{aligned} \tag{3.60}$$

The energy difference across the stroke gives the work done on the system:

$$\langle H\rangle^A - \langle H\rangle^{D'} = \left(\frac{\mu_h}{\mu_c} - 1\right)\mathrm{tr}\left[H_S^C\rho_c\right]. \tag{3.61}$$

Under weak coupling assumptions this simplifies to

$$\langle H\rangle^A_{weak} - \langle H\rangle^{D'}_{weak} = \left(\frac{\mu_h}{2} - \frac{\mu_c}{2}\right)\left[1 - \tanh\left(\frac{\mu_c}{2k_BT_c}\right)\right]. \tag{3.62}$$

Then we switch on the coupling to the hot reservoir instantaneously and return to point A'. The Hamiltonian contains the term H_{I_h} and the average energy is given by

$$\begin{aligned}\langle H\rangle^{A'} =& \mathrm{tr}\left[(H_S^B + H_{R_h} + H_{R_c} + H_{I_h})\chi^{A'}\right] \\ =& \frac{\mu_h}{\mu_c}\mathrm{tr}\left[H_S^C\rho_c\right] + \mathrm{tr}\left[H_{R_c}\rho_c\right] + \langle H_{R_h}\rangle_{th} \\ =& \langle H\rangle^A,\end{aligned} \tag{3.63}$$

where, in the last line, as in the cold reservoir case, we make the point that there is no cost associated with the switch on of the coupling to the hot reservoir, as it is in thermal equilibrium at this point.

3.2.4 Work output and efficiency at finite coupling

Now that we have analysed the cycle in detail and obtained expressions for the average energy at all points around the cycle, Eqns. (3.30), (3.36), (3.49), (3.52), (3.56) and (3.60), we are in a position to evaluate the net work output and energy conversion efficiency of the finite coupling Otto cycle.

We sum the energetic changes along each isentropic stroke to evaluate the net work output W. Note that this includes contributions from the cost of decoupling the reservoirs (although not from coupling - as explained in the preceding section):

$$\begin{aligned} W =& \langle H^{B'}\rangle - \langle H^{B}\rangle + \langle H^{C}\rangle - \langle H^{B}\rangle + \langle H^{D'}\rangle - \langle H^{D}\rangle + \langle H^{A}\rangle - \langle H^{D'}\rangle \\ =& \left(\frac{\mu_c}{\mu_h} - 1\right) \mathrm{tr}\left[H_S^B \rho_h\right] + \left(\frac{\mu_h}{\mu_c} - 1\right) \mathrm{tr}\left[H_S^C \rho_c\right] - \mathrm{tr}\left[H_{I_h} \rho_h\right] - \mathrm{tr}\left[H_{I_c} \rho_c\right]. \end{aligned} \tag{3.64}$$

In the weak coupling treatment, the interaction terms evaluate to zero. The expression for the net work output then reduces to the standard form

$$\begin{aligned} W_{weak} =& \langle H\rangle^{C'} - \langle H\rangle^{B} + \langle H\rangle^{A'} - \langle H\rangle^{D} \\ =& \frac{1}{2}\left(\mu_c - \mu_h\right)\left[\tanh\left(\frac{\mu_h}{2k_B T_h}\right) - \tanh\left(\frac{\mu_c}{2k_B T_c}\right)\right]. \end{aligned} \tag{3.65}$$

It follows from equation (3.65), that $\mu_h/\mu_c < T_h/T_c$ must hold for there for be a net output of work from the engine. This is known as the positive work condition. When this condition is violated, the effective temperature of the TLS at the end of the hot isentrope is greater than the temperature of the hot reservoir. At the end of the cold isentrope, it is colder than the cold reservoir. This means heat flows in the opposite direction to that required for an output of work, and instead, a net amount of work is invested into the system for it to operate as a refrigerator enabling heat to flow from the cold to the hot reservoir. The energy transferred into the system from the hot reservoir is evaluated as the change in energy along the hot isochore:

$$\begin{aligned} Q =& \langle H\rangle^{B} - \langle H\rangle^{A'} \\ =& \mathrm{tr}\left[H_S^B \rho_h\right] - \frac{\mu_h}{\mu_c}\mathrm{tr}\left[H_S^C \rho_c\right] + \mathrm{tr}\left[H_{R_h}\left(\rho_h - \rho_{th_h}\right)\right] + \mathrm{tr}\left[H_{R_c}\left(\rho_{th_c} - \rho_c\right)\right] + \mathrm{tr}\left[H_{I_h}\rho_h\right]. \end{aligned} \tag{3.66}$$

Once again, In the weak coupling treatment, this reduces to a standard form because the

reservoirs remain in thermal equilibrium such that their internal energies cancel out:

$$Q_{weak} = \frac{\mu_h}{2}\left[\tanh\left(\frac{\mu_c}{2k_BT_c}\right) - \tanh\left(\frac{\mu_h}{2k_BT_h}\right)\right]. \tag{3.67}$$

The efficiency of the engine is defined as the ratio of the net work output to the energy absorbed from the hot reservoir by the TLS along the hot isochore,

$$\eta = \frac{W}{Q}. \tag{3.68}$$

For weak coupling, using equations (3.65) and (3.67), this simplifies to

$$\eta_{weak} = 1 - \frac{\mu_c}{\mu_h}, \tag{3.69}$$

which is commonly known as the Otto efficiency (for a two-level system).

Before turning to some results, we will briefly describe in the next section a method by which some of the costs incurred due to the reservoir decoupling may be recovered.

3.2.5 Adiabatic reservoir decoupling

In this section we consider a modification of the Otto cycle which allows us to mitigate some of the work cost associated with decoupling from the hot and cold reservoirs at points B' and D', respectively. We consider decoupling the TLS from each reservoir adiabatically at the end of each isochore. In this case the global state at point B' has evolved from point B. Turning the interaction off adiabatically means doing so infinitesimally slowly such that the state at B' is the steady state solution of a weak coupling master equation describing the interaction between the system and the hot reservoir. The global state is therefore given by a tensor product of three thermal states:

$$\chi^{B'} = \rho_{S_h} \otimes \rho_{th_h} \otimes \rho_{th_c}, \tag{3.70}$$

see Eqs. (3.31) - (3.33). The energetic cost of decoupling now evaluates to

$$\langle H\rangle^{B'} - \langle H\rangle^{B} = \mathrm{tr}\left[H_S^B(\rho_{S_h} - \rho_h)\right] + \mathrm{tr}\left[H_{R_h}(\rho_{th_h} - \rho_h)\right] - \mathrm{tr}\left[H_{I_h}\rho_h\right]. \tag{3.71}$$

This cost remains zero in the standard weak coupling analysis since the reservoirs remain thermal and the interaction term is vanishing. At finite coupling, however, it contains a work contribution and a component of heat dissipation into the hot reservoir. In order to separate the two we compute the change in free energy, $F = E - TS$, of the full state:

$$\begin{aligned} F_{B'} - F_B =& \langle H\rangle^{B'} - \frac{1}{\beta_h}S(\chi^{B'}) - \left[\langle H\rangle^{B} - \frac{1}{\beta_h}S(\chi^{B})\right] \\ =& \frac{1}{\beta_h}\ln \mathrm{tr}\left[\exp\left(-\beta_h\left(H_S^B + H_{R_h} + H_{I_h}\right)\right)\right] - \frac{1}{\beta_h}\ln Z_{S_h} - \frac{1}{\beta_h}\ln Z_{R_h}, \end{aligned} \tag{3.72}$$

where $S(\rho) = -\mathrm{tr}\left[\rho\ln\rho\right]$ is the von Neumann entropy, $Z_{S_h} = \mathrm{tr}\left[\exp\left(-\beta_h H_S^B\right)\right]$, and $Z_{R_h} = \mathrm{tr}\left[\exp\left(-\beta_h H_{R_h}\right)\right]$ are standard partition functions involving the TLS and reservoir Hamiltonians. We define this as the work contribution to the decoupling cost. The heat dissipated into the bath during decoupling is then given by the change in energy minus this work contribution

$$Q_{BB'} \;=\; \langle H\rangle^{B'} - \langle H\rangle^{B} - \left[F_{B'} - F_B\right]. \tag{3.73}$$

The RC approach may be employed to perform these calculations, as discussed in earlier sections.

A similar procedure holds for the cost of decoupling from the cold reservoir at point D. If the interaction is switched off adiabatically then the state at D' is given by

$$\chi^{D'} = \rho_{S_c}\otimes\rho_{th_h}\otimes\rho_{th_c}, \tag{3.74}$$

where ρ_{S_c} is the Gibbs state given by

$$\rho_{S_c} = \frac{\exp\left(-\beta_c H_S^C\right)}{\mathrm{tr}\left[\exp\left(-\beta_c H_S^C\right)\right]}. \tag{3.75}$$

In complete analogy to Eq. (3.71) the energetic cost is evaluated as

$$\langle H\rangle^{D'} - \langle H\rangle^{D} = \mathrm{tr}\left[H_S^C(\rho_{S_c} - \rho_c)\right] + \mathrm{tr}\left[H_{R_c}(\rho_{th_c} - \rho_c)\right] - \mathrm{tr}\left[H_{I_c}\rho_c\right]. \tag{3.76}$$

This may be partitioned once again into a work contribution and energy dissipated into the cold reservoir in the same way as was done in Eqns. (3.72) and (3.73).

For adiabatic decoupling, the expression for the net work output around a complete cycle then evaluates to

$$\begin{aligned} W &= \left(\frac{\mu_c}{\mu_h} - 1\right)\mathrm{tr}\left[H_S^B\rho_{S_h}\right] + \left(\frac{\mu_h}{\mu_c} - 1\right)\mathrm{tr}\left[H_S^C\rho_{S_c}\right] \\ &\quad + \frac{1}{\beta_h}\ln\mathrm{tr}\left[\exp\left(-\beta_h\left(H_S^B + H_{R_h} + H_{I_h}\right)\right)\right] + \frac{1}{\beta_c}\ln\mathrm{tr}\left[\exp\left(-\beta_c\left(H_S^C + H_{R_c} + H_{I_c}\right)\right)\right] \\ &\quad - \frac{1}{\beta_h}\ln Z_{S_h} - \frac{1}{\beta_h}\ln Z_{R_h} - \frac{1}{\beta_c}\ln Z_{S_c} - \frac{1}{\beta_c}\ln Z_{R_c}. \end{aligned} \tag{3.77}$$

The total energy dissipated into the hot reservoir comprises both the contribution from the hot isochore and the subsequent decoupling, $Q = Q_{A'B} + Q_{BB'}$. It reads

$$\begin{aligned} Q &= -\frac{\mu_h}{\mu_c}\mathrm{tr}\left[H_S^A\rho_{S_c}\right] - \mathrm{tr}\left[H_S^B\rho_{S_h}\right] + \frac{1}{\beta_h}\ln Z_{S_h} + \frac{1}{\beta_h}\ln Z_{R_h} \\ &\quad - \ln\mathrm{tr}\left[\exp\left(-\beta_h\left(H_S^B + H_{R_h} + H_{I_h}\right)\right)\right]. \end{aligned} \tag{3.78}$$

We clarify that we do not consider the possibility of switching on the coupling to either reservoir adiabatically. There is no cost associated with this, in any case, but doing so would negate the need for the hot/cold isochores that follow. Adiabatic coupling therefore has no equivalent in the standard Otto cycle.

3.2.6 Results for the equilibrium quantum Otto cycle

With the groundwork in place, we now explore the impact of strong coupling and system-reservoir correlations on the engine's performance. First we consider the example of adiabatic isentropic strokes, as outlined above. Later we will extend the analysis to the opposite limit of

sudden isentropes. In both cases, we will see that strong coupling acts to reduce the performance of the cycle compared with the weak coupling version. This is consistent with findings for continuous heat engines in the strong coupling regime [64]. However, additionally in our case, we are able to identify the primary reason for the reduced performance in the shape of the work costs imposed in decoupling the system and reservoirs after each isochore. This distinguishes these results from considerations for continuous engines which operate such that system-reservoir coupling is always present. In fact, as we shall see, were it not for this cost, it would be possible for the strong coupling engine to output more work than its weak coupling counterpart.

Adiabatic isentropic strokes

In the adiabatic limit the isentropic strokes of the cycle are carried out slowly enough for the quantum adiabatic theorem to hold. In Fig. 3.2 we show representative plots of the work output and energy absorbed from the hot reservoir in this regime. The parameter which is tuned along the horizontal axis is the ratio of the TLS bias at the start and at the end of the isentropic expansion. Note that this also dictates the bias ratio along the isentropic compression stroke. This effectively controls the extent to which the energy gap between the two eigenlevels of the TLS Hamiltonian is changed during the isentropic strokes. We compare the strong coupling regime with the weak coupling limit (dashed curves), Eqs. (3.65) and (3.67). In the case of strong coupling, we consider the two alternative cycles with either instantaneous (dotted curves) or adiabatic (solid curves) decoupling of the reservoirs from the TLS as outlined previously. For strong coupling, all calculations have been performed using the RC formalism.

In the weak coupling limit, net work output vanishes when $\epsilon_h/\epsilon_c = 1$. Since tunneling Δ is maintained fixed here, a ratio of 1 means that there is no change in the energy spacing of the TLS across the isentropic strokes. In other words, there are no isentropic strokes and only two thermalisation strokes. As such no work is extracted from the engine. Work output vanishes also when $\mu_h/\mu_c = T_h/T_c$. This is known as the positive work condition derived from Eq. (3.65) which implies that for W_{weak} to be negative (our sign convention for positive work output) we require $\mu_h/\mu_c < T_h/T_c$. This is also the point at which the energy absorbed from the hot

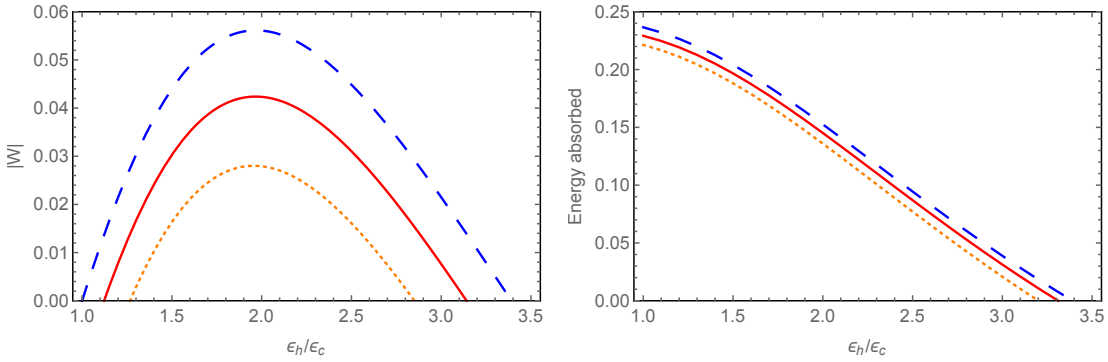

(a) (b)

Figure 3.2: **Adiabatic limit.** (a) Work output and (b) energy absorbed from the hot reservoir for a TLS quantum Otto cycle plotted as a function of the TLS bias at point A, ϵ_h. We choose to plot ϵ_h/ϵ_c on the horizontal axis rather than μ_h/μ_c because we are keeping Δ fixed. *Blue dashed curves*: weak coupling; *Yellow dotted curves*: strong coupling with instantaneous decoupling of the reservoirs; *Red solid curves*: strong coupling with adiabatic decoupling of the reservoirs. Parameters (in units of ϵ_c): $\Delta_h = \Delta_c = 1$, $\beta_h = 1$, $\beta_c = 2.5$, $\omega_c = 2$, $\alpha = 0.005$, and $n = 30$ states are taken in the RC calculations. We see that work output and energy absorbed from the hot reservoir are both reduced at stronger coupling, but that this effect can be mitigated by adiabatic decoupling of the reservoirs. Even at what could be argued as still relatively weak coupling compared with the energy scale of the TLS, we still see large enough interaction costs to have an impact on work output. Figure is reproduced from Ref. [16].

reservoir vanishes: at this ratio the TLS has the same effective temperature as the hot reservoir and so no thermalisation occurs during the hot isochore. Beyond this point, for weak coupling we have that $\mu_h/\mu_c > T_h/T_c$ and the engine turns over to operate instead as a refrigerator, absorbing energy from the cold reservoir and dissipating into the hot reservoir.

The strong coupling treatments both yield lower work outputs than the weak coupling calculations. Contrary to the weak coupling treatment where there is a net work output as soon as $\mu_h/\mu_c > 1$, at stronger coupling, there is a regime where $\mu_h/\mu_c > 1$ but the engine still consumes a net amount of work. This is because of the decoupling cost which must be overcome before net output is seen. Work, also, cannot be extracted right up to the limit of $\mu_h/\mu_c = T_h/T_c$ (positive work condition). Strong coupling, however, leads to a reduction in the energy absorbed from the hot reservoir which would entail an efficiency gain were it not for decoupling costs. In contrast to the weak coupling case, for strong coupling the work output and energy absorbed do not change sign at the same point, meaning that these regimes where there is net output at weak coupling but not so at strong coupling are regimes in which the cycle acts neither as an engine nor as a refrigerator. It simply consumes work while still being a conduit for heat to flow from the hot reservoir to the cold one. Comparing the adiabatic decoupling case with the instantaneous one, we see that a large proportion of the decoupling cost may be recovered.

To illustrate that decoupling costs account for the majority of the loss in performance, we have separated these contributions from the remaining work output in Fig. 3.3. In the case of instantaneous decoupling we see that even when we neglect the cost of switching off the reservoir interactions (dotted curve), slightly less net work is extracted along the isentropic strokes than in the weak coupling case (dashed curve). This is because the TLS state differs from the thermal state obtained in the adiabatic decoupling and standard weak coupling treatments at the start of the isentropic strokes. The size of the cost term (dashed line) is the dominant effect though. This emphasises just how severe a simplification is made by neglecting interaction effects in the weak coupling treatment. We see that the cost can be mitigated to a certain extent by the adiabatic decoupling procedure (solid line). The work extracted neglecting the decoupling cost still only recovers to the weak coupling limit in this case, thus the total work output is still

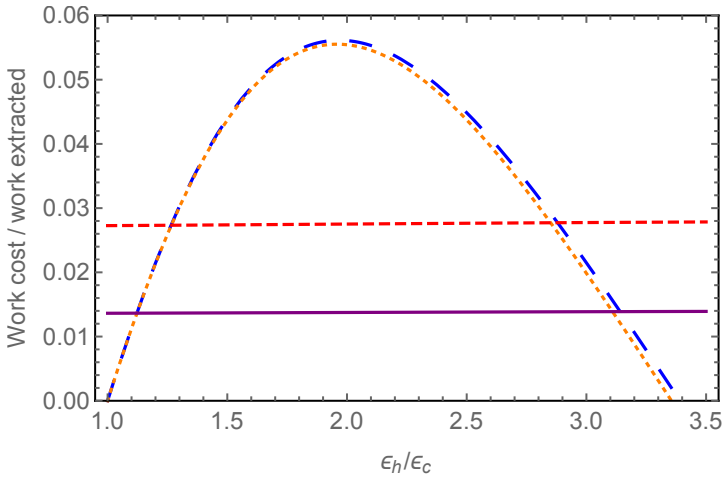

Figure 3.3: **Adiabatic limit.** Net work output of the Otto cycle separated into decoupling work cost and magnitude of the remaining work extracted components. The parameter which is varied along the horizontal axis is the ratio of the TLS bias ϵ_h/ϵ_c. *Blue dashed curve:* weak coupling (no decoupling cost) and strong coupling work extracted ignoring work cost (adiabatic decoupling case); *Yellow dotted curve:* strong coupling work extracted ignoring work cost (instantaneous decoupling case); *Red dashed line:* strong coupling cost of instantaneous decoupling; *Purple solid line:* strong coupling cost of adiabatic decoupling. Parameters as in Fig. 3.2. It is the cost of decoupling the reservoirs which accounts primarily for the loss in work output at stronger coupling. The beneficial effect of adiabatic decoupling in mitigating this cost is seen in the difference between the *red dashed* and *purple* lines. Figure is reproduced from Ref. [16].

lower and costs cannot be fully overcome. Moreover we see that costs remain flat with the ratio ϵ_h/ϵ_c which means there are regions at small and large ratios where, as mentioned above, net work output goes negative and the engine consumes both energy from the reservoir and a net amount of work.

We now consider how efficient the engine is, with efficiency defined as in Eq. (3.68). In Fig. 3.4, we show a parametric plot of the work output against the efficiency of the engine for both strong and weak coupling. The parameter which is varied as we move along a curves is the TLS bias, ϵ_h. In the weak coupling regime, the efficiency increases monotonically with ϵ_h (although, as we have seen, work output does not) and saturates at the Carnot limit, $\eta_C = 1 - T_c/T_h$. This is the point at which the net work output vanishes, $\mu_h/\mu_c = T_h/T_c$. Maximum work output occurs prior at an efficiency lower than the Carnot bound, and in practice this is the efficiency of the working engine. At stronger coupling, the efficiency of the engine is inferior. This is

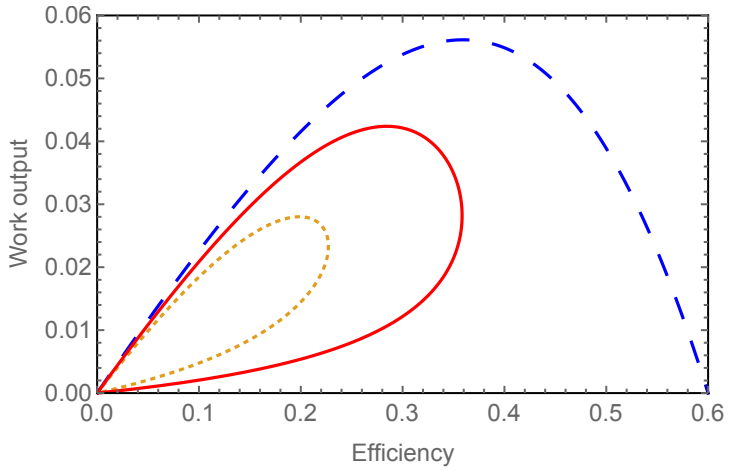

Figure 3.4: **Adiabatic limit.** Parametric plots of work output versus efficiency in the adiabatic isentropes regime for a quantum Otto cycle. The parameter which is varied along these curves is TLS bias during the hot part of the cycle, ϵ_h. *Blue dashed curve*: weak coupling; *Red solid curve*: strong coupling with adiabatic decoupling of the reservoirs; *Yellow dotted curve*: Strong coupling with instantaneous decoupling of the reservoirs. Parameters (in units of ϵ_c): $\Delta_h = \Delta_c = 1$, $\beta_h = 1$, $\beta_c = 2.5$, $\omega_c = 2$, $\alpha = 0.005$, and $n = 30$ states are taken in the RC calculations. Figure is reproduced from Ref. [16].

because work output is reduced in this regime and the energy absorbed from the hot reservoir is not reduced sufficiently to prevent a reduction in efficiency. We also note that qualitatively different behaviour is observed compared with the weak coupling limit: the Carnot limit is never reached and maximum efficiency, although not coinciding with maximal work output, is much closer than in the weak coupling case. This means that the engine, during practical operation, operates at close to its optimal efficiency. Efficiency is not monotonic with TLS bias in this regime and falls to zero as the work output vanishes. This creates the loop structure of both the instantaneous decoupling and adiabatic decoupling curves, evocative of studies of classical heat engines containing some source of internal frictional loss, for example in Ref. [31]. The efficiency can be improved with the adiabatic decoupling protocol, since there is some mitigation of the decoupling costs. In this case we notice a loop which lies outside the instantaneous decoupling case.

We point out at this stage that, for instantaneous decoupling in certain parameter regimes, it is possible for the the work output in the strong coupling case to beat the weak coupling limit, if one were to ignore the decoupling cost. Obviously, there is no escaping this cost but we

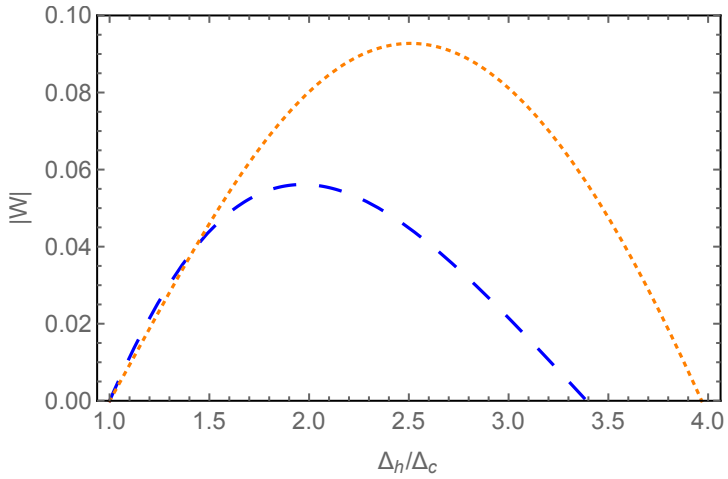

Figure 3.5: **Adiabatic limit.** Work output of the Otto cycle plotted as a function of the TLS tunneling, Δ_h, during the hot part of the cycle. Here, we ignore the decoupling cost for strong coupling (we are only considering instantaneous decoupling). *Blue dashed curve:* weak coupling; *Yellow dotted curve:* strong coupling. Parameters (in units of Δ_c): $\epsilon_h = \epsilon_c = 1$, $\beta_h = 1$, $\beta_c = 2.5$, $\omega_c = 2$, $\alpha = 1$, and $n = 30$ states are taken in the RC calculations. Figure is reproduced from Ref. [16].

simply wish to make the point that, on taking the isentropic strokes in isolation, it is possible to find parameter regimes in which more work is extracted because of stronger coupling with the reservoirs. An example is shown in Fig. 3.5. Here the tunnelling, Δ_h, is tuned along the isentropic strokes rather than ϵ_h. Note this still results in changing the TLS energy gap along this stroke. The decoupling costs far outweigh such enhancements still, and the cycle as a whole always displays a reduction in work output for the strong coupling calculations. But the example serves to show that strong coupling itself does not always act to the detriment of possible work extraction.

Finally, in Fig. 3.6, we examine how the engine performance scales with system-reservoir coupling strength α . At weak coupling, we make the approximation that the magnitude of the interaction term is negligible and hence the weak coupling efficiency is flat with α. At stronger coupling, the first sanity check is that, as expected, the weak coupling efficiency is recovered as $\alpha \to 0$. It is clear that the detrimental effect of the decoupling cost is more pronounced at higher couplings. The adiabatic decoupling procedure becomes increasingly valuable as coupling is increased, despite being unable to fully recover the weak coupling efficiency. In fact, for

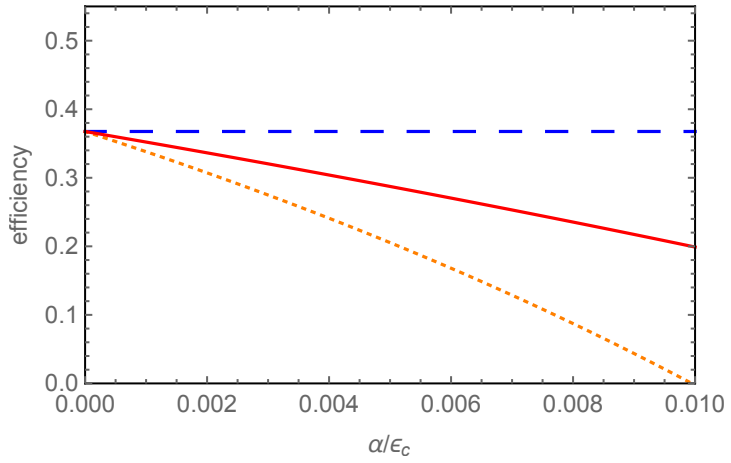

Figure 3.6: **Adiabatic limit.** Efficiency of the Otto engine plotted as a function of coupling strength α. *Blue dashed line:* weak coupling - the efficiency is constant and equal to $1 - \frac{\mu_c}{\mu_h}$ as in equation (3.69); *Yellow dotted curve:* strong coupling with instantaneous decoupling of the reservoirs; *Red solid curve:* strong coupling with adiabatic decoupling of the reservoirs. Parameters as in Fig. 3.2 with $\epsilon_h/\epsilon_c = 2$. Figure is reproduced from Ref. [16].

large enough couplings, it allows the cycle to perform as an engine even when the work output has vanished in the instantaneous decoupling case. It is also worth recognising that the sensitivity of the cycle performance to the system-reservoir decoupling procedure (instantaneous or adiabatic) could be used (even at fixed α) to signify the presence of strong coupling effects in experimental realisations of quantum heat engines. This is because it is a feature inherent to the strong coupling regime and completely absent in the weak coupling treatment.

Sudden isentropic strokes

Until now, we have been considering the case where the isentropic strokes are carried out in the adiabatic limit. We move now to the sudden limit of the Otto cycle. This means we carry out the isentropic strokes so quickly that the quantum state has no time to evolve along the isentropic strokes between points B' and C or between D' and A. The global states at C and A are therefore given by $\chi^C = \chi^{B'}$ and $\chi^A = \chi^{D'}$. This changes the respective energy expressions at these end points of the isentropic strokes. In the instantaneous decoupling limit, considering

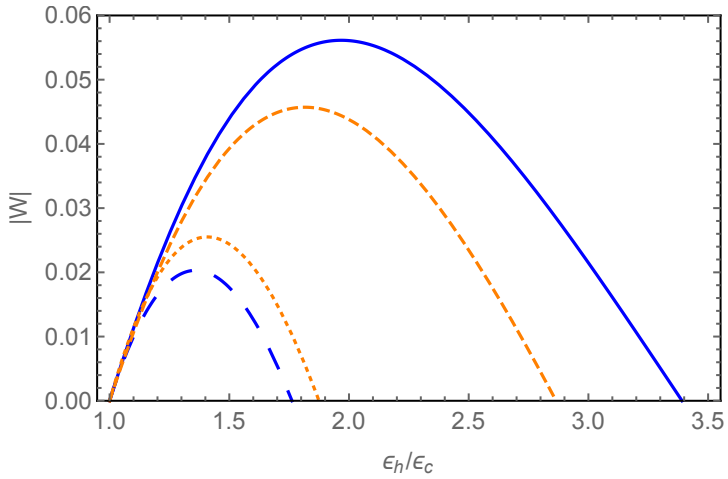

Figure 3.7: **Comparing the adiabatic and sudden limits.** Work output of the Otto cycle plotted as a function of the TLS bias during the hot part of the cycle, ϵ_h. We ignore the decoupling cost for the strong coupling curves here. *Blue solid curve:* weak coupling adiabatic; *Yellow (small) dashed curve:* strong coupling adiabatic with instantaneous decoupling; *Blue (large) dashed curve:* weak coupling sudden; *Yellow dotted curve:* strong coupling sudden. Parameters as in Fig. 3.2 though with $\alpha/\epsilon_c = 0.1$. Figure is reproduced from Ref. [16].

the cycle as a whole, we find that in the sudden limit the net work output reads

$$W = \mathrm{tr}\left[H_S^B(\rho_c - \rho_h)\right] + \mathrm{tr}\left[H_S^C(\rho_h - \rho_c)\right] - \mathrm{tr}[H_{I_h}\rho_h] - \mathrm{tr}[H_{I_c}\rho_c]. \tag{3.79}$$

The energy absorbed from the hot reservoir is now given by

$$Q^{A'B} = \mathrm{tr}\left[H_S^B(\rho_h - \rho_c)\right] + \mathrm{tr}\left[H_{R_h}(\rho_h - \rho_{R_h})\right] + \mathrm{tr}\left[H_{R_c}(\rho_{R_c} - \rho_c)\right] + \mathrm{tr}[H_{I_h}\rho_h]. \tag{3.80}$$

Both expressions may be evaluated within the RC formalism, as was the case in the adiabatic treatment.

It is well understood that engines which operate outside of the adiabatic regime are hampered by coherence developing during work extraction strokes between the energy eigenlevels of the working fluid [23, 29, 43]. This effect, known as quantum friction, is always detrimental to the engine's work output when compared with an adiabatic version. This is the reason for the severe reduction in the weak coupling work output as compared to the adiabatic limit in Fig. 3.7. Interestingly, in this example, we note the effect of quantum friction is less pronounced

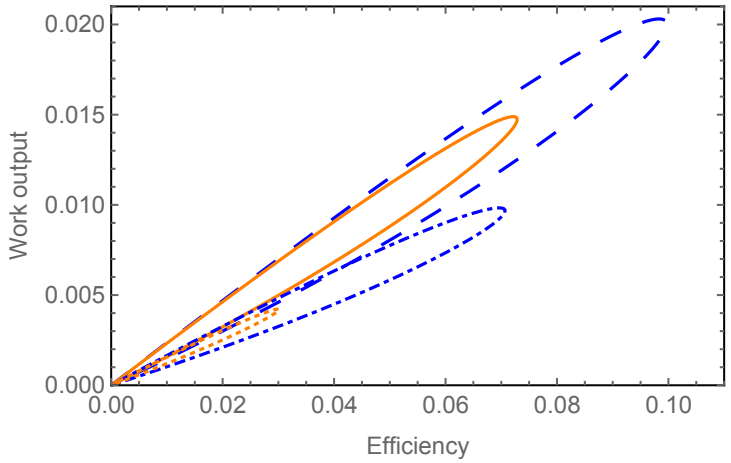

Figure 3.8: **Sudden limit.** Parametric plots of work output against efficiency in the sudden regime for a quantum Otto cycle. The parameter which is varied along each curve is the TLS bias during the hot part of the cycle, ϵ_h. We consider two different temperatures of the cold reservoir. *Blue dashed curve*: weak coupling and $\beta_c = 2.5$; *Yellow solid curve*: strong coupling and $\beta_c = 2.5$; *Blue dot-dashed curve*: weak coupling $\beta_c = 1.75$; *Orange dotted curve*: strong coupling $\beta_c = 1.75$. Parameters (in units of ϵ_c): $\Delta_h = \Delta_c = 1$, $\beta_h = 1$, $\omega_c = 2$, $\alpha = 0.001$, and $n = 30$ states are taken in the RC calculations. Figure is reproduced from Ref. [16].

in the strong coupling regime. Indeed, were it not for the cost of decoupling (which outweighs the benefit), the strong coupling engine would outperform its weakly coupled counterpart. The impacts of the decoupling cost on the work output and energy conversion efficiency are highlighted in Fig. 3.8. There, we see both the effect of quantum friction leading to a loop-like structure qualitatively similar to those seen in Fig. 3.4, as well as the impact of finite coupling costs reducing work output and efficiency resulting in smaller loops. We find that the scaling of engine performance with coupling strength is qualitatively similar to the adiabatic isentropic limit in Fig. 3.6.

3.2.7 Summary

We have analysed an equilibrium quantum heat engine in the regime of strong coupling between the system and reservoirs, employing the RC formalism to properly account for the generation of system-reservoir correlations. We have seen that this results in costs incurred by decoupling the system and reservoirs. These costs impact negatively on the performance of the engine. We have seen that it is possible to recover some of this lost performance by operating a variation

of the cycle which involves adiabatic decoupling, pertinent only to the strong coupling regime.

Let us finally emphasize that it is thanks to the RC formalism that we have been able to compute explicitly the work costs involved in coupling and decoupling the system and the reservoirs around a heat engine cycle. These costs are typically ignored in the weak coupling limit. In that regime, it is assumed that the interaction term in the Hamiltonian is small enough that the reservoirs remain in thermal equilibrium, and so linear interaction terms may be considered as being without any associated energetic costs. This assumption is frequently valid in classical thermodynamic systems, where energetic costs associated with interactions between large systems are typically restricted to the surface of macroscopic objects. For small surface area to volume ratios, these costs can be safely neglected. At the quantum scale this need not necessarily be so. It may be argued that in considering such costs, we have had to specify a particular microscopic model of a heat engine and that, as a result, the emerging thermodynamics becomes dependent on our choice of model, which departs from the spirit of classical thermodynamics and its universality. In response to this, we would argue that at strong coupling, whether on the quantum or classical scale, a model specific description of thermodynamics may be inevitable since one is forced to consider the type of interaction between the working fluid and heat reservoir. In such cases, a formalism such as the RC method that allows for a physically intuitive treatment of these interactions holds great promise.

We have so far restricted ourselves to an idealised reversibe version of the Otto cycle where full equilibration occurs along the isochores and where the isentropic strokes are carried out either in the adiabatic or sudden limit. This cycle theoretically requires an infinite amount of time to complete, although, for sufficiently long times, the deviations from the metrics presented here as a result of finite time isochores would be minimal. This engine, in any case, produces negligible power output and is therefore of little practical use, beyond the fundamental concepts explored here. In the next chapter we will consider a more practical, non-equilibrium version of the engine, which operates in finite time and therefore generates finite power output, albeit at the cost of irreversibility.

There have been various proposals for experimental realisations of nanoscale heat engines [72, 73,

74, 75, 76, 77]. Although the protocols presented in this chapter are idealised in that they involve complete decoupling of the system from the reservoirs at various points during the engine cycle, it is certainly possible to control very precisely parameters such as the bias and tunnelling, for example, in experimental realisations of double well quantum dots in semiconductor nanowires [67, 68]. An experimental realisation of a single-atom heat engine has recently been achieved [72], indicating that tuning the interaction strength as required for protocols such as those outlined here is possible. As such, let us now turn our attention to a more practical treatment of the quantum Otto cycle at finite time.

Chapter 4

Non-equilibrium quantum heat engine

To operate the Otto cycle in finite time, there is the option of performing the isentropic strokes away from the adiabatic regime as well as the possibility of performing the isochoric strokes such that the relevant reservoir is decoupled before full equilibration has occurred. In the laboratory, of course, both of these will be the case. It is well understood that quantum engines operating outside the adiabatic regime are hampered by coherence developing between the energy eigenlevels of the working fluid during the work extraction strokes [29]. This effect, known as quantum friction, degrades the engine's work output when compared with a stroke performed infinitely slowly in which the quantum adiabatic theorem holds. Avoiding the costs imposed by quantum friction, negating this quantum disadvantage, may be possible by employing techniques known as shortcuts to adiabaticity, which enable the engine work strokes to remain adiabatic despite being carried out in finite time [32, 78] or through quantum lubrication in the form of an appropriate form of environmental noise [79]. Nevertheless, quantum coherence accrued through non-adiabatic work strokes can prove to be advantageous when comparing instead with the equivalent non-adiabatic stochastic (classical) engines in the particular limit of small action which is discussed in Refs. [80, 81]. Away from this limit, it has been argued that coherence

acts as a disadvantage over the classical non-adiabatic case [82]. Nanoscale heat engines have recently become an experimental reality [72] and these effects have been seen in the laboratory [83].

In what follows, we analyse the same quantum Otto heat engine cycle as in the previous chapter, however now operating in finite time. We will spend some time discussing the advantages of strong coupling when it comes to maximising power output before shifting our focus onto the effect of coherence between the TLS energy eigenlevels resulting from system-reservoir correlations accrued during the heat exchange strokes rather than the isentropic strokes. In typical treatments of the quantum Otto cycle, a weak coupling assumption is made which results in system and environmental reduced quantum states remaining separable at all times. In the adiabatic regime, where no coherence accrues in the TLS during the work extraction strokes, the weak coupling assumption also means the TLS reduced state remains diagonal in its energy eigenbasis during the heat exchange strokes. By going beyond the weak coupling assumption, but remaining approximately adiabatic along the work extraction strokes, we will see how coherence caused by system-environment correlations leads to power losses even where quantum friction plays no role. By considering a version of the strongly coupled engine where coherence is suppressed, we will see that a fully coherent engine, despite generating greater power output than a weakly coupled version as in Ref. [84], suffers from this distinctly quantum disadvantage.

We have already seen how finite reservoir coupling is detrimental to the performance of infinite time heat engine cycles when compared to cases in which the coupling strength is vanishingly weak. This is due primarily to the energetic costs imposed when decoupling the working system and reservoirs around the cycle in the finite coupling case. Our focus here is markedly different. Instead of purely focusing on a comparison between weak and strong coupling, we are interested in the relative performance of coherent and incoherent heat engine cycles where both are operating at finite coupling strength. We shall see that strong system-reservoir coupling imposes a distinct quantum coherent limit on heat engine performance when compared with the equivalent incoherent cycle.

As in the previous chapter, in order to access the strong coupling regime, we make use of RC

formalism. We will therefore restrict our description of this technique here to only the features salient to the present analysis of the finite time Otto cycle. We refer the reader to preceding chapters for a more in depth presentation of the formalism. We proceed first, for clarity, by refreshing our memory of the Otto cycle TLS model which was first introduced at the start of the previous chapter.

4.1 The Otto cycle model at finite time

We consider a TLS with self-Hamiltonian H_S which may interact separately with two heat reservoirs, at temperatures T_h and T_c with $T_h > T_c$, operating in an Otto cycle as described in section 3.2.1. Adopting the same labels, the cycle proceeds as $A'BB'CC'DD'A$, with the following adaptations:

- *Hot isochore*: at A' the TLS is coupled to the hot reservoir and interacts with it for a finite time τ_i to reach B. In the standard, infinite time version of the cycle, $\tau_i \to \infty$ and the global state of system plus reservoir at point B is taken to be a Gibbs thermal state with respect to the total Hamiltonian at inverse temperature $\beta_h = \frac{1}{k_B T_h}$. However, in what follows we consider a finite τ_i where the state at the end of the stroke may be out of equilibrium. The interaction between the TLS and the hot reservoir is then instantaneously set to zero and we do not consider here the possibility of adiabatic decoupling ($B \to B'$).

- *Isentropic expansion ($B' \to C$)*: H_S is tuned such that the gap between the two energy eigenvalues is reduced. The finite time taken for this stroke is given by τ. In what follows, we consider the adiabatic limit, where τ is large enough that the adiabatic theorem may be applied to give a very good approximation to the state at the end of the stroke, but where we still have $\tau \ll \tau_i$. Now, the interaction between the TLS and the cold reservoir is switched on instantaneously as before ($C \to C'$).

- *Cold isochore ($C' \to D$)*: The TLS interacts with the cold thermal reservoir at temperature

T_c for a finite time τ_i. As with the hot isochore, in the infinite time version of the cycle the global state at the end of the cold isochore is a Gibbs state with respect to the total Hamiltonian, now at inverse temperature $\beta_c = \frac{1}{k_B T_c}$. For a finite τ_i the global state will not have reached equilibrium. The system is then decoupled from the cold reservoir instantaneously ($D' \to D'$).

- *Isentropic compression ($D' \to A$)*: H_S is tuned for a time τ such that the gap between energy eigenstates is increased back to the same level it was at point A', and the adiabatic approximation again holds. The cycle is completed by instantaneously turning on the interaction with hot reservoir ($A \to A'$).

These four strokes are repeated until a limit cycle is reached [85] and all transient states have settled to their limit values. In this limit, the global quantum state at any particular point in the cycle is the same from one cycle to the next.

The full Hamiltonian for the internal energy of the TLS and the two reservoirs plus interaction terms reads the same as in the previous section and given in equations (3.1), (3.4), (3.5), (3.6) and (3.7). Once again, In order to access the strong coupling regime, we make use of the RC mapping as described in Refs. [14, 13] and in particular for the infinite time Otto cycle in Ref. [16] and the previous section.

As before, in order to numerically solve the RC master equation it is necessary to truncate the Hilbert space for the quantum state of the enlarged system S'. In practice this means truncating the number of excitations N_{RC} we consider in the RC mode. We choose the truncation such as to reach a reasonable compromise between computation time and convergence of the engine metrics (in particular the work output of the cycle).

We wish to emphasize now some points which have already been discussed in the infinite time version of the cycle, but are equally important in the present context. Whereas in standard treatments of heat engines, one is accustomed to applying the weak coupling assumption such that the quantum state for the total system of TLS plus each reservoir remains separable at all times in the TLS and reservoir degrees of freedom, here the weak coupling approximation

is applied to the residual environments. This results in a total state which is separable at all times in the degrees of freedom of S', R'_h and R'_c, namely $\rho_{S'} \otimes \rho_{R'_h} \otimes \rho_{R'_c}$, but where correlations between the TLS, the hot and the cold RC will form and indeed persist even in the limit cycle. These correlations are crucial to the performance of the engine in the stronger coupling regime. We show in the following section that the resulting coherence leads to limits on the engine's output which are not present in an incoherent version of the cycle.

4.2 Rethermalising reservoirs

Before turning to the characteristics of the finite time quantum Otto cycle, we must first address an implicit assumption which was made during the infinite time treatment of the cycle and that requires some adaptation here at finite times. In the infinite time version of the cycle, we assumed that when the TLS was decoupled from a particular reservoir, by the time the coupling was turned back on again this reservoir had returned to thermal equilibrium. Indeed, that the TLS is only ever coupled to a thermal reservoir at the start of an isochoric stroke is the reason why the particular form for the TLS-reservoir interaction in equations (3.6) and (3.7) yields no coupling costs. In the finite time version of the cycle, we also wish to make this assumption because, for the sake of our strong coupling comparison with weak coupling, we want to remain as close in spirit as possible to standard thermodynamic treatments which consider thermal reservoir resources. Since we shall be explicitly computing the dynamics of the full global state around the cycle, we need to build in to our model some phenomenologically motivated mechanism which explicitly ensures that an uncoupled reservoir returns to thermal equilibrium by the time it is coupled once more to the TLS.

In this section therefore, we briefly discuss how to modify the master equation governing the motion of the enlarged system S' in order to additionally induce damping of the uncoupled RC. The master equation for the enlarged system S' for the spin-boson model (the model used here for the interaction between the TLS working system and the reservoirs) for the case of one RC

takes the form

$$\frac{d\rho(t)}{dt} = -i\left[H_{S'}, \rho(t)\right] - \left[A, \left[\chi, \rho(t)\right]\right] + \left[A, \left\{\Xi, \rho(t)\right\}\right], \tag{4.1}$$

where the first term on the right hand side governs the unitary evolution of S' and the other Liouvillian terms induce decoherence and dissipation in the energy eigenbasis of S'. Here, $A = a + a^\dagger$, $H_{S'}$ is defined in equation (3.18) and the operators χ and Ξ are given by

$$\chi = \gamma \int_0^\infty d\tau \int_0^\infty d\omega \omega \cos(\omega\tau) \coth\left(\frac{\beta\omega}{2}\right) e^{-iH_{S'}\tau} A e^{iH_{S'}\tau} \tag{4.2}$$

$$\Xi = \gamma \int_0^\infty d\tau \int_0^\infty d\omega \cos(\omega\tau) \left[H_{S'}, e^{-iH_{S'}\tau} A e^{iH_{S'}\tau}\right]. \tag{4.3}$$

While the hot reservoir is coupled to the TLS, we wish to ensure that the cold reservoir rethermalises, and vice versa. This is because we wish to isolate effects on the engine metrics (work, heat, power, efficiency) which are due to strong coupling. Were the reservoirs not to thermalise while they are uncoupled from the system, it might be argued that any changes in the engine metrics might be due to the effects of coupling to non-thermal reservoirs. We can do this by adding terms to equation (4.1) which act only on the uncoupled RC space and hence do not depend on the full system plus RC eigenstructure. The uncoupled RC is a simple harmonic oscillator so we may add standard weak coupling dissipators, for example as can be found in [1]

$$\begin{aligned} L_{damp} &= \gamma_{damp}(N+1)\left\{a\rho(t)a^\dagger - \frac{1}{2}a^\dagger a\rho(t) - \frac{1}{2}\rho(t)a^\dagger a\right\} \\ &+ \gamma_{damp} N\left\{a^\dagger\rho(t)a - \frac{1}{2}aa^\dagger\rho(t) - \frac{1}{2}\rho(t)aa^\dagger\right\}. \end{aligned} \tag{4.4}$$

Here, $N = \frac{e^{-\beta\Omega}}{1-e^{-\beta\Omega}}$ is the thermal occupation number for the RC with frequency Ω at inverse

temperature β. We choose the rate γ_{damp} to ensure thermalisation occurs over a timescale such that the TLS re-couples to a thermal reservoir at the start of the subsequent isochore. The operators a ($a^\dagger$) represent the annihilation (creation) operations of the uncoupled RC.

4.3 Computing out of equilibrium engine states around the Otto cycle

The work output of the Otto cycle is given by the net energy change of the system across each of the isentropic strokes. This also involves accounting for the energetic costs associated with turning on or off the interaction term at the start and end of these strokes. As discussed previously, this leads to the following expression for work output

$$W = \mathrm{tr}\left[H_S^c \rho^C\right] - \mathrm{tr}\left[H_S^h \rho^B\right] + \mathrm{tr}\left[H_S^h \rho^A\right] - \mathrm{tr}\left[H_S^c \rho^D\right] - \mathrm{tr}\left[H_{I_h} \rho^B\right] - \mathrm{tr}\left[H_{I_c} \rho^D\right]. \quad (4.5)$$

Here, h (c) superscripts on the Hamiltonian operators indicate that the splitting in the TLS is set to ϵ_h (ϵ_c). The density operator ρ is labelled with superscripts $A - D$ indicating the various points around the cycle. In the infinite time version of the cycle, ρ represented the quantum state of the enlarged system S' consisting of the TLS and the RC from the hot reservoir for points A and B and from the cold reservoir for points C and D. Here we consider S' to be the enlarged system which consists of the TLS and two RCs (both hot and cold).

The first four terms in equation (4.5) are the usual energetic contributions for the work output of the cycle, which arise also in the weak coupling treatment. The final two terms are a distinct feature of the strong coupling treatment and arise because of costs of decoupling the TLS from either the hot or the cold reservoir. Since we include terms which bring about a rethermalisation of the non-interacting RC once it is decoupled, according to equation (4.4), we are still faced with the situation where there are no coupling costs, as explained previously.

The energy transferred into the system during the hot isochore is given by

$$Q = \mathrm{tr}\left[H^h_{S'}\rho^B\right] - \mathrm{tr}\left[H^h_{S'}\rho^A\right]. \tag{4.6}$$

We have previously discussed how this expression contains contributions from the interaction energy between the TLS and the RC as well as a contribution from the RC being pulled out of equilibrium. These contributions are neglected in weak coupling treatments but are important at stronger coupling and computable within the RC framework.

To evaluate equations (3.64) and (4.6), one needs to calculate the quantum states of S' at each of the points A, B, C and D when the engine is operating in the limit cycle. In the infinite time version of the cycle, this involves taking the steady state solution of an enlarged RC master equation along each isochore to obtain ρ^B and ρ^D. ρ^C and ρ^A can be obtained by unitary evolution along the isentropic strokes. In the present work, for finite time isochores, the calculation is much more involved and we must solve the dynamical equation of motion for the full state S'. For point B, we must solve the dynamical equation of motion for the hot isochore which is given by

$$\frac{d}{dt}\rho(t) = L_{A'\to B}[\rho(t)], \tag{4.7}$$

where $L_{A'\to B} = L_h[\rho(t)] + L_{damp}[\rho(t)]$. L_h is given by the right hand side of equation (4.1) with parameters set according to the hot isochore. The other Liouvillian term is as described in section 4.2 and is responsible for rethermalisation of the non-interacting RC representing the cold reservoir. For a particular isochore time, τ_i, the solution to this equation is

$$\rho^B = \mathcal{U}_h(\tau_i)[\rho^A] \equiv \exp(L_{A'\to B}\ \tau_i)[\rho^A]. \tag{4.8}$$

Decoupling from the hot reservoirs happens instantaneously and so the state is unchanged between B and B'. The state then evolves unitarily to point C under the time dependent Hamiltonian given in equation (3.1). Here we choose a time dependence for $\epsilon(t)$ and $\Delta(t)$ such

that $(\epsilon_h, \Delta_h) \to (\epsilon_c, \Delta_c)$ in a time τ which is much smaller than τ_i but such that the state still evolves adiabatically to a very good approximation:

$$H_S(t) = \frac{\epsilon_h}{2}\left(\frac{\epsilon_c}{\epsilon_h}\right)^{\frac{t}{\tau}}\sigma_z + \frac{\Delta_h}{2}\left(\frac{\Delta_c}{\Delta_h}\right)^{\frac{t}{\tau}}\sigma_x. \tag{4.9}$$

The state at point C can then be computed by solving for the time dependent unitary evolution governed by the Liouville von-Neumann equation of motion

$$\frac{d}{dt}\rho(t) = -i[H_S(t), \rho(t)]. \tag{4.10}$$

The interaction term for the cold bath is turned on instantaneously with no change in the system state and then the subsequent two strokes are carried out completely analogously to the previous two, but with the cold reservoir taking the place of the hot, and with $(\epsilon_c, \Delta_c) \to (\epsilon_h, \Delta_h)$ along the cold adiabatic stroke. In general, one complete cycle will return a different state at A' than that which was injected. However, after a number of cycles, these transient dynamics vanish and the limit cycle is reached [43], where the state at any one particular point is the same from one cycle to the next. This is the regime in which the engine's figures of merit are computed.

4.4 Non-equilibrium engine metrics

An Otto cycle heat engine outputs an optimal amount of work when it is permitted to absorb the maximum amount of heat during the hot isochore and convert this into work adiabatically along the hot isentropic stroke. For the process to be cyclic, a further heat exchange must occur with a heat reservoir and some work done on the working system before it is brought back into contact with the hot reservoir once more. Performing the isochoric strokes in finite time means that a less than maximal amount of heat can be exchanged between the working system and the reservoirs, with the knock on effect that a less than optimal amount of net work is performed by the engine. However, in reality engines are designed to operate out of equilibrium in order that they may generate a finite amount of power. There is therefore a tradeoff to be had between

extracting as much work as possible, and reducing the amount of time needed to perform a cycle.

Increasing the interaction strength between the TLS and the reservoirs in this engine speeds up the process of equilibration. The working system approaches its equilibrium state more quickly than with the interaction strength kept very weak. The closer the TLS is permitted to get to its eventual equilibrium state before embarking on the isentropic strokes, the more heat is absorbed (or dissipated) during the hot (or cold) isochore. This then translates into a larger population difference between the two energy eigenlevels of the TLS during the isentropic strokes, which is desired for optimal work extraction. Increasing the coupling strength is therefore one way of mitigating the loss in work output by performing the isochoric strokes in finite time. One has to pay an energetic cost due to system-reservoir decoupling at stronger coupling, as has been previously discussed. But for intermediate coupling strengths, before these costs begin to dominate too severely, the time gained in reaching close to equilibrium along the isochores translates into a greater power output at stronger coupling.

We show this behaviour of the engine in figure 4.1. Two different types of cycle are plotted there: an incoherent and a coherent version of the engine. We shall discuss the difference between these two shortly, but for the moment, let us note the general behaviour in both cases is for the work output of the engine to increase with coupling strength up to a point where there is a turnover as reservoir decoupling costs begin to dominate. Note that we are considering here a finite isochore time, τ_i, and that therefore the system has not reached its strongly coupled equilibrium state (at which point, as we have seen in the previous discussion of the equilibrium engine, work always decreases with coupling strength). The energy absorbed from the hot reservoir increases with coupling strength too and this leads to a decrease in efficiency over weaker coupling scenarios. However, as we have explained, the metric one often seeks to improve upon in practice is the power output, and we see here that, at finite coupling before costs begin to dominate, there is a region where it is beneficial to increase the system-reservoir coupling. A similar finding is also reflected in the analysis of the strong coupling regime for a heat engine via a different approach in Ref. [84], where the isochores are long enough that the engine is considered to have reached

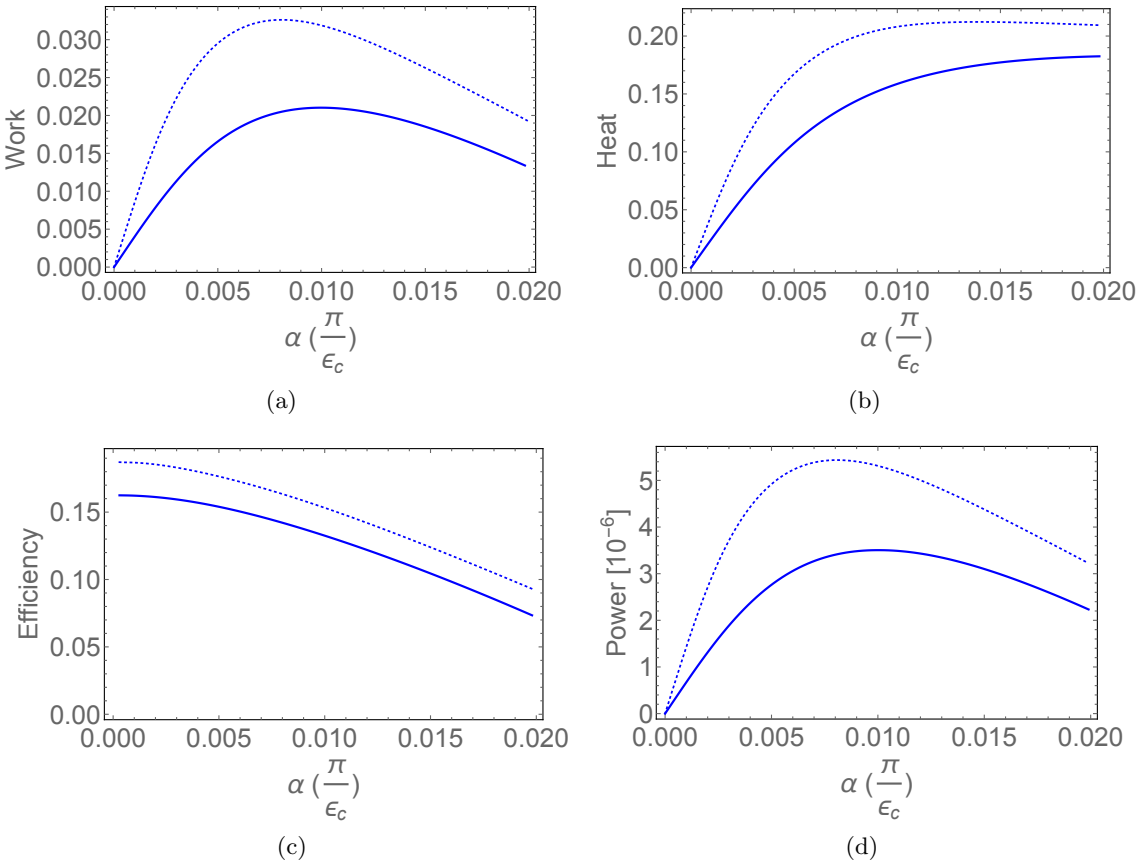

Figure 4.1: (a) work output, (b) heat absorbed, (c) efficiency and (d) power output of the non-equilibrium TLS Otto cycle engine, each as a function of coupling strength α for $\tau_i = 3000$. The metrics are plotted for two types of cycle: *blue dotted curve* the incoherent engine, *blue solid curve* the coherent engine. Parameters: $\epsilon_c = 1$, $\epsilon_h = 1.5$, $\Delta_h = \Delta_c = 1$, $\omega_c = 0.265$, $\beta_h = 0.95$, $\beta_c = 2.5$, $\gamma_{damp} = 0.1$, $N_{RC} = 9$. We see that work output and power increase with coupling strength up to a point where interaction costs begin to dominate and subsequently reverse this trend. The heat absorbed from the hot reservoir increases with coupling strength. Efficiency monotonically decreases with coupling strength. For all these metrics, an improvement is seen in the case where the build up of quantum coherence in the engine is suppressed.

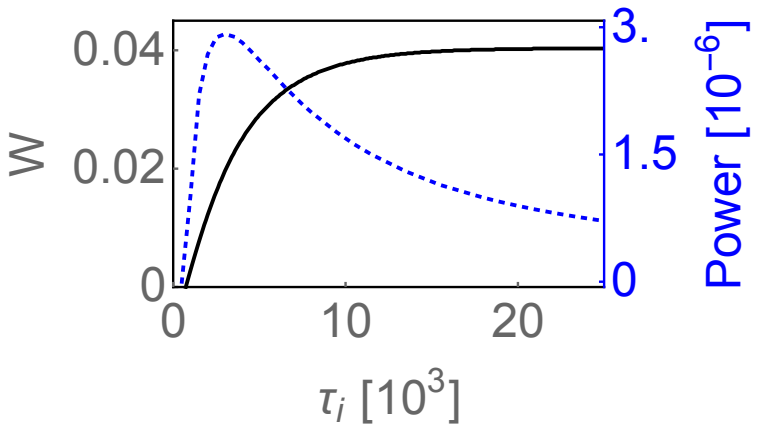

Figure 4.2: A joint plot of power and work against isochore time for $\alpha = 0.0055/\pi$, with work plotted in *black* on the left hand axis and power plotted in *blue dashed* on the right hand axis. Parameters: $\epsilon_c = 1$, $\epsilon_h = 1.5$, $\Delta_h = \Delta_c = 1$, $\omega_c = 0.265$, $\beta_h = 0.95$, $\beta_c = 2.5$, $N_{RC} = 9$. We see that power is maximised at isochore times which are shorter than those required for the engine to have equilibrated (where work output saturates).

arbitrarily close to equilibrium.

This latter point is reflected in figure 4.2 where we show the work output and power output as a function of τ_i for an intermediate coupling strength at which costs do not yet outweigh the benefits. As the system S' approaches equilibrium, the work output saturates. Power output, however, is in fact maximised before the working fluid has reached its equilibrium. If the desired metric for the engine is how much power it can produce, it is therefore preferable for it to operate out of equilibrium, by choosing shorter isochore times and intermediate coupling strengths.

4.5 Quantum nature of the heat engine

So far we have discussed the benefits of the strongly coupled engine over that of its weakly coupled counterpart in terms of increased power output. This of course has a significant practical importance for future technologies where nanoscale devices like heat engines may be key com-

ponents. Another benefit of analysing this particular model at strong coupling is that it affords us some insight into some fundamental effects on the thermodynamics of the engine which are purely quantum in nature. In a traditional weak coupling treatment of the Otto cycle, when the isochores are long enough, the TLS equilibrates to a Gibbs state, which is diagonal in the energy eigenbasis. This is a probabilistic distribution of classical energy eigenstates. With the isentropic strokes carried out adiabatically, populations in these energy eigenstates are kept constant and no coherence in the working system state accumulates. In fact, if the isentropic strokes remain approximately adiabatic when the cycle is treated at finite time, then no coherence is present during the isochores. Therefore quantum coherence does not play a role in the traditional, weak coupling treatment of the Otto cycle. At non-negligible system-reservoir interaction strength, quantum coherence in the energy eigenbasis is present in the TLS state at the end of the isochores because of correlations present between the TLS and the reservoir as the reservoir is pulled out of thermal equilibrium. This coherence will, in general, persist during the isentropes even if they are performed adiabatically. In this way, the strongly coupled TLS Otto cycle is inherently quantum in nature.

We wish to isolate the effects on engine performance of coherence in the working system developing during the heat exchange isochoric strokes as a result of non-negligible interactions with the heat reservoirs. To do so, we need to distinguish this fully quantum version of the cycle and one where coherence is prevented from accumulating. We achieve this distinction by introducing into equation (4.1) some terms which will induce pure dephasing [1, 3, 86, 87] in the energy eigenbasis of the system of interest, while taking care that these have no energetic contribution. To meet with these criteria, these purely dephasing terms must commute with $H_{S'}$, which we diagonalise and write as

$$H_{S'} = \sum_n E_n |E_n\rangle\langle E_n|. \tag{4.11}$$

We then construct a purely dephasing Liouvillian term as

$$L_{dep} = \gamma_{dep} \sum_n \left[|E_n\rangle\langle E_n|, [|E_n\rangle\langle E_n|, \rho(t)] \right]. \tag{4.12}$$

We are free to choose γ_{dep} to ensure dephasing occurs on an appropriate timescale, such that coherence is prevented from developing during the isochoric strokes of the engine. We can then compute the states of the working system at various points around the cycle as previously described in section 4.3. We define the incoherent engine as the version of the cycle where these pure dephasing terms have been including during the isochoric strokes. We stress here that these terms achieve pure dephasing in the energy eigenbasis of the enlarged TLS + RC eigenbasis rather than just the TLS energy eigenbasis. This is the natural choice for a system interacting strongly with an environment, rather than introducing purely dephasing terms into the master equation which only act on the TLS. The latter would be inappropriate as they have an energetic effect since they do not commute with the unitary part of the equation which depends on $H_{S'}$. The RC treatment, therefore, provides a route to choosing purely dephasing terms at strong reservoir coupling.

We compare these two versions of the Otto cycle, coherent and incoherent, and analyse the effect of quantum coherence on engine performance in figures 4.1 as a function of coupling strength and 4.3 as a function of isochore time. In the solid curves we depict the behaviour of the fully coherent engine. The dotted curves represent the incoherent version of the cycle. At longer isochore times, i.e. larger τ_i, the incoherent and coherent engines converge. Determining precisely how the timescale of this convergence relates to the coupling strength is the subject of ongoing work, however early indications are that thermalisation is inversely proportional to the coupling strength, rather than inversely proportional to its square which is true in a fully weak coupling treatment. At longer times, the state of S' approaches thermal equilbrium with the relevant residual reservoir which is maintained at the hot or cold temperature. This state is then diagonal in the energy eigenbasis of S', and so no coherence is present in either type of engine at points B or D if the isochore is long enough. For shorter times however, this is not the case, and pure dephasing does have an appreciable effect on the engine metrics.

The dephased engine absorbs more heat along the hot isochore and outputs a net work larger enough to yield a higher efficiency than the fully coherent engine. Decoupling costs remain comparable. These are dominated by the RC state being pulled out of equilibrium along the

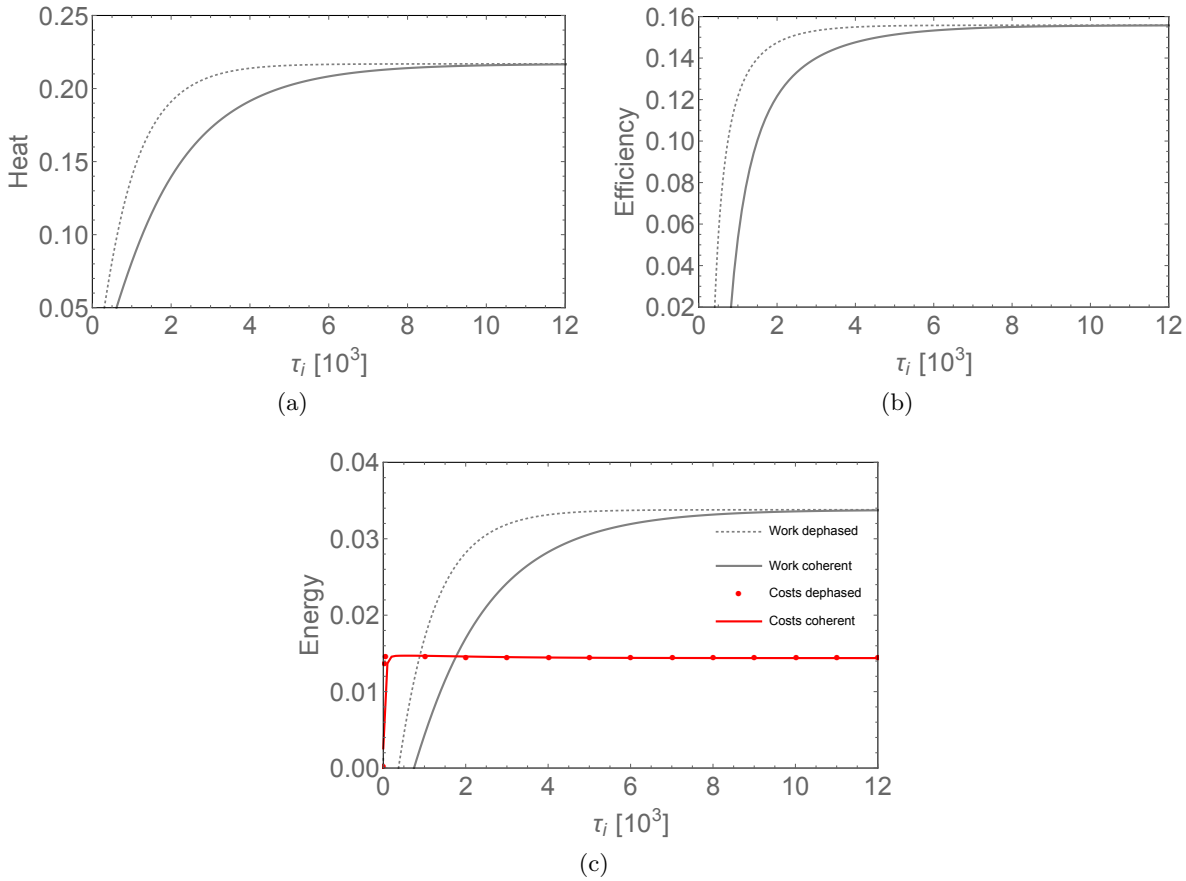

Figure 4.3: (a) Heat, (b) efficiency, (c) work and decoupling costs plotted against isochore time τ_i for the non-equilibrium TLS Otto cycle. *Solid curves* represent the fully coherent engine while *dotted curves* depict the behaviour of the incoherent engine where quantum coherence has been suppressed by pure dephasing in the energy eigenbasis of S'. Parameters: $\alpha = 0.01/\pi$, $\epsilon_c = 1$, $\epsilon_h = 1.5$, $\Delta_c = \Delta_h = 1$, $\omega_c = 0.265$, $\beta_h = 0.95$, $\beta_c = 2.5$, $N_{RC} = 9$. We see that dephasing leads to a quicker approach to equilibrium values for heat, work output and therefore efficiency. Decoupling costs remain comparable in both types of engine.

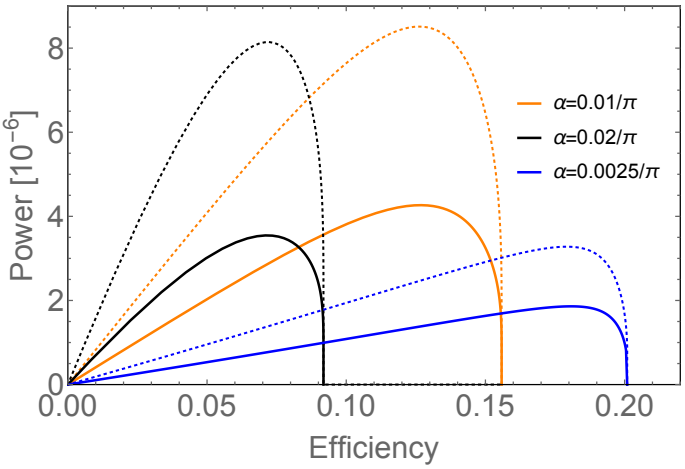

Figure 4.4: Parametric plot of power output against efficiency for the non-equilibrium TLS Otto cycle for various values of coupling strength α. Solid curves represent the fully coherent engine while dotted curves depict the behaviour of the incoherent engine. The parameter which is varied along the curves is the isochore time τ_i. Other parameters: $\epsilon_c = 1$, $\epsilon_h = 1.5$, $\Delta_c = \Delta_h = 1$, $\omega_c = 0.265$, $\beta_h = 0.95$, $\beta_c = 2.5$, $N_{RC} = 9$. We see that dephasing in the energy eigenbasis of S' leads to an engine that outperforms its quantum coherent counterpart for a range of coupling strengths. At weaker coupling, this effect is less pronounced.

isochores and this is not prevented by dephasing terms. In figure 4.4, we show this improved engine performance in parametric power versus efficiency plots for a selection of coupling strengths. Even at weaker but finite coupling, where coherence development is minimal, a pronounced improvement in power and efficiency over the coherent engine can be achieved by dephasing.

Dephasing in the TLS+RC basis accelerates the process of equilibration of the working system S'. Of crucial importance for heat and work calculations, which result from average energy differences between the points of the Otto cycle, are the ground and excited state populations of the TLS (in the eigenbasis of H_S), or rather the difference between these populations. In figure 4.5 we show how these are affected by dephasing in the full TLS+RC energy eigenbasis at point B, just before the hot adiabatic stroke begins, and at point D, just before the cold adiabatic stroke begins.

At point B, we wish to have as much population as possible in the excited state and therefore as small a population difference as possible. Recall that, for a two-level system, the maximally mixed state with half its population in the ground state and half in the excited state corresponds

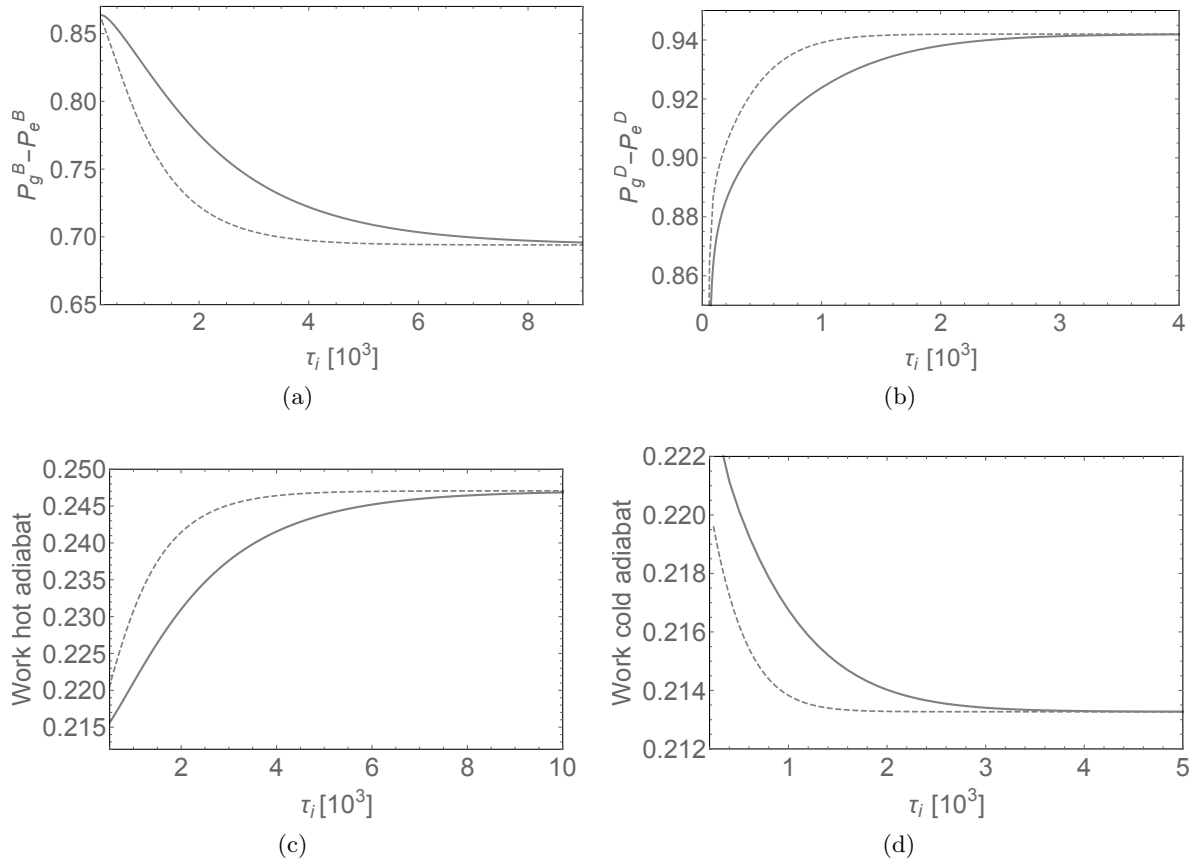

Figure 4.5: (a) The difference in population of the TLS eigenstates at point B in the Otto cycle, (b) The difference in population of the TLS eigenstates at point D in the cycle, (c) work extracted during the hot adiabatic stroke and (d) work input during the cold adiabatic stroke, each plotted against isochore time τ_i. *Solid curves* represent the fully coherent engine while *dotted curves* depict the behaviour of the incoherent engine. Parameters: $\alpha = 0.01/\pi$, $\epsilon_c = 1$, $\epsilon_h = 1.5$, $\Delta_c = \Delta_h = 1$, $\omega_c = 0.265$, $\beta_h = 0.95$, $\beta_c = 2.5$, $N_{RC} = 9$. We see that dephasing in the energy eigenbasis of S' leads to a population difference at crucial points around the cycle which is more beneficial for net work extraction. At shorter isochore times, there is a smaller population difference at point B in the version of the engine where coherence has been suppressed, meaning more heat has been absorbed during the hot isochore and more work can be extracted on the subsequent stroke. At point D, there is a larger population difference in the dephased engine, meaning more heat has been dumped into the cold reservoir during the cold isochore, and less work is done on the subsequent stroke.

to a theoretical thermal state at infinite temperature. The smaller the population difference at point B therefore, the higher the temperature reached by the TLS. This entails that more heat has been absorbed from the hot reservoir during the hot isochore and that the subsequent hot adiabatic stroke can extract an optimal amount of work. We recall that this stroke is carried out approximately adiabatically and the population difference in the TLS is preserved up to point C.

At point D, after interacting with the cold reservoir, it is desirable to have as little population in the excited state as possible and therefore as large a population difference as possible. This corresponds to a low temperature (recall that the ground state is the theoretical thermal state with zero temperature). It means that as much heat as possible has been dumped into the cold reservoir and that on the subsequent adiabatic stroke, the work performed on the system can be kept to a minimum.

We see this behaviour well illustrated in figure 4.5. For longer isochore times, the population difference at points B and D is the same in both the fully coherent and dephased (incoherent) engines. As previously discussed, this is what we would expect since we know that the engine metrics at longer times are the same for both types (heat, work, efficiency). At shorter times, the dephased engine displays a faster approach to the level reached at longer times than the fully coherent engine. At point B there is therefore a smaller population difference (plot (a)) at shorter τ_i and at point D a larger population difference (b). We see the effect this has on the work extracted during the hot adiabat (c) and invested during the cold adiabat (d). The dephased engine allows from greater work extraction and smaller work investment during these strokes when the previous isochore time has been shorter than that required for close to equilibrium levels to be reached.

4.6 Summary

We have looked at how a quantum system undergoing an Otto cycle can operate as a heat engine in a regime not typically considered: that of finite coupling and finite time. Yet, both of these

conditions are more readily met in any practical application of such a device. Vanishingly small interactions are harder to engineer and control. Very slow operation of the engine, yielding maximum work output, is not as practical as maximising finite power output for completing whatever task the engine may be designed for in a realistic time. In these, more realistic regimes, we have seen that finite system-reservoir interaction strength leads to a greater power output of the engine.

We have also compared a distinctly quantum version of the Otto cycle with one where quantum effects are minimized. In the coherent cycle, the working system is able to populate distinctly quantum states and develops coherence in the energy eigenbasis at finite isochore times due to its appreciable interaction with the environment. In an incoherent cycle, this coherence is dephased and the working system optimises its population of the ground and excited energetic states, desirable for a work extraction calculation.

This is a distinct effect from that of quantum friction, which degrades the work extraction strokes of quantum heat engines when these strokes are carried out in non-adiabatic conditions. We still operate in a close to adiabatic regime where there are negligibly small non-adiabatic transitions during the work strokes. Here, quantum coherence enters the cycle only through strong system-reservoir interactions.

In the case of quantum friction, superadiabatic schemes have been proposed to allow quantum engines to remain in the adiabatic regime despite operating in finite time, thus negating the detrimental effect of coherence build up along the isentropes. We argue here that schemes to dephase the working fluid of a quantum engine during isochoric strokes will also mitigate a degrading effect, accountable to strong coupling, and lead to enhanced performance.

We have explained in the main part of this chapter, how dephasing has been applied in the TLS+RC energy eigenbasis as a natural basis for systems strongly interacting with the reservoirs. We have also considered the effect of dephasing in the reduced TLS energy eigenbasis. This is done in Ref. [80] as a means of representing the classical counterpart to a quantum coherent engine, where coherence develops along the isentropes. We found that the behaviour

of such a stochastic engine was qualitatively similar to the case presented here: engine performance was enhanced. For the sake of avoiding repetition we therefore do not present that work here. However, we wish to note that dephasing in the TLS energy eigenbasis was also problematic. When included in a master equation for the enlarged system S', purely dephasing terms on the TLS subsystem could lead to unphysical population differences at the end of the isochores. This issue arises because terms which induce pure dephasing on the TLS in a weak coupling master equation have a different effect in the enlarged RC master equation. They can also act to change the population difference in the TLS since they do not commute with the enlarged system self-Hamiltonian $H_{S'}$, which includes a coupling term between the system and the RC. These terms therefore also entail an undesired energetic contribution (leading to erroneous population differences). The RC treatment thus allows us to identify the correct basis in which to apply pure dephasing.

This draws to a close this chapter on heat engines in the strong coupling regime. In the final chapter, to follow, we shall stick with the theme of quantum effects in thermodynamics at strong coupling. In the sections to follow, we seek to address the question of whether decoherence, i.e. the erasure of the quantum content of a particular state, entails an unavoidable thermodynamic cost.

Chapter 5

Thermodynamic cost of quantum information erasure

5.1 Introduction

Information theory and thermodynamics are intricately related through Landauer's erasure principle [88]. The latter establishes that there is an inherent work cost associated with an irreversible computation, specifically the cost of memory erasure. This principle is most commonly formulated in terms of a process which involves the resetting of a classical bit of information. The bit may be in the 0 or 1 state and therefore represents some information which an observer, unaware of the state, is not privy to. Resetting the bit involves wiping this information and forcing the bit into a known state, for example the 0 state. Landauer's principle tells us that this erasure of information must be accompanied by a dissipation of heat equivalent to at least $k_B T \ln 2$ into the environment (which is assumed to be in thermal equilibrium at temperature T). Here, k_B is the Boltzmann constant. Conservation of energy tells us therefore that there must be an equivalent amount of work done on the physical system used to represent the bit of information, representing the cost of information erasure. This simple, fundamental observation reverberates widely across physics and information theory. It may be employed in a resolution

of the Szilard engine and Maxwell's demon paradox [89]. It leads to a fundamental bound on the capacity of a noisy communication channel (one that is open to the environment) for the transmission of information encoded in both classical systems [90] and quantum systems [91, 92]. It can be used to determine an upper bound on the amount of classical information which can be encoded in a quantum state, as an alternative means of proving that quantum states cannot be cloned, and as a means of setting a bound to how efficient any stochastic process of enhancing the degree of entanglement in a multi-partite quantum state can be [93].

Landauer's erasure principle is by its very nature a statement about open physical systems. It has been argued that it holds for the erasure of classical information in the both the case where this is encoded in a classical physical system (i.e. a macroscopic one which is well described without recourse to quantum theory) and also the case where a quantum physical system is used to represent the classical information. It holds in both the weak and strong environmental coupling regimes [88, 94, 95].

The question we seek to address in this chapter concerns the erasure of quantum information in the form of coherence. This is the degree to which a given quantum state represents a superposition of classical states. Can this type of erasure, the decoherence of a single quantum bit, be understood in a thermodynamic setting, in the same spirit as the thermodynamic connotations of erasing a single bit. In answering the question we have just posed concerning the erasure of quantum information, we shall see that we are led to consider the issue of anomalous information flow in a setting where a Born-Markov treatment is invalid, i.e. a non-Markovian setting.

Recently, attempts have been made to establish a correlation between anomalous information flow and anomalous heat flow in non-Markovian open quantum systems [96]. In Markovian open quantum systems, information which passes from the system into the reservoir is lost, since the reservoir is modelled as static. However in non-Markovian open quantum systems, one accounts for how the interaction may alter the reservoir state to one which may transfer some information back to the system through subsequent interactions with the system. In the case of the spin-boson model studied in Ref. [96] and for the definitions of information flow and

heat flow considered therein, no conclusive correlation is seen between anomalous flows of each kind. We shall revisit this question of whether there is any correlation between the behaviour of a thermodynamic quantity and the behaviour of information transfer beyond the realm of weak coupling.

We will explore all of this, at first, within the simplified version of the spin-boson model which we discussed in sections 1.4.2 and 2.3.2, the independent boson model. We will then extend our treatment to the more complicated spin-boson model. The independent boson model induces pure decoherence of the spin in its energy eigenbasis. The question of properly accounting for quantum coherence in the thermodynamics of open quantum systems is the subject of much debate in the literature. We are, of course, particularly interested in cases where system-environment interactions are non-negligible. We have seen in chapter 3 that in these situations, when a system is left to thermalise by exchanging heat with a thermal reservoir, a canonical Gibbs state with respect to the system self-Hamiltonian is in fact not the steady state equilibrium. The difficulties with associating heat flow into a system with changes in its von Neumann entropy in such settings are discussed in Ref. [97]. The approach advocated for there is for a special definition of quantum heat which contains two components, one associated with entropic changes in the system and another, excess heat, associated with the preservation of quantum coherence into the steady state. The approach relies on a definition of thermodynamic entropy which assumes that coherence in the system prevents a steady state which would otherwise be Gibbsian. A different approach is discussed in Refs [98, 99]. Key to this strategy is to assume a thermal reservoir is capable of exchanging both heat and work with the system. Elsewhere the argument is made for associating thermodynamic entropy solely with diagonal entropy [100, 101]. The latter coincides with von Neumann entropy only in the case of states with no coherence in the energy eigenbasis. This approach rules out any thermodynamic interpretation to decoherence.

Here, we make use of the exact definitions of reversible entropy flow and irreversible entropy production for a time independent open quantum system, as derived in Ref. [61]. We shall see how these come into play in the context of the independent boson model. We will explore

decoherence within that framework, with the objective of discovering whether it uncovers a thermodynamic signature associated with the erasure of quantum information. We will see how entropy flow and entropy production can be extracted using the RC framework and this will allow us to extend our analysis beyond the exactly solvable independent boson model to the spin-boson model where these quantities are less easily computed otherwise.

5.2 Information flow in the independent boson model

We begin by recalling from sections 1.4.1 and 2.2 that the global Hamiltonian for the independent boson model is given by

$$H = \frac{\epsilon}{2}\sigma_z + \sigma_z \sum_k g_k \left(b_k^\dagger + b_k\right) + \sum_k \omega_k b_k^\dagger b_k, \tag{5.1}$$

where all symbols retain their meaning from those previous sections and we identify each term as the self-Hamiltonian of the system $H_S \equiv \frac{\epsilon}{2}\sigma_z$, the self-Hamiltonian of the environment $H_E \equiv \sum_k \omega_k b_k^\dagger b_k$ and the interaction term $H_I \equiv \sigma_z \sum_k g_k \left(b_k^\dagger + b_k\right)$.

The information content of a physical system is encoded in its entropy. In the present case of a TLS interacting with a bosonic reservoir we are interested in information flow into and out of the TLS, and therefore in the von Neumann entropy of the reduced TLS density operator as a function of time:

$$S_S(t) = -k_B \mathrm{tr}\left[\rho_S(t) \ln \rho_S(t)\right]. \tag{5.2}$$

For ease of notation, we shall henceforward drop the Boltzmann constant proportionality factor by setting $k_B = 1$. More specifically we are interested in the change in the system's entropy $\Delta S_S(t)$ as it interacts with the environment between times $t = 0$ and t,

$$\Delta S_S(t) = -\mathrm{tr}\left[\rho_S(t) \ln \rho_S(t)\right] + \mathrm{tr}\left[\rho_S(0) \ln \rho_S(0)\right]. \tag{5.3}$$

We will proceed by manipulating equation (5.3) into an expression which isolates two distinct contributions: one reversible, associated with heat exchange with a reservoir, and the other irreversible, associated with entropy generation within the system. The derivations which follow are due to Ref. [61], and we work through them here for the dual purposes of keeping this document self-contained and clarifying precisely which assumptions about the system and its interaction with the reservoir are made. We begin with the common assumption that the initial global state of system and environment is separable, $\rho(0) = \rho_S(0) \otimes \rho_E(0)$. Because this global system is closed, the von Neumann entropy remains constant:

$$-\mathrm{tr}\left[\rho(t)\ln\rho(t)\right] = -\mathrm{tr}\left[\rho(0)\ln\rho(0)\right] \equiv -\mathrm{tr}\left[\rho_S(0)\ln\rho_S(0)\right] - \mathrm{tr}\left[\rho_E(0)\ln\rho_E(0)\right]. \tag{5.4}$$

In the above, we have substituted in for the separable initial global state at $t = 0$. Rearranging equation (5.4) and substituting in for the second term on the right hand side of equation (5.3) yields

$$\Delta S_S(t) \;=\; -\mathrm{tr}\left[\rho_S(t)\ln\rho_S(t)\right] + \mathrm{tr}\left[\rho(t)\ln\rho(t)\right] - \mathrm{tr}\left[\rho_E(0)\ln\rho_E(0)\right]. \tag{5.5}$$

We may now expand the first term on the right hand side of equation (5.5) by adding and subtracting a term proportional to the logarithm of the initial environment state to give

$$\begin{aligned}\Delta S_S(t) &= -\mathrm{tr}\left[\rho(t)\ln\rho_S(t)\otimes\rho_E(0)\right] + \mathrm{tr}\left[\rho_E(t)\ln\rho_E(0)\right] + \mathrm{tr}\left[\rho(t)\ln\rho(t)\right] - \mathrm{tr}\left[\rho_E(0)\ln\rho_E(0)\right] \\ &= -\mathrm{tr}\left[\rho(t)\ln\rho_S(t)\otimes\rho_E(0)\right] + \mathrm{tr}\left[\rho(t)\ln\rho(t)\right] + \mathrm{tr}\left[\left(\rho_E(t)-\rho_E(0)\right)\ln\rho_E(0)\right], \end{aligned} \tag{5.6}$$

where in the second line we have merely performed a rearrangement in order to group together system terms and, separately, environmental terms.

Now, let us define heat flow as energy leaving the reservoir, positive if there is a net flow of energy out of the reservoir and negative if there is a net flow of energy into the reservoir. By extension, this is consistent with the sign convention we have taken elsewhere for work in the case of time dependent Hamiltonians, positive if there is a flow of energetic work done into

the working system and negative if there is a flow of work out of the system. Heat flow is therefore computed as the change in the expectation value of the environment Hamiltonian: $Q(t) \equiv \langle H_E(0)\rangle - \langle H_E(t)\rangle$ (note that this ensures the correct sign convention). We take the environment to be initialised in the thermal equilibrium state $\rho_E(0) = \rho_E^{eq} = \frac{\exp(-\beta H_E)}{Z_E}$ and note that in our model there is no time dependence on the global Hamiltonian, given in equation (5.1), and more specifically for our purposes here, no time dependence in the environment term. This means we may manipulate the expression for heat flow as follows

$$\begin{aligned} Q(t) &= \mathrm{tr}\left[\rho_E(0)H_E\right] - \mathrm{tr}\left[\rho_E(t)H_E\right] \\ &= \frac{1}{\beta}\mathrm{tr}\left[(\rho_E(t) - \rho_E(0))\ln\rho_E(0)\right]. \end{aligned} \tag{5.7}$$

We note that the right hand side of equation (5.7) is equivalent to the final term on the right hand side of equation (5.6) up to the factor of $\frac{1}{\beta}$. We will therefore label this term reversible entropy flow and associate it with heat flow, $\Delta_e(t) = \beta Q(t)$, as defined by energy leaving the environment. If the energy of the reservoir falls, i.e. $Q(t) > 0$ then entropy flows into the TLS, i.e. $\Delta_e(t) > 0$. The alternative situation where entropy flows out of the system, i.e. $\Delta_e(t) < 0$, is associated with heat dissipation into the reservoir and $Q(t) < 0$.

The other two terms on the right hand side of equation (5.6) may be written more compactly as the relative entropy between the correlated full system-environment state $\rho(t)$ and a separable state composed of the tensor product of the reduced TLS state $\rho_S(t)$ and an environment which has remained in equilibrium, $\left[\rho(t)||\rho_S(t)\otimes\rho_E^{eq}\right] \equiv \mathrm{tr}\left[\rho(t)\ln\rho(t)\right] - \mathrm{tr}\left[\rho(t)\ln\rho_S(t)\otimes\rho_E(0)\right]$. Collectively these two terms define the irreversible entropy production within the TLS, $\Delta_i(t)$, for which there is no associated heat flow. In summary, we have partitioned the change in entropy of the TLS into a reversible and an irreversible component as follows

$$\Delta S_S(t) = \Delta_i(t) + \Delta_e(t) \tag{5.8}$$

$$\Delta_i(t) = D\left[\rho(t)||\rho_S(t)\otimes\rho_E^{eq}\right] \tag{5.9}$$

$$\Delta_e(t) = \mathrm{tr}\left[(\rho_E(t) - \rho_E^{eq})\ln\rho_E^{eq}\right]. \tag{5.10}$$

The superscript on the environment state signifies the initial thermal equilibrium state. We note that equation (5.9) implies $\Delta_i(t) \geq 0$ and that our sign convention is that positive entropy flow, $\Delta_e(t)$, is associated with heat flowing out of the reservoir and into the system.

For the independent boson model, we can write down exact analytical expressions for reversible and irreversible entropy production. The total energy is partitioned into an internal energy term for the TLS, an interaction term and an environment internal energy, see equation (5.1). An exact expression is given in equation (2.96) for the expectation value of the interaction energy as a function of time. We also know from equations (1.93) and (1.94) that the TLS populations are unchanging. The TLS internal energy is therefore constant, $\Delta\langle H_S\rangle(t) = 0$. As the total Hamiltonian is time independent, by energy conservation we therefore obtain

$$Q(t) = 2\int_0^\infty d\omega \frac{J(\omega)}{\omega}[1-\cos(\omega t)], \tag{5.11}$$

$$\Delta_e(t) = 2\beta\int_0^\infty d\omega \frac{J(\omega)}{\omega}[1-\cos(\omega t)]. \tag{5.12}$$

By equation (5.8), we can also arrive at the following expression for entropy production in the independent boson model

$$\Delta_i(t) = \Delta S_S(t) - 2\beta\int_0^\infty d\omega \frac{J(\omega)}{\omega}[1-\cos(\omega t)], \tag{5.13}$$

where, in practice, one can compute the TLS entropy change, $\Delta S_S(t)$, using the expression derived in section 1.4.2 for the exact time evolution of the TLS density operator given in equation (1.100), for a given spectral density and decoherence function.

In figure 5.1 we perform this computation for two different initial TLS states, one with no coherence and the other a maximally coherent superposition of the two system energy eigenstates. We define $|g\rangle$ and $|e\rangle$ as the ground and excited eigenstates respectively of $H_S = \frac{\epsilon}{2}\sigma_z$ and $|\pm\rangle \equiv \frac{1}{\sqrt{2}}(|g\rangle \pm |e\rangle)$. Reversible entropy flow, in (a), is independent of the initial state and is proportional to the change in energy held within the interaction term, equation (5.12). This implies that for non-negligible system-environment coupling there is a flow of heat into the

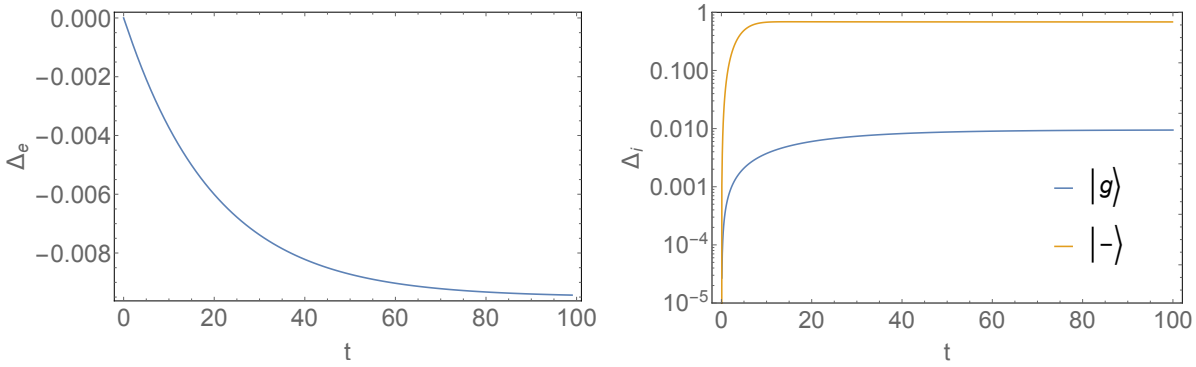

(a) (b)

Figure 5.1: Reversible entropy flow (a) and irreversible entropy production (b) for an initial state with coherence in the energy eigenbasis, (*yellow curve*), and without, (*blue curve*) as a function of time for the independent boson model. Entropy flow is independent of the initial state. For the $|g\rangle$ state (ground eigenstate of H_S), irreversible entropy production is equal in magnitude and opposite in sign to entropy flow. For the $|-\rangle \equiv \frac{1}{\sqrt{2}}(|g\rangle - |e\rangle)$ state (an equal superposition of ground and excited eigenstates of H_S) there is an additional contribution from the erasure of the quantum coherence of the state. Parameters: $\epsilon = 1$, $\omega_0 = 1$, $\Gamma = 20$, $\alpha = 0.01/\pi$, $\beta = 0.95$.

reservoir even though the system dynamics are static. Irreversible entropy production, plotted in (b), does depend on the amount of coherence within the TLS initial state. For a state with no coherence in the energy eigenbasis, it is equal in magnitude and opposite in sign to the entropy flow. This is the case for all states which lie on the z-axis of the Bloch sphere, i.e. all states which are mixtures of $|g\rangle$ and $|e\rangle$. All such states are fixed points under the independent boson model, and therefore there is no change in the system entropy, $\Delta S_S = 0$, implying $\Delta_i = -\Delta_e$ by equation 5.8. For states with coherence in the energy eigenbases, there is an additional contribution Δ_i due to the erasure of this coherence as the TLS state tends to a mixed state which lies on the Bloch sphere z-axis. This accounts for the additional amount of irreversible entropy production seen for the $|-\rangle$ initial state. In the independent boson model therefore, the thermodynamic cost of decoherence appears as an additional contribution to irreversible entropy production, which is not detectable as dissipation of heat into or out of the reservoir.

5.3 Information flow in the independent boson model according to the RC framework

It is also possible to evaluate approximations for entropy flow and entropy production within the RC framework. This is not necessary in the case of an exactly solvable model such as the independent boson model, where exact analytical expressions are available, but we wish to show here how the RC framework can alternatively be employed, when done so with care. We will then employ it in the case of the full spin-boson model where exact expressions for entropy flow and entropy production are not available.

In the RC picture, the system-reservoir interaction is captured by an interaction between ρ_S and the collective environmental degree of freedom ρ_{RC}, the joint state of which we label as $\rho_{S'}$. $\rho_{S'}$ remains at all times in a separable state with a residual environment $\rho_{E'}$, which, in turn, remains in its initial equilibrium state. We now proceed by re-deriving equation (5.6) in the RC frame. The change is entropy of the TLS is then

$$\begin{aligned}\Delta S_S(t) &= -\mathrm{tr}\left[\rho_S(t)\ln\rho_S(t)\right] + \mathrm{tr}\left[\rho(t)\ln\rho(t)\right] - \mathrm{tr}\left[\rho_E(0)\ln\rho_E(0)\right] \\ &\approx -\mathrm{tr}\left[\rho_S(t)\ln\rho_S(t)\right] + \mathrm{tr}\left[\rho_{S\prime}(t)\otimes\rho_{E'}\ln\left(\rho_{S'}(t)\otimes\rho_{E'}\right)\right] \\ &\quad -\mathrm{tr}\left[\rho_{RC}(0)\otimes\rho_{E'}\ln\left(\rho_{RC}(0)\otimes\rho_{E'}\right)\right]. \end{aligned} \tag{5.14}$$

In the second line we have recast $\rho(t)$ and $\rho_E(t)$ into the RC picture in the second two terms on the right hand side under the assumption that the initial state is given by $\rho(0) = \rho_S(0)\otimes\rho_{RC}(0)\otimes\rho_{E'}(0)$. By adding and subtracting tensor products with environmental states to the first term, this may be rewritten as

$$\begin{aligned}\Delta S_S(t) \approx &- \mathrm{tr}\left[\rho_{S'}(t)\otimes\rho_{E'}\ln\left(\rho_S(t)\otimes\rho_{RC}(0)\otimes\rho_{E'}\right)\right] + \mathrm{tr}\left[\rho_{RC}(t)\otimes\rho_{E'}\ln\left(\rho_{RC}(0)\otimes\rho_{E'}\right)\right] \\ &+ \mathrm{tr}\left[\rho_{S'}(t)\otimes\rho_{E'}\ln\left(\rho_{S'}(t)\otimes\rho_{E'}\right)\right] - \mathrm{tr}\left[\rho_{RC}(0)\otimes\rho_{E'}\ln\left(\rho_{RC}(0)\otimes\rho_{E'}\right)\right]. \end{aligned} \tag{5.15}$$

Collecting terms we arrive at the following more succinct expression for TLS entropy change

$$\begin{aligned}\Delta S_S(t) \approx & - \mathrm{tr}\left[\rho_{S'}(t)\ln\left(\rho_S(t)\otimes\rho_{RC}(0)\right)\right] + \mathrm{tr}\left[\rho_{S'}(t)\ln\rho_{S'}(t)\right] \\ & + \mathrm{tr}\left[\left(\rho_{RC}(t)-\rho_{RC}(0)\right)\ln\rho_{RC}(0)\right], \end{aligned} \tag{5.16}$$

and at the following expressions for entropy flow and entropy production within the RC picture

$$\Delta_i(t) \approx D\left[\rho_{S'}(t)||\rho_S(t)\otimes\rho_{RC}(0)\right], \tag{5.17}$$

$$\Delta_e(t) \approx \mathrm{tr}\left[\left(\rho_{RC}(t)-\rho_{RC}(0)\right)\ln\rho_{RC}(0)\right]. \tag{5.18}$$

However, proceeding in this way involves making severely restricting approximations on the environmental dynamics which we would expect to adversely affect the accuracy of any computation of entropy flow and entropy production. In equation (5.14) we have replaced the global state $\rho(t)$ with the global state in the RC frame $\rho_{S'}(t)\otimes\rho_{E'}$. This involves making the Born-Markov approximations on the residual reservoir E'. We have seen in chapter 2 how these approximations are valid for computing the dynamics of the reduced original system state $\rho_S(t)$ in regimes where they are invalid when made on the original environment E. But we cannot expect the framework to reproduce the correct dynamics of the full environment. Indeed the framework is designed for situations where this computation is not possible. Since the expressions for entropy flow, and by extension entropy production, in equations (5.10) and (5.9) rely on expressions being available for the full global state and the reduced state of a dynamical non-Markovian environment, we anticipate that approximating them with expressions from the RC framework, as we have done here, will lead to inaccuracies.

We will show, in due course, how despite this the RC framework may still be used to provide accurate estimates. However, for the time being we observe these anticipated inaccuracies in figure 5.2 when the RC framework is employed in the manner outlined so far. Here, we plot Δ_e and Δ_i for two initial states of the TLS at both weak and strong coupling to the bosonic reservoir, computed exactly according to equations (5.12) and (5.13) and also using equations (5.17) and (5.18). It is clear that, although we saw in chapter 2 that the RC picture leads to

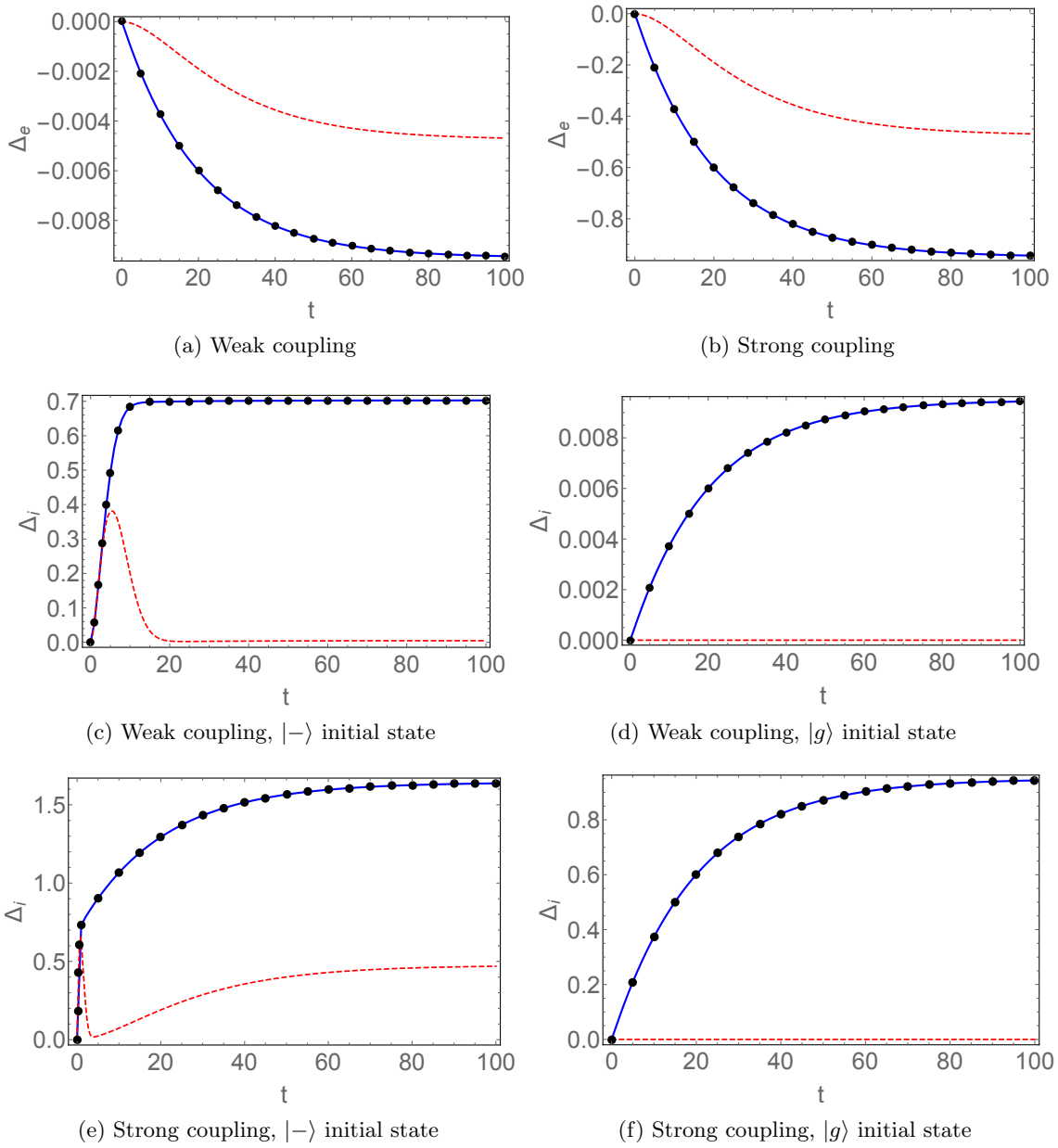

(a) Weak coupling

(b) Strong coupling

(c) Weak coupling, $|-\rangle$ initial state

(d) Weak coupling, $|g\rangle$ initial state

(e) Strong coupling, $|-\rangle$ initial state

(f) Strong coupling, $|g\rangle$ initial state

Figure 5.2: (a) Reversible entropy flow $\Delta_e(t)$ at weak coupling and (b) at strong coupling. The results are independent of initial TLS state. (c) Irreversible entropy production $\Delta_i(t)$ at weak coupling for an initial TLS state $|-\rangle$ and (d) for an initial TLS state $|g\rangle$. (e) Irreversible entropy production $\Delta_i(t)$ at strong coupling for an initial TLS state $|-\rangle$ and (f) for an initial TLS state $|g\rangle$. *Blue curves* - exact solution; *red dashed curves* - calculated in RC picture according to equations (5.17) and (5.18); *black points* - calculated in the RC picture using equations (5.20) and (5.8). Parameters: $\epsilon = 1$, $\omega_0 = 1$, $\Gamma = 20$, $\beta = 0.95$, strong coupling $\alpha = 1/\pi$, weak coupling $\alpha = 0.01/\pi$. When the RC framework is instead used to compute the interaction energy in equation (5.20) and the system entropy change in equation (5.8) we obtain good agreement with the exact solutions for $\Delta_e(t)$ and $\Delta_i(t)$ at weaker and stronger coupling.

excellent agreement with the exact results for TLS dynamics as a function of time, employing equations (5.17) and (5.18) does not yield a good approximation to the exact results for entropy flow between the TLS and the reservoir, or entropy production within the TLS, at either strong or weak coupling, for either initial TLS state, with or without coherence.

In the case of entropy flow ((a), (b)), the qualitative behaviour is reproduced in the RC frame, but the predictions are quantitatively inaccurate. Entropy production ((c)-(f)) is very poorly represented in the RC frame, when using equations (5.17) and (5.18), except at short timescales in the case where there is initial coherence in the system state.

A better approach is to employ the RC framework to compute a good approximation for the interaction energy and the TLS energy (via the dynamics of the TLS). The change in energy for the global state in the independent boson model is given by

$$\Delta E(t) = \Delta\langle H_S\rangle(t) + \Delta\langle H_I\rangle(t) + \Delta\langle H_E\rangle(t), \tag{5.19}$$

where $\Delta\langle\bullet\rangle(t) \equiv \mathrm{tr}[\bullet(\rho(t) - \rho(0))]$, and the Hamiltonian terms are as written in equation (5.1). We have seen in section 2.3.2 and in figure 2.7 how the RC framework can be used to compute an accurate approximation for the second term in equation (5.19). In figure 2.6 we saw how the dynamics of $\rho_S(t)$ can also be obtained to a high level of accuracy. We may therefore employ these dynamics in a computation of the first term in equation (5.19), in cases where this term is not constant such as the full spin-boson model to which we shall extend our analysis in section 5.4. Since we are dealing with a time independent total Hamiltonian, we have that $\Delta E(t) = 0$. Therefore, armed with accurate approximations for the first two terms, we may tackle the third term, the change in energy in the environment, which we also know how to relate to reversible entropy flow according to

$$\begin{aligned} \Delta_e(t) &= \beta Q(t) \\ &= -\beta\Delta\langle H_E\rangle(t) \\ &= \beta\left[\Delta\langle H_S\rangle(t) + \Delta\langle H_I\rangle(t)\right]. \end{aligned} \tag{5.20}$$

Furthermore, the change in the von Neumann entropy of the TLS, $\Delta S_S(t)$, can be well approximated by means of the RC version of the system dynamics. This means we now have good approximations for two of the three terms in equation (5.8), which we may therefore combine to yield a more accurate approximation for the third term, irreversible entropy production $\Delta_i(t)$. Proceeding in this manner yields the black dots plotted in figure 5.2 which agree well with the exact results.

We can therefore avoid the pitfalls of computation by means of equations (5.17) and (5.18), which fail to yield accurate approximations because the RC fails to capture the dynamics of the whole environment sufficiently well to allow for it to serve as an approximation for the environment terms in equations (5.9) and (5.10). We simply need to take care that the RC framework is used to obtain approximations for either system observables or the interaction energy, rather than full environment observables. This is the method we shall employ in the next section to look at information flow in the spin-boson model.

5.4 Information flow in the spin-boson model

The total Hamiltonian for the spin-boson model is given by

$$H_{SB} = \frac{\epsilon}{2}\sigma_z + \frac{\Delta}{2}\sigma_x + \sigma_z \sum_k g_k(b_k^\dagger + b_k) + \sum_k \omega_k b_k^\dagger b_k. \tag{5.21}$$

Here, we have an additional term proportional to σ_x known as the tunnelling term, with amplitude Δ. The TLS self-energy is now given by $H_S = \frac{\epsilon}{2}\sigma_z + \frac{\Delta}{2}\sigma_x$, which differs from the definition in section 5.2 as it now contains this additional tunnelling term. The interaction energy and reservoir energy terms remain unchanged from the independent boson case. This model is no longer exactly analytically solvable and as we have discussed in previous chapters, the RC approach is a powerful method for computing the dynamics of the TLS beyond weak coupling, as it can accurately keep track of correlations between it and the reservoir. Crucially, we may employ the RC framework to obtain an accurate approximation for the expectation value of

the interaction energy as a function of time which is a key ingredient for our present task of obtaining accurate approximations for information dynamics in the form of entropy flow and entropy production.

We therefore proceed exactly as outlined at the end of section 5.3 and consider information flow in the spin-boson model by computing the change in von Neumann entropy of the TLS ΔS_S, partitioned into entropy flow Δ_e and entropy production Δ_i for various initial states of the TLS in figure 5.3. In (a) and (c), we consider the ground and excited energy eigenstates of H_S, $|g\rangle$ and $|e\rangle$, in (b) an equal superposition of these eigenstates, $|-\rangle \equiv \frac{1}{\sqrt{2}}(|g\rangle - |e\rangle)$, and in (d) we consider an initial Gibbs state of the TLS, $\rho_S^{eq} \equiv \frac{\exp(-\beta H_S)}{Z_S}$. For all of these initial TLS states, the RC is initialised in a Gibbs state at inverse temperature β with respect to the RC self-Hamiltonian and the composite system S' starts in a tensor product state. In (e) we consider the special case of an initial ground energy eigenstate of the composite system of S' with respect to the TLS+RC self-Hamiltonian, $|g_{S'}\rangle$.

For each of the initial states which are pure states of the TLS, the steady state value for ΔS_S is the same (dashed lines), since each of these begins with $S_{VN} = 0$ and reaches the same equilibrium steady state. In the case of ρ_S^{eq}, the change in von Neumann entropy ΔS_S is much smaller. This is because this initial state is already close to the long time equilibrium state but we note that $\Delta S_S \neq 0$ as a result of strong reservoir coupling effects pulling the TLS state away from a canonical Gibbs thermal state. The approach to this equilibrium value for ΔS_S is not monotonic, with oscillations present at shorter times fading away to a steady approach at later times.

The two components of entropy change, Δ_e and Δ_i also display this oscillatory behaviour at shorter times before transitioning to a steady approach to their respective equilibrium values. Entropy production Δ_i is always positive by equation (5.9), but non-monotonic dynamics, as observed here, are not forbidden. Entropy flow Δ_e, on the other hand, can be positive or negative and we recall that according to the sign convention we have adopted in the previous section, heat flowing into the TLS is accompanied by a positive entropy flow, while heat dissipating out of the TLS entails a negative entropy flow. As we might expect heat, and therefore entropy

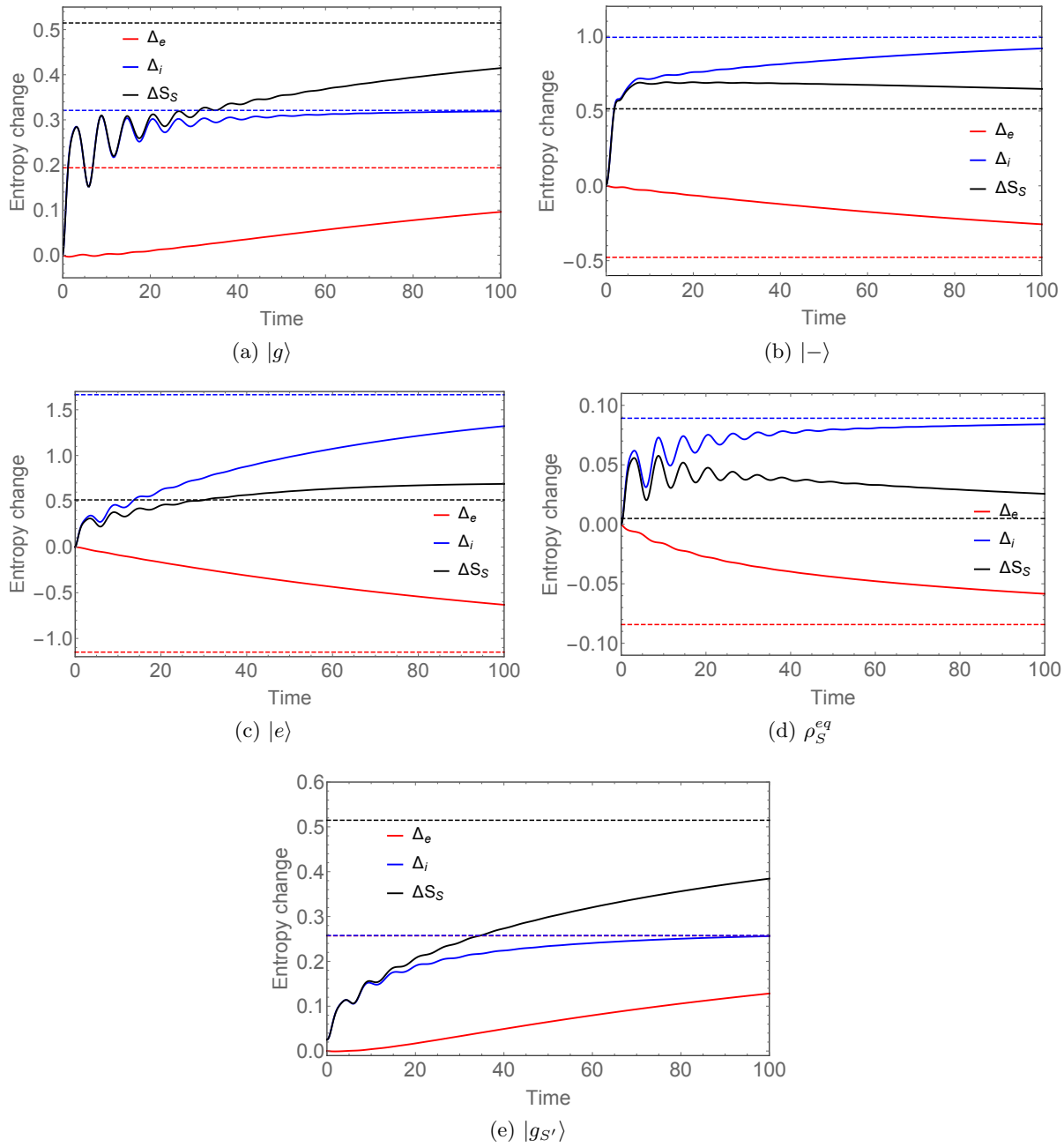

(a) $|g\rangle$ (b) $|-\rangle$

(c) $|e\rangle$ (d) ρ_S^{eq}

(e) $|g_{S'}\rangle$

Figure 5.3: Change in the von Neumann entropy of the TLS, ΔS_S, and its partitioning into reversible entropy flow, Δ_e, and irreversible entropy production, Δ_i, for various initial states: (a) $|g\rangle$, ground energy eigenstate of the TLS; (b) $|-\rangle = \frac{1}{\sqrt{2}}(|g\rangle - |e\rangle)$, a superposition of the two TLS energy eigenstates; (c) $|e\rangle$, excited energy eigenstate of the TLS; (d) ρ_S^{eq} a Gibbs thermal state of the TLS at temperature β; (e) $|g_{S'}\rangle$, the ground energy eigenstate of the enlarged TLS+RC system S'. *Solid curves* show the dynamical behaviour of ΔS_S (*black*), Δ_e (*red*) and Δ_i (*blue*). *Dashed curves* mark the steady state values (and note that in (e) the steady state values for Δ_i and Δ_e are approximately the same). Parameters: $\epsilon = 1$, $\Delta = 1$, $\omega_0 = 1$, $\Gamma = 20$, $\beta = 0.95$, $\alpha = 0.1/\pi$.

flow, is positive for the ground states $|g\rangle$, and $|g_{S'}\rangle$ as these represent Gibbs thermal states at a theoretical temperature $T = 0$ with respect to their relevant self-Hamiltonians. The $|-\rangle$ state is not a thermal state, but a projection onto the its closest Gibbs state would be one at infinite temperature and so heat and entropy flow are negative for this state. Likewise, the state $|e\rangle$ is not a thermal state but one would expect heat to dissipate out of the system as it approaches the equilibrium state and so $\Delta_e < 0$ here too. When the system is initialised in a Gibbs thermal state at the temperature of the reservoir, i.e. a thermal state at inverse temperature β, ρ_S^{eq}, strong coupling effects lead to heat dissipation into the reservoir and $\Delta_e < 0$ as the system is pulled towards its non-canonical equilibrium state. In all these cases, non-monotonic behaviour can be observed in Δ_e at shorter times, signifying anomalous heat flow resulting from strong coupling between the system and reservoir.

Quantifying non-Markovianity is the subject of a vast body of literature in the field of open quantum systems [102]. A common approach for studying the non-Markovianity of interactions between a two-level system and an environment is to examine the dynamics of the trace distance, $D(\rho(t), \sigma(t)) \equiv \frac{1}{2}\sqrt{(\rho(t) - \sigma(t))^\dagger(\rho(t) - \sigma(t))}$, between two initially orthogonal pairs of TLS states ρ and σ [103, 104]. The trace distance is non increasing under trace preserving quantum operations. Specifically this means that for a Markovian evolution $\mathcal{E}(\rho)$, then $D(\mathcal{E}(\rho), \mathcal{E}(\sigma)) \leq D(\rho, \sigma)$. If the dynamics of the trace distance are such that it increases at any stage in its evolution, then this is a signature for non-Markovianity and it acts as a witness. In Ref. [96], this witness for non-Markovianity is used to examine whether any correlation is present between information backflow from an environment into an open quantum system and heat flow, in a similar spirit to the concepts under investigation in this chapter. In the situation studied there, it was inconclusive whether any correlations were seen between anomalous heat flows and signatures of non-Markovianity indicated by witness events in the trace distance measure. As such the question of whether information backflow was related to anomalous heat flows in non-Markovian systems was left open.

In our case, heat is defined in such a way as it is intricately related to a component of the information content of the TLS, namely the reversible entropy flow. When the rate of entropy

flow changes sign, this indicates sections of the equilibration process that involve heat flow contrary to the overall net flow across the total equilibration process. For the states $|g\rangle$ and $|g_{S'}\rangle$ this means heat flow back from the system into the reservoir, and in the other cases, this means heat flow back from the reservoir to the system. Likewise, the other component of the rate of change of TLS entropy, the irreversible entropy production rate which is not associated with any heat flow, is negative for some sections of the equilibration process. It has been argued recently that such negative entropy production rates are indicators of the non-Markovian nature of the reservoir in open quantum systems [105].

We notice that, in general, the magnitude of Δ_i is larger than the magnitude of Δ_e for the initial state with coherence in the TLS energy eigenbasis. For other initial states without coherence, the magnitudes of each component of entropy change are similar. Indications from what we learned in the previous section on the independent boson model suggest that this is a signature of the erasure of this initial quantum coherence. But, beyond this, it is less straightforward, in the case of the full spin-boson model, to associate entropy production solely with the erasure of quantum information in the form of coherence, as we have previously done in the independent boson model. All the initial states shown in figure 5.3, whether quantum coherent or not, generate irreversible entropy production in a non-monotonic fashion. The dynamics of TLS populations and coherence in the energy eigenbasis are intricate. Under this Hamiltonian, the reduced density operator for the TLS undergoes dynamics with terms in the master equation responsible for both decoherence and dissipation. So we expect to see complex dynamics in both the TLS populations and the coherence, unlike in the independent boson model where there were only coherence dynamics. In figure 5.4 we see the behaviour of the population in the ground energy eigenstate and the real and imaginary parts of the coherence for the different initial states considered in figure 5.3.

The population in the ground state, P_g, will tend towards an equilibrium value given by the steady state solution of the RC master equation, as discussed in previous chapters. Strong coupling and non-Markovian effects manifest themselves in the non-monotonic behaviour of P_g as it tends to this equilibrium value for all the initial states considered here. Coherence also

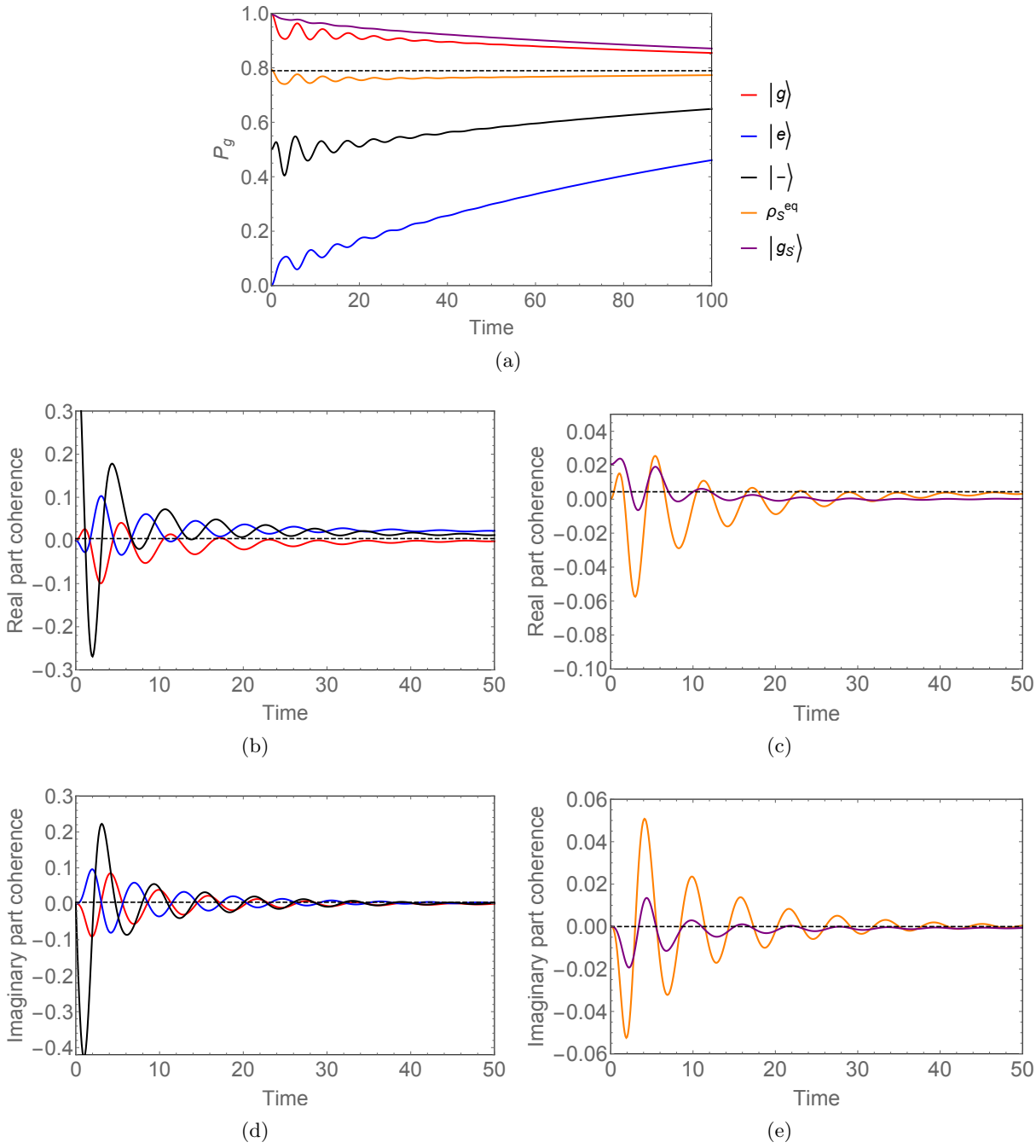

Figure 5.4: (a) Population in the ground energy eigenstate of the TLS; (b) and (c) real part of the coherence of the TLS in its energy eigenbasis; (d) and (e) imaginary part of the coherence of the TLS in its energy eigenbasis for the spin boson model at finite coupling, for the various initial states from figure 5.3, and as indicated in the legend on plot (a). For clarity with have separated these five states into two plots for each component of the coherence, and note the difference in scale on the vertical axis. *Black dashed line* represents steady state equilibrium values. Parameters: $\epsilon = 1$, $\Delta = 1$, $\omega_0 = 1$, $\Gamma = 20$, $\beta = 0.95$, $\alpha = 0.1/\pi$.

oscillates and will tend to an equilibrium level according to the RC master equation steady state. We note that, even for initial states with no quantum coherence in the TLS energy eigenbases, transitions to quantum coherent states occur as a result of the finite strength of system-environment coupling. This is the behaviour responsible for the quantum nature of the heat engine discussed in the previous chapter, for instance, and is not behaviour which is seen in a standard weak coupling treatment of the spin-boson model. It is also now the reason it is less straightforward to associate Δ_i purely with coherence destruction, as we were able to in the case of the independent boson model.

5.5 Summary

We have seen in this chapter how to employ exact definitions of entropy flow and entropy production and apply them in the analysis of an open quantum system which is strongly interacting with its environment. We showed how the decoherence of the TLS in the independent boson model manifests itself purely in terms of irreversible entropy production, thus giving a thermodynamic interpretation to the erasure of quantum information in that context. In contrast, the erasure of classical information is always accompanied by heat dissipation according to Landauer's principle.

Beyond this model of pure decoherence, we used the RC method and the partitioning of entropy to look at information flow, and backflow, in the spin-boson model under strong coupling non-Markovian regimes. We were able to associate anomalous heat flow with entropy flow in the opposite direction to that expected, identifying a connection between a thermodynamic quantity and an information theoretic one which had not been successfully achieved previously when employing the trace distance as a witness to non-Markovianity [96].

Concluding remarks

This project has sought to address an area which has, as yet, been largely lacking in recent efforts at extending the theory of thermodynamics to the quantum regime. We have developed a framework for tackling open quantum systems which interact strongly with their environment and this has allowed us to examine aspects of quantum thermodynamics at strong working system-reservoir coupling.

In chapter 2, we saw how the RC framework could be used to give excellent agreement with exact results for open quantum system dynamics. It allows for a treatment which goes beyond standard techniques which restrict us to weak coupling and afford us only the ability to compute system dynamics and observables. The RC framework tracks, in addition to the system, some environmental dynamics which allows insight into system-environmental correlations.

This toolbox was applied to the cases of equilibrium and non-equilibrium heat engines in chapters 3 and 4. We saw how these engines behaved differently from their weakly coupled counterparts in terms of work and power output, efficiency and heat absorption. All of which are the metrics classical and weakly coupled quantum engines are judged by. In addition, by keeping track of system-environment correlations, we were able to identify the source of additional operational costs in the case of strongly coupled engines and proposed a method by which these could be mitigated. The non-equilibrium, strongly coupled engine gave us insight into quantum effects not present in weakly coupled counterparts of the engine which are not able to develop quantum coherence during their operational cycles. We saw how this coherence caused a resistive effect which was detrimental to the engine's performance.

In chapter 5, we examined coherence in a more general setting than that of the workings of a heat engine. In the case of a quantum system undergoing decoherence alone as a result of its interaction with an environment, we saw how the erasure of quantum coherence was associated only with irreversible entropy production within the system. We saw how the RC framework allows for an accurate calculation of this quantity which would otherwise require a full treatment of environmental dynamics, which, in general, is not possible with standard methods from open quantum systems. We then looked at the spin-boson model, within the RC framework, and partitioned the system's entropy change into reversible entropy flow and irreversible entropy production. We discussed signatures therein of non-Markovianity and anomalous heat flow which result from strong system-reservoir interaction strength.

Bibliography

[1] Heinz-Peter Breuer and F Petruccione. *The theory of open quantum systems*. Oxford University Press, Oxford, 2002.

[2] Howard Carmichael. *Statistical methods in quantum optics: master equations and fokker-planck equations*. Springer, New York, 1999.

[3] Maximilian A Schlosshauer. *Decoherence and the quantum-to-classical transition*. Springer, Berlin, 2007.

[4] Manabendra N. Bera, Arnau Riera, Maciej Lewenstein, and Andreas Winter. Generalized laws of thermodynamics in the presence of correlations. *Nature Communications*, 8(1):2180, 2017.

[5] U Weiss. *Quantum dissipative systems*. World Scientific, New Jersey, 4th ed edition, 2012.

[6] A. Caldeira and A. Leggett. Path integral approach to quantum brownian motion. *Physica A: Statistical Mechanics and its Applications*, 121:587–616, 1983.

[7] A. J. Leggett, S. Chakravarty, A. T. Dorsey, Matthew P. A. Fisher, Anupam Garg, and W. Zwerger. Dynamics of the dissipative two-state system. *Rev. Mod. Phys.*, 59:1–85, Jan 1987.

[8] Joel Gilmore and Ross H McKenzie. Spin boson models for quantum decoherence of electronic excitations of biomolecules and quantum dots in a solvent. *Journal of Physics: Condensed Matter*, 17(10):1735, 2005.

[9] Ahsan Nazir and Dara P S McCutcheon. Modelling exciton–phonon interactions in optically driven quantum dots. *Journal of Physics: Condensed Matter*, 28(10):103002, 2016.

[10] Yoshitaka Tanimura. Nonperturbative expansion method for a quantum system coupled to a harmonic-oscillator bath. *Phys. Rev. A*, 41:6676–6687, Jun 1990.

[11] Yoshitaka Tanimura and Ryogo Kubo. Two-time correlation functions of a system coupled to a heat bath with a gaussian-markoffian interaction. *Journal of the Physical Society of Japan*, 58(4):1199–1206, 1989.

[12] A. Nazir and G. Schaller. The reaction coordinate mapping in quantum thermodynamics. *arXiv:1805.08307*, 2018.

[13] Jake Iles-Smith, Neill Lambert, and Ahsan Nazir. Environmental dynamics, correlations, and the emergence of noncanonical equilibrium states in open quantum systems. *Phys. Rev. A*, 90:032114, Sep 2014.

[14] Jake Iles-Smith, Arend G. Dijkstra, Neill Lambert, and Ahsan Nazir. Energy transfer in structured and unstructured environments: Master equations beyond the born-markov approximations. *The Journal of Chemical Physics*, 144(4), 2016.

[15] Philipp Strasberg, Gernot Schaller, Neill Lambert, and Tobias Brandes. Nonequilibrium thermodynamics in the strong coupling and non-markovian regime based on a reaction coordinate mapping. *New Journal of Physics*, 18(7):073007, 2016.

[16] David Newman, Florian Mintert, and Ahsan Nazir. Performance of a quantum heat engine at strong reservoir coupling. *Phys. Rev. E*, 95:032139, Mar 2017.

[17] Philipp Strasberg, Gernot Schaller, Thomas L. Schmidt, and Massimiliano Esposito. Fermionic reaction coordinates and their application to an autonomous maxwell demon in the strong-coupling regime. *Phys. Rev. B*, 97:205405, May 2018.

[18] Ahsan Nazir and Dara P S McCutcheon. Modelling exciton–phonon interactions in optically driven quantum dots. *Journal of Physics: Condensed Matter*, 28(10):103002, feb 2016.

[19] S. Barnett, J. Cresser, and S. Cooke. Theory of the strongly damped harmonic oscillator. *ArXiv: 1508.02442v1*, 2015.

[20] Sadi Carnot. *Réflexions sur la puissance motrice du feu: et sur les machines propres à développer cette puissance.* Chez Bachelier, libraire, quai des Augustins, no. 55, A Paris, 1824.

[21] Stephen Blundell and Katherine M Blundell. *Concepts in thermal physics.* Oxford University Press, Oxford, 2nd ed edition, 2010.

[22] P. L. Curto-Risso, A. Medina, and A. Calvo Hernández. Theoretical and simulated models for an irreversible otto cycle. *Journal of Applied Physics*, 104(9):094911, 2008.

[23] P. L. Curto-Risso, A. Medina, and A. Calvo Hernández. Optimizing the operation of a spark ignition engine: Simulation and theoretical tools. *Journal of Applied Physics*, 105(9):094904, 2009.

[24] R Alicki. The quantum open system as a model of the heat engine. *Journal of Physics A: Mathematical and General*, 12(5):L103, 1979.

[25] Paul Skrzypczyk, Anthony J. Short, and Sandu Popescu. Work extraction and thermodynamics for individual quantum systems. *Nat Commun*, 5, 06 2014.

[26] H. E. D. Scovil and E. O. Schulz-DuBois. Three-level masers as heat engines. *Phys. Rev. Lett.*, 2:262–263, Mar 1959.

[27] H. T. Quan, Yu-Xi Liu, C. P. Sun, and Franco Nori. Quantum thermodynamic cycles and quantum heat engines. *Phys. Rev. E*, 76:031105, Sep 2007.

[28] Tien D. Kieu. The second law, maxwell's demon, and work derivable from quantum heat engines. *Phys. Rev. Lett.*, 93:140403, Sep 2004.

[29] Ronnie Kosloff and Tova Feldmann. Discrete four-stroke quantum heat engine exploring the origin of friction. *Phys. Rev. E*, 65:055102, May 2002.

[30] F. Plastina, A. Alecce, T. J. G. Apollaro, G. Falcone, G. Francica, F. Galve, N. Lo Gullo, and R. Zambrini. Irreversible work and inner friction in quantum thermodynamic processes. *Phys. Rev. Lett.*, 113:260601, Dec 2014.

[31] A Alecce, F Galve, N Lo Gullo, L Dell'Anna, F Plastina, and R Zambrini. Quantum otto cycle with inner friction: finite-time and disorder effects. *New Journal of Physics*, 17(7):075007, 2015.

[32] M V Berry. Transitionless quantum driving. *Journal of Physics A: Mathematical and Theoretical*, 42(36):365303, 2009.

[33] A. del Campo, J. Goold, and M. Paternostro. More bang for your buck: Super-adiabatic quantum engines. *Scientific Reports*, 4:6208 EP –, 08 2014.

[34] Shujin Deng, Aurélia Chenu, Pengpeng Diao, Fang Li, Shi Yu, Ivan Coulamy, Adolfo del Campo, and Haibin Wu. Superadiabatic quantum friction suppression in finite-time thermodynamics. *Science Advances*, 4(4), 2018.

[35] Marlan O. Scully, M. Suhail Zubairy, Girish S. Agarwal, and Herbert Walther. Extracting work from a single heat bath via vanishing quantum coherence. *Science*, 299(5608):862–864, 2003.

[36] Marlan O. Scully. Quantum afterburner: Improving the efficiency of an ideal heat engine. *Phys. Rev. Lett.*, 88:050602, Jan 2002.

[37] J. Roßnagel, O. Abah, F. Schmidt-Kaler, K. Singer, and E. Lutz. Nanoscale heat engine beyond the carnot limit. *Phys. Rev. Lett.*, 112:030602, Jan 2014.

[38] R. Dillenschneider and E. Lutz. Energetics of quantum correlations. *EPL (Europhysics Letters)*, 88(5):50003, 2009.

[39] Obinna Abah and Eric Lutz. Efficiency of heat engines coupled to nonequilibrium reservoirs. *EPL (Europhysics Letters)*, 106(2):20001, 2014.

[40] D. Gelbwaser-Klimovsky, R. Alicki, and G. Kurizki. Minimal universal quantum heat machine. *Phys. Rev. E*, 87:012140, Jan 2013.

[41] David Gelbwaser-Klimovsky, Wolfgang Niedenzu, and Gershon Kurizki. Thermodynamics of quantum systems under dynamical control. *Advances In Atomic, Molecular, and Optical Physics*, 64:329 – 407, 2015.

[42] Ronnie Kosloff and Amikam Levy. Quantum heat engines and refrigerators: Continuous devices. *Annual Review of Physical Chemistry*, 65(1):365–393, 2014.

[43] Yair Rezek and Ronnie Kosloff. Irreversible performance of a quantum harmonic heat engine. *New Journal of Physics*, 8(5):83, 2006.

[44] A. Friedenberger and E. Lutz. When is a quantum heat engine quantum? *arXiv:1508.04128*, 2015.

[45] Udo Seifert. First and second law of thermodynamics at strong coupling. *Phys. Rev. Lett.*, 116:020601, Jan 2016.

[46] K. Słowik, R. Filter, J. Straubel, F. Lederer, and C. Rockstuhl. Strong coupling of optical nanoantennas and atomic systems. *Phys. Rev. B*, 88:195414, Nov 2013.

[47] T. Hümmer, F. J. García-Vidal, L. Martín-Moreno, and D. Zueco. Weak and strong coupling regimes in plasmonic qed. *Phys. Rev. B*, 87:115419, Mar 2013.

[48] Karyn Le Hur. Kondo resonance of a microwave photon. *Phys. Rev. B*, 85:140506, Apr 2012.

[49] Moshe Goldstein, Michel H. Devoret, Manuel Houzet, and Leonid I. Glazman. Inelastic microwave photon scattering off a quantum impurity in a josephson-junction array. *Phys. Rev. Lett.*, 110:017002, Jan 2013.

[50] B. Peropadre, D. Zueco, D. Porras, and J. J. García-Ripoll. Nonequilibrium and nonperturbative dynamics of ultrastrong coupling in open lines. *Phys. Rev. Lett.*, 111:243602, Dec 2013.

[51] Yu-Jia Wei, Yu He, Yu-Ming He, Chao-Yang Lu, Jian-Wei Pan, Christian Schneider, Martin Kamp, Sven Höfling, Dara P. S. McCutcheon, and Ahsan Nazir. Temperature-

dependent mollow triplet spectra from a single quantum dot: Rabi frequency renormalization and sideband linewidth insensitivity. *Phys. Rev. Lett.*, 113:097401, Aug 2014.

[52] Ulrich Vogl and Martin Weitz. Laser cooling by collisional redistribution of radiation. *Nature*, 461(7260):70–73, 09 2009.

[53] D. Gelbwaser-Klimovsky, K. Szczygielski, U. Vogl, A. Saß, R. Alicki, G. Kurizki, and M. Weitz. Laser-induced cooling of broadband heat reservoirs. *Phys. Rev. A*, 91:023431, Feb 2015.

[54] Joachim Ankerhold and Jukka P. Pekola. Heat due to system-reservoir correlations in thermal equilibrium. *Phys. Rev. B*, 90:075421, Aug 2014.

[55] M Carrega, P Solinas, A Braggio, M Sassetti, and U Weiss. Functional integral approach to time-dependent heat exchange in open quantum systems: general method and applications. *New Journal of Physics*, 17(4):045030, 2015.

[56] Massimiliano Esposito, Maicol A. Ochoa, and Michael Galperin. Quantum thermodynamics: A nonequilibrium green's function approach. *Phys. Rev. Lett.*, 114:080602, Feb 2015.

[57] Michele Campisi, Peter Talkner, and Peter Hänggi. Fluctuation theorem for arbitrary open quantum systems. *Phys. Rev. Lett.*, 102:210401, May 2009.

[58] Michele Campisi, Peter Hänggi, and Peter Talkner. *Colloquium* : Quantum fluctuation relations: Foundations and applications. *Rev. Mod. Phys.*, 83:771–791, Jul 2011.

[59] Peter Hanggi and Peter Talkner. The other qft. *Nat Phys*, 11(2):108–110, 02 2015.

[60] Christian Hörhammer and Helmut Büttner. Information and entropy in quantum brownian motion. *Journal of Statistical Physics*, 133(6):1161–1174, 2008.

[61] Massimiliano Esposito, Katja Lindenberg, and Christian Van den Broeck. Entropy production as correlation between system and reservoir. *New Journal of Physics*, 12(1):013013, 2010.

[62] Sebastian Deffner and Eric Lutz. Nonequilibrium entropy production for open quantum systems. *Phys. Rev. Lett.*, 107:140404, Sep 2011.

[63] Lorenzo Pucci, Massimiliano Esposito, and Luca Peliti. Entropy production in quantum brownian motion. *Journal of Statistical Mechanics: Theory and Experiment*, 2013(04):P04005, 2013.

[64] David Gelbwaser-Klimovsky and Alán Aspuru-Guzik. Strongly coupled quantum heat machines. *The Journal of Physical Chemistry Letters*, 6(17):3477–3482, 2015.

[65] Gil Katz and Ronnie Kosloff. Quantum thermodynamics in strong coupling: Heat transport and refrigeration. *Entropy*, 18(5):186, 2016.

[66] R Gallego, A Riera, and J Eisert. Thermal machines beyond the weak coupling regime. *New Journal of Physics*, 16(12):125009, 2014.

[67] Y.-Y. Liu, J. Stehlik, C. Eichler, M. J. Gullans, J. M. Taylor, and J. R. Petta. Semiconductor double quantum dot micromaser. *Science*, 347(6219):285–287, 2015.

[68] Y.-Y. Liu, K. D. Petersson, J. Stehlik, J. M. Taylor, and J. R. Petta. Photon emission from a cavity-coupled double quantum dot. *Phys. Rev. Lett.*, 113:036801, Jul 2014.

[69] M. J. Gullans, Y.-Y. Liu, J. Stehlik, J. R. Petta, and J. M. Taylor. Phonon-assisted gain in a semiconductor double quantum dot maser. *Phys. Rev. Lett.*, 114:196802, May 2015.

[70] S.N. Shevchenko, S. Ashhab, and Franco Nori. Landau–zener–stückelberg interferometry. *Physics Reports*, 492(1):1 – 30, 2010.

[71] M. Born and V. Fock. Beweis des adiabatensatzes. *Zeitschrift für Physik*, 51(3):165–180, Mar 1928.

[72] Johannes Roßnagel, Samuel T. Dawkins, Karl N. Tolazzi, Obinna Abah, Eric Lutz, Ferdinand Schmidt-Kaler, and Kilian Singer. A single-atom heat engine. *Science*, 352(6283):325–329, 04 2016.

[73] O. Abah, J. Roßnagel, G. Jacob, S. Deffner, F. Schmidt-Kaler, K. Singer, and E. Lutz. Single-ion heat engine at maximum power. *Phys. Rev. Lett.*, 109:203006, Nov 2012.

[74] Andrew N. Jordan, Björn Sothmann, Rafael Sánchez, and Markus Büttiker. Powerful and efficient energy harvester with resonant-tunneling quantum dots. *Phys. Rev. B*, 87:075312, Feb 2013.

[75] Björn Sothmann, Rafael Sánchez, and Andrew N Jordan. Thermoelectric energy harvesting with quantum dots. *Nanotechnology*, 26(3):032001, 2015.

[76] Patrick P. Hofer and Björn Sothmann. Quantum heat engines based on electronic mach-zehnder interferometers. *Phys. Rev. B*, 91:195406, May 2015.

[77] Patrick P. Hofer, J.-R. Souquet, and A. A. Clerk. Quantum heat engine based on photon-assisted cooper pair tunneling. *Phys. Rev. B*, 93:041418, Jan 2016.

[78] E. Torontegui, S Ibanez, S Martinez-Garaot, M. Modugno, A del Campo, D Guery-Odelin, A Ruschhaupt, Xi Chen, and J G Muga. Shortcuts to adiabaticity. *arXiv:1212.6343*, 2012.

[79] Tova Feldmann and Ronnie Kosloff. Quantum lubrication: Suppression of friction in a first-principles four-stroke heat engine. *Phys. Rev. E*, 73:025107, Feb 2006.

[80] Raam Uzdin, Amikam Levy, and Ronnie Kosloff. Equivalence of quantum heat machines, and quantum-thermodynamic signatures. *Phys. Rev. X*, 5:031044, Sep 2015.

[81] Raam Uzdin, Amikam Levy, and Ronnie Kosloff. Quantum heat machines equivalence, work extraction beyond markovianity, and strong coupling via heat exchangers. *Entropy*, 18(4), 2016.

[82] Kay Brandner, Michael Bauer, and Udo Seifert. Universal coherence-induced power losses of quantum heat engines in linear response. *Phys. Rev. Lett.*, 119:170602, Oct 2017.

[83] J. Klatzow, J. Becker, P. Ledingham, C Weinzetl, K. Kaczmarek, D. Saunders, J. Nunn, I. Walmsley, R. Uzdin, and E. Poem. Experimental demonstration of quantum effects in the operation of microscopic heat engines. *arXiV:1710.08716*, 2017.

[84] M. Perarnau-Llobet, H. Wilming, A. Riera, R. Gallego, and J. Eisert. Fundamental corrections to work and power in the strong coupling regime. *arXiv:1704.05864*, 2017.

[85] R. Kosloff and Y. rezek. The quantum harmonic otto cycle. *Entropy*, 19(4):136, 2017.

[86] David G. Tempel and Alán Aspuru-Guzik. Relaxation and dephasing in open quantum systems time-dependent density functional theory: Properties of exact functionals from an exactly-solvable model system. *Chemical Physics*, 391(1):130 – 142, 2011. Open problems and new solutions in time dependent density functional theory.

[87] Patrick Rebentrost, Masoud Mohseni, Ivan Kassal, Seth Lloyd, and Alán Aspuru-Guzik. Environment-assisted quantum transport. *New Journal of Physics*, 11(3):033003, 2009.

[88] R. Landauer. Irreversibility and heat generation in the computing process. *IBM Journal of Research and Development*, 5(3):183–191, July 1961.

[89] C.H. Bennett. *Int J Theor Phys*, 21(905), 1982.

[90] Richard P Feynman, Anthony J. G Hey, and Robin W Allen. *Feynman lectures on computation*. Addison-Wesley, Reading, Mass., 1996.

[91] M Plenio. The holevo bound and landauer's principle. *Phys Lett A*, 263:281, 1999.

[92] M Plenio. *arXiV:quant-ph/9910086v1*, 2018.

[93] M Plenio and Vincenzo Vitelli. The physics of forgetting: Landauer's erasure principle and information theory. 42, 03 2001.

[94] Barbara Piechocinska. Information erasure. *Phys. Rev. A*, 61:062314, May 2000.

[95] Stefanie Hilt, Saroosh Shabbir, Janet Anders, and Eric Lutz. Landauer's principle in the quantum regime. *Phys. Rev. E*, 83:030102, Mar 2011.

[96] R. Schmidt, S. Maniscalco, and T. Ala-Nissila. Heat flux and information backflow in cold environments. *Phys. Rev. A*, 94:010101, Jul 2016.

[97] Bartłomiej Gardas and Sebastian Deffner. Thermodynamic universality of quantum carnot engines. *Phys. Rev. E*, 92:042126, Oct 2015.

[98] U. Singh, M. N. Bera, A. Misra, and A. K. Pati. Erasing quantum coherence: An operational approach. *ArXiv:1506.08186*, 2015.

[99] P. Kammerlander and J. Anders. Coherence and measurement in quantum thermodynamics. *Scientific Reports*, 6:22174 EP –, 02 2016.

[100] Anatoli Polkovnikov. Microscopic diagonal entropy and its connection to basic thermodynamic relations. *Annals of Physics*, 326(2):486 – 499, 2011.

[101] Tatsuhiko N. Ikeda, Naoyuki Sakumichi, Anatoli Polkovnikov, and Masahito Ueda. The second law of thermodynamics under unitary evolution and external operations. *Annals of Physics*, 354:338 – 352, 2015.

[102] Angel Rivas et al. Quantum non-markovianity: characterization, quantification and detection. *Rep. Prog. Phys.*, 77:094001, 2014.

[103] Michael A Nielsen and Isaac L. Chuang. *Quantum computation and quantum information*. Cambridge University Press, Cambridge, 2000.

[104] Heinz-Peter Breuer, Elsi-Mari Laine, and Jyrki Piilo. Measure for the degree of non-markovian behavior of quantum processes in open systems. *Phys. Rev. Lett.*, 103:210401, Nov 2009.

[105] P. Strasberg and M. Esposito. Non-markovianity and negative entropy production rates. *arXiv:1806.09101v2*, 2018.